NEURAL RESPONSES TO INJURY:
PREVENTION, PROTECTION, AND REPAIR
Annual Technical Report
1996

Submitted by

Nicolas G. Bazan, M.D., Ph.D.
Project Director

Period Covered: 20 September, 1995, through 19 September, 1996
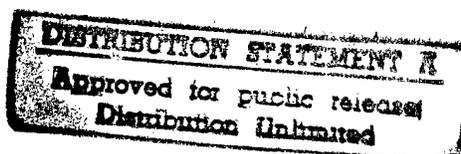
Cooperative Agreement DAMD17-93-V-3013

between

United States Army Medical Research and Development Command
(Walter Reed Army Institute of Research)

and

Louisiana State University Medical
Center
Neuroscience Center of Excellence

Volume 7 of 9

DTIC QUALITY INSPECTED 4/

Role of Growth Factors and Cell Signaling in the Response of Brain and Retina to Injury

Project Directors:
Prescott Deininger, Ph.D.
Nicolas G. Bazan, M.D., Ph.D.

19980323 153

FOREWORD

Opinions, interpretations, conclusions and recommendations are those of the authors and are not necessarily endorsed by the U.S. Army.

( )   Where copyrighted material is quoted, permission has been obtained to use such material.

( )   Where material from documents designated for limited distribution is quoted, permission has been obtained to use the material.

( )   Citations of commercial organizations and trade names in this report do not constitute an official Department of Army endorsement or approval of the products or services of these organizations.

(x)   In conducting research using animals, the investigator(s) adhered to the "Guide for the Care and Use of Laboratory Animals," prepared by the Committee on Care and use of Laboratory Animals of the Institute of Laboratory Resources, National Research Council (NIH Publication No. 86-23, Revised 1985).

( )   For the protection of human subjects, the investigator(s) adhered to policies of applicable Federal Law 45 CFR 46.

( )   In conducting research utilizing recombinant DNA technology, the investigator(s) adhered to current guidelines promulgated by the National Institutes of Health.

( )   In the conduct of research utilizing recombinant DNA, the investigator(s) adhered to the NIH guidelines for Research Involving Recombinant DNA Molecules.

( )   In the conduct of research involving hazardous organisms, the investigator(s) adhered to the CDC-NIH Guide for Biosafety in Microbiological and Biomedical Laboratories.

_____ 10/18/96
Investigator Signature   Date

ANIMAL USE
SEPTEMBER 20, 1995 THROUGH SEPTEMBER 19, 1996

DAMD17-93-V-3013

The experimental animals used during this period for the project, Neural Responses to Injury: Prevention, Protection, and Repair, **Subproject: Role of Growth Factors and Cell Signaling in the Response of Brain and Retina to Injury**, are as follows:

Species	Number Allowed	Number Used	LSU IACUC#
Rat (Albino Wistar)	78	78	1032
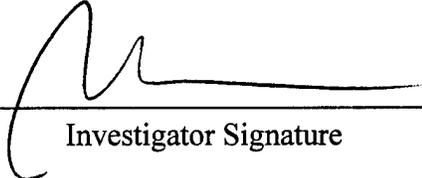
_____
Investigator Signature

Volume 7 Role of Growth Factors and Cell Signaling in the Response of Brain and Retina to Injury

Project Directors: Prescott Deininger, Ph.D.
                                   Nicolas G. Bazan, M.D., Ph.D.

Participating Scientists: Julia Cook, Ph.D.
                                   Haydee E. P. Bazan, Ph.D.
                                   William C. Gordon, Ph.D.
                                   Elena Rodriguez De Turco, Ph.D.
                                   Victor Marcheselli, Ph.D.

Publications

Rodriguez de Turco EB, Deretic D, Bazan NG, Papermaster DS (1996) Post-Golgi Vesicles Cotransport
Docosahexaenoyl-Phospholipids and Rhodopsin During Frog Photoreceptor Membrane
Biogenesis. J Biol Chem. Submitted.

Rodriguez de Turco EB, Marcheselli VL, Gordon WC, Bazan NG (1996) The onset of light damage
selectively induces the early response gene inducible cyclooxygenase in the rat retina. The Joint
Meeting of the American Society for Biochemistry and Molecular Biology, 2-6 June, New
Orleans, LA.

Bazan NG, Marcheselli VL, Gordon WC, Zhang D (1997) Enhanced expression of the inducible
prostaglandin synthase gene precedes light-induced photoreceptor apoptosis. 1997 Keystone
Symposia Conference on Ocular Cell and Molecular Biology, 7-12 January, Tamarron, Colorado.

Bazan NG (1997) PAF is a transcriptional activator of PGS-2 (COX-2): Significance for neuronal
survival after injury. 1997 Keystone Symposia Conference on Lipid Mediators: Recent Advances
in Molecular Biology, Understanding of Regulation, and Pharmacology, 26-31 January, Keystone
Resort, Colorado.

PROJECT 1: GENE EXPRESSION FOLLOWING BRAIN INJURY

The objective of this study is to assay for changes in expression of genes involved in neural growth and differentiation as a function of wound healing. We have used the Chalifour procedure (1) to assay for changes in panels of brain cortex RNAs.

Materials and Methods

Rat Brain Cryogenic Injury

Winstar rats weighing 250-275 g were ether anesthetized and a 9 mm diameter probe cooled in liquid nitrogen was placed on the right parietal region of the rat skull for 1 min. The animals were then euthanized and the brains dissected at the specified times.

Analysis of Gene Expression Patterns

Double-stranded radiolabeled cDNAs were synthesized from rat cortex RNAs isolated at various time points following brain injury. Panels of nitrocellulose filter-fixed cDNA clones were then screened according to the method of Chalifour *et al.* (1). Modifications included the use of 50 μg of RNA, 2000u reverse transcriptase, 120 μCi ^{32}P-dCTP, and 2u of klenow per sample. Nitrocellulose filters were hybridized to 10^6 cpm/ml of brain cDNA in 10 ml of hybridization solution.

RNA Collection and Northern Blots

RNAs from rat brain were collected by the method of Chomczynski and Sacchi (2). Northern blots were performed using standard techniques.

Results   See pages which follow.

Discussion and Future Directions

Our final data show the relative steady-state levels of various polyadenylated mRNAs in total brain. Transferrin receptor, myelin basic protein, IGF-1 and IL-2 are all highly represented mRNAs. In contrast, many mRNAs including PLP, PDGF A and B, p53 and transferrin are relatively poorly represented. Many RNAs exhibit dramatic increases following injury. Among these are the Sst, MBP, PLP, renin and PDGF A chain mRNAs.

We further performed northern blot analysis of two representative RNAs in order to show that the trends observed in the dot blots are, indeed, accurate. Both PLP and MBP show patterns of RNA expression by northern analysis that are consistent with those exhibited in the dot blots.

Increases in growth factors may play a role in stimulating cell growth. Increases in glial markers such as PLP and MBP may reflect increased rates of myelination in the healing brain tissue. Those growth factors which increase during wound healing may be reasonable candidates for peptide-based brain therapies following injury. Alternatively, viral vector-directed gene therapy may be useful to overexpress therapeutically relevant peptides.

We will conduct similar experiments using rat hippocampus mRNAs.

References, Project 1

1) Chalifour, L. E., Fahmy, R., Holder, E. L., Hutchinson, E. W., Osterland, C. K., Schipper, H. M., Wang, E. 1994. Anal. Biochem. 216:299-304.

2) Chomczynski, P., Sacchi, N. 1987. Anal. Biochem. 162:156-159.

Table 1. Clone numerical designations and corresponding abbreviations.

Clone Number	Clone Name
A1	pBr322
B1	pUC118
C1	somatostatin (Sst)
D1	myelin basic protein (MBP)
E1	thymidine kinase (TK)
A2	α-tubulin (αTub)
B2	insulin-like growth factor-1 (IGF-1)
C2	renin (Ren)
D2	β-actin
E2	transferrin receptor (Tr-R)
A3	interleukin-2 (IL-2)
B3	v-Fos
C3	laminin
D3	proteolipid protein (PLP)
E3	p53
A4	platelet-derived growth factor receptor α (PDGFαR)
B4	platelet-derived growth factor A (PDGF A)
C4	platelet-derived growth factor β receptor (PDGFβR)
D4	(PDGF B)
E4	transferrin (Tr)

Figure Legend, Project 1

Figure 1. Dot blot analysis of brain mRNA expression at various times following injury using the method of Chalifour. Filter-fixed DNA clones are identified in Table 1.

Figure 2. Same as Figure 1. Repeat of experiment.

Figure 3. Densitometric analysis of dot blot hybridizations presented in Figure 2.

Figure 4. Same as Figure 3.

Figure 5. Northern blot analyses of PLP and MBP RNAs derived from brain tissue at various times following injury. A rRNA probe was used to re-screen the MBP blot in order to confirm accurate gel-loading.
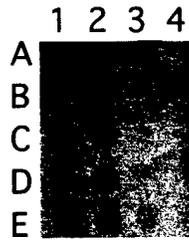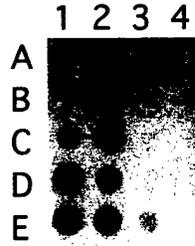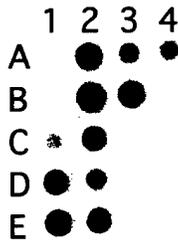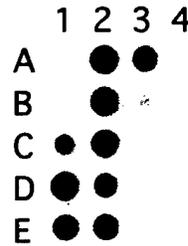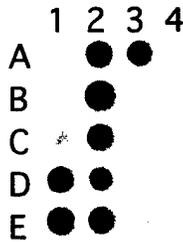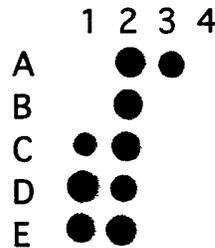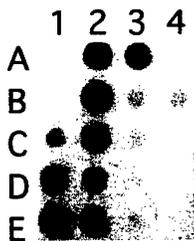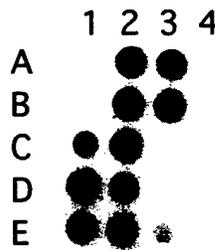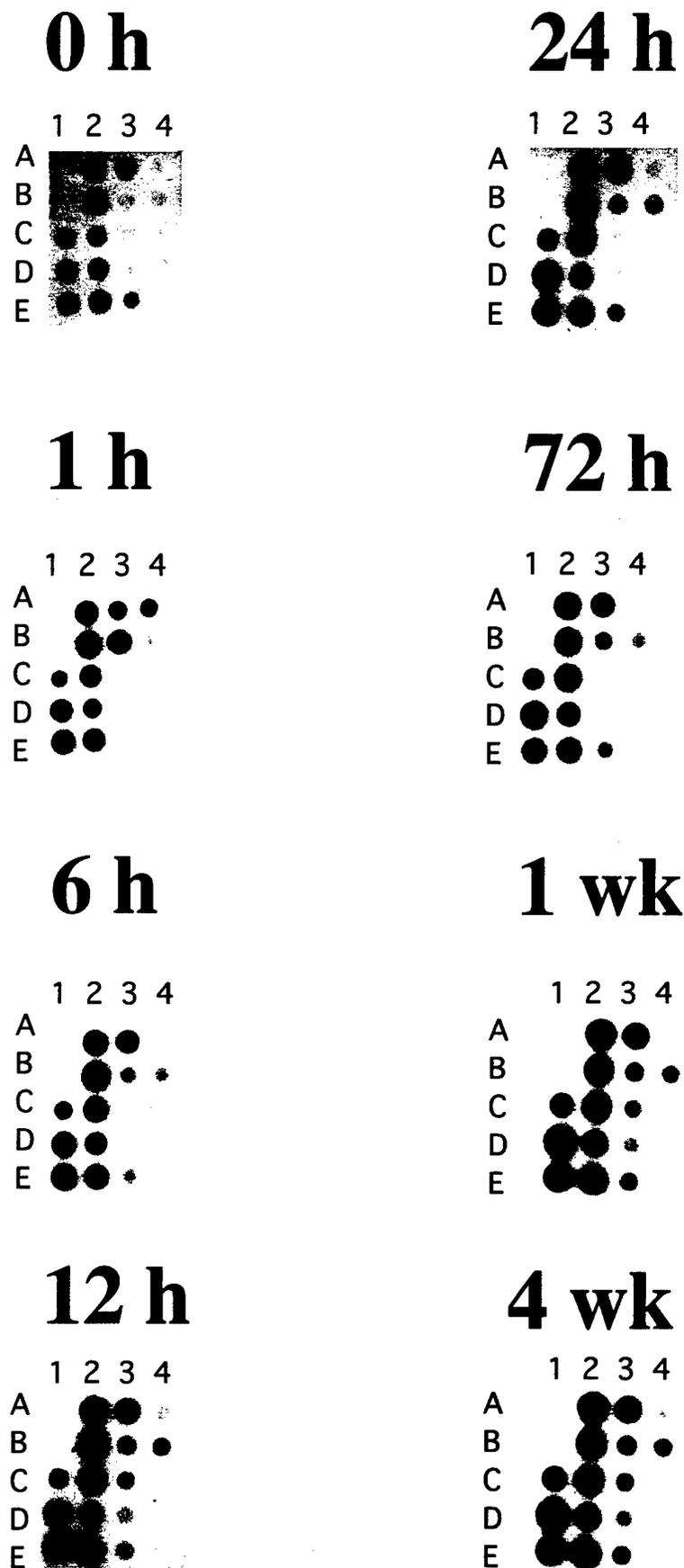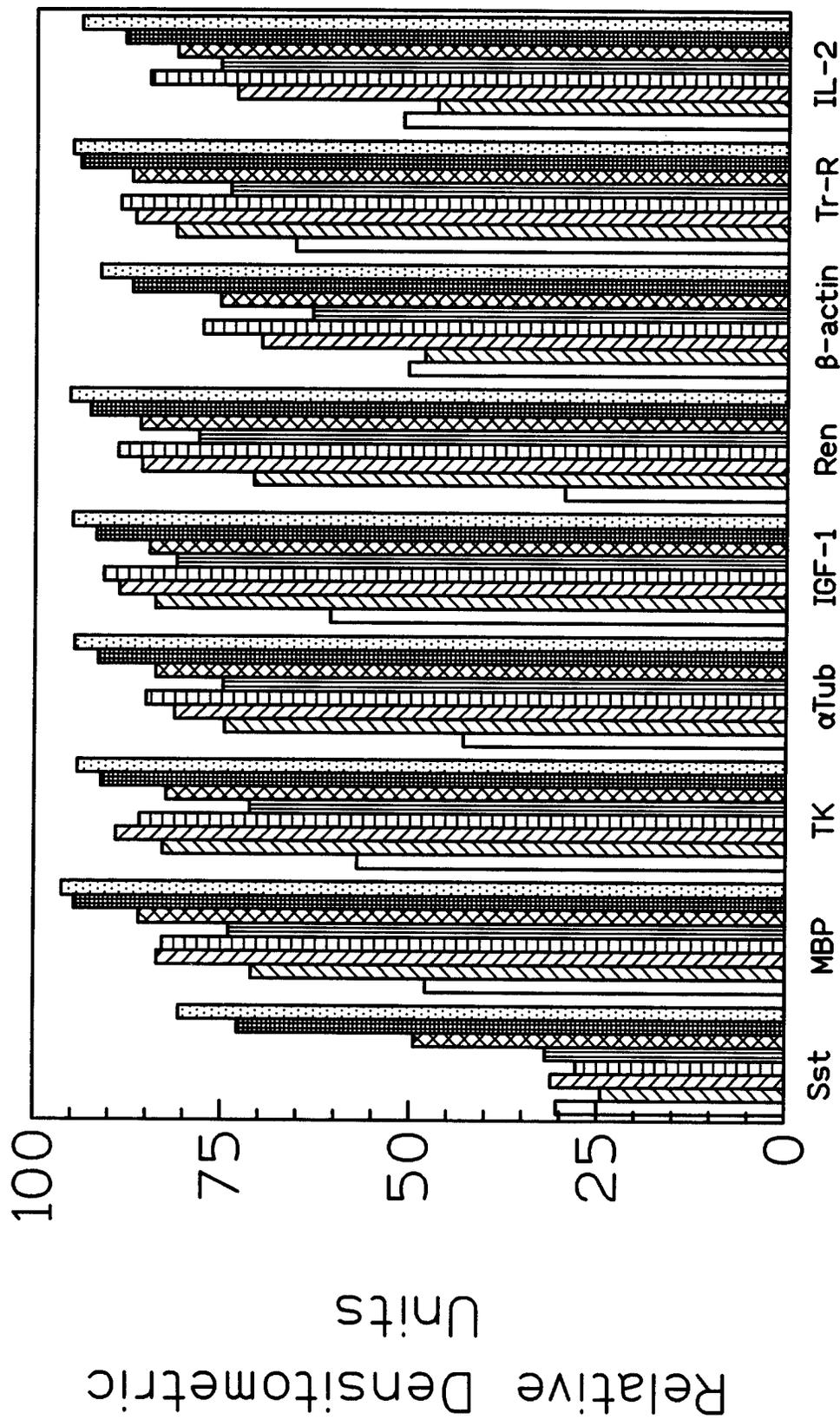
FIGURE 1

FIGURE 2

FIGURE 3
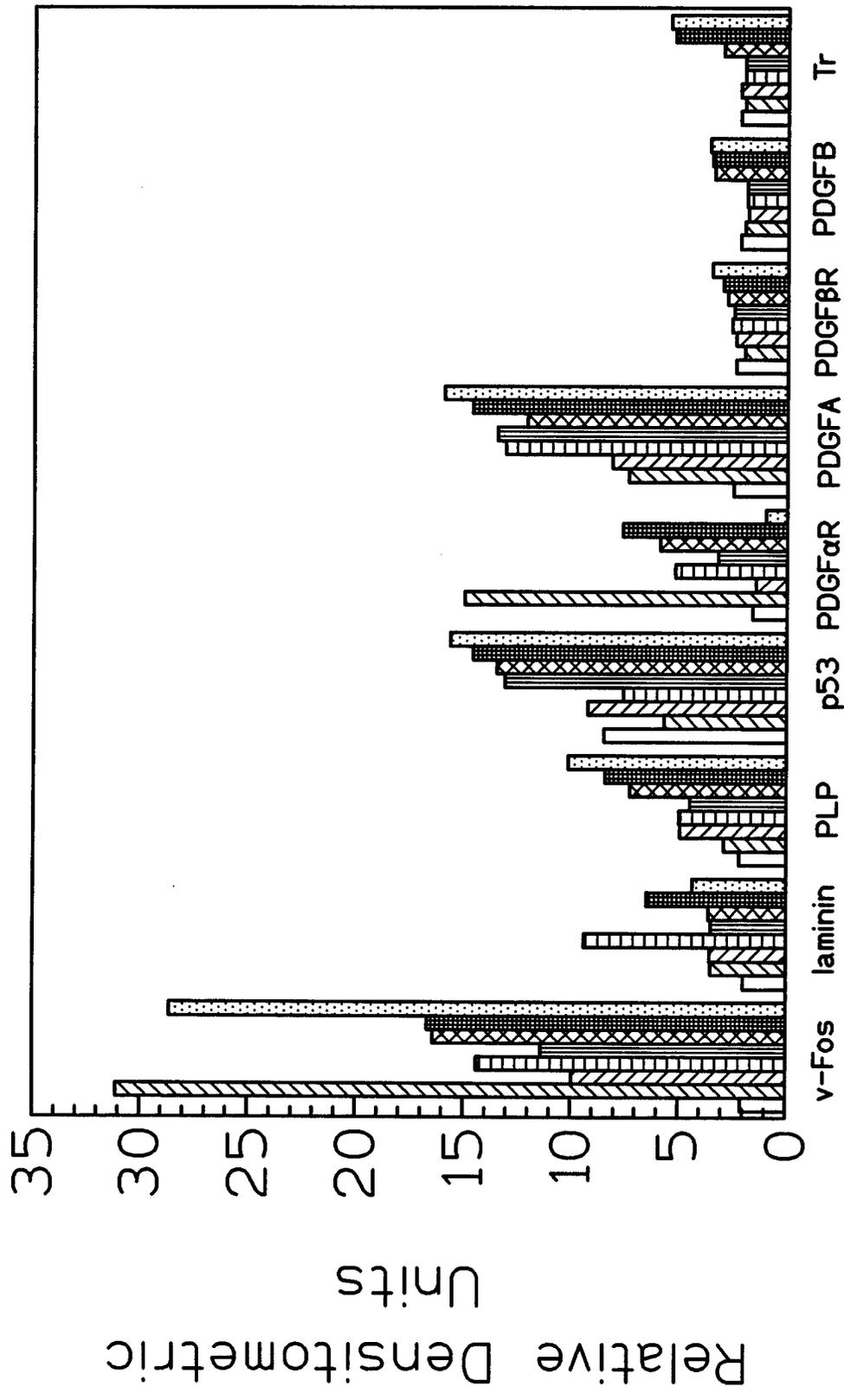
FIGURE 4

PLP

0h 6h 12h 1d 3d 1wk 4wk
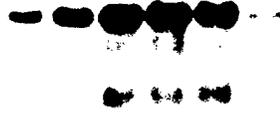
MBP

0h 6h 1d 3d 4wk

rRNA

0h 6h 12h 1d 3d 1wk 4wk

FIGURE 5

PROJECT 2: DEVELOPMENT OF UNIVERSAL HIGH EXPRESSION RETROVIRAL VECTORS

Background: Retroviral Vectors

Retroviral vectors (RVVs) infect cells through specific cell-surface receptors and integrate into genomic DNA prior to transcription (see 1 and 2 for reviews). RVVs have been frequently employed in animal studies and human clinical trials to target brain tumors with high efficiency. Any mitotically active cell, such as those stimulated to divide following injury, are potential targets for efficient RVV uptake.

RVV DNA is reasonably stable in the genome though it is sometimes deleted (3). Transcriptional inactivation of genes encoded by RVVs occurs frequently, however, and is presumed to reflect changes in chromatin structure or methylation patterns in the regions of the promoters (3). Clearly then, both genetic and epigenetic mechanisms are responsible for proviral shutdown. It is believed that viral promoters are quite susceptible to these inactivations and that cellular promoters are more stably expressed. However, it is also clear that viral promoters are typically expressed at much higher levels than are cellular promoters. Viral promoters must be strong in order for viruses to invade and successfully monopolize the transcription machinery of the host cell. Inder Verma's group (4, 5) was one of the first to suggest that long-term expression might be better achieved through the use of housekeeping promoters (those involved in expression of genes integral to cellular functions). They infected mouse embryo fibroblasts with retroviral vectors possessing the β-galactosidase gene linked to either the cytomegalovirus immediate early promoter or the dihydrofolate reductase promoter. The transduced fibroblasts were embedded in a collagen matrix and grafted onto the mid-back of recipient mice. They found long-term expression with the DHFR promoter (2 months) construct but not with the CMV-IE promoter. Consequently, they suggested that the CMV-IE promoter is inducible and may require actively growing cells to be expressed while the DHFR gene is "housekeeping" and should be expressed constitutively. In our early experiments in the area of *in vivo* gene transfer into arteries (6), we demonstrated that the α-actin smooth muscle-specific promoter also increases duration of expression over that obtained from the CMV or Rous sarcoma virus promoters.

Ideally, therefore, our RVVs should possess cellular promoters (since they are less subject to inactivation than are viral promoters), and very strong promoters (so that the gene of interest will be expressed at necessary levels). Our studies in the area of the p53 tumor suppressor DNA-binding consensus sequence suggest that we may apply its unique characteristics towards this goal.

Background: p53 Tumor Suppressor DNA-Binding Consensus Sequence

Our unrelated studies in the area of the p53 tumor suppressor gene have suggested to us a novel approach for increasing the magnitude and duration of expression of cellular genes ligated into RVVs. This may be useful in targeting brain tissue following injury. As we stated previously, viral enhancers are frequently turned off, presumably by methylation or changes in chromatin structure.

10

Cellular enhancers, on the other hand, tend to be weaker than viral enhancers and tend to be very tissue-specific, limiting their broad-application. We have explored two different variations on a p53-regulated DNA transcriptional region (referred to as the p53 DNA-binding consensus sequence (7, 8, 9)) and found that they enhance expression of basal promoters in a promoter-independent manner and respond to very low levels (undetectable by ELISA assays) of wild-type p53 (10, see accompanying manuscript). The consensus is of sequence $5'$-(RRRCWWGYYY)N_{0-13}(RRRCWWGYYY)-$3'$ where R=purine, W=A or T, and Y=pyrimidine. In particular, we find that one of these sequences, hereafter referred to as PG ($5'$-AGACATGCCTAGACATGCCT-$3'$), causes a >60-fold increase in the basal expression of the herpes simplex virus thymidine kinase (TK) promoter when ligated 21 bp upstream of the TATA box and transfected into HCT 116 cells (without co-transfection of a p53 expression construct). The same sequence induces the TK promoter 11-fold in HeLa cells and 50-fold in HJC cells (again, without co-transfection of a p53 expression construct). We find that two tandem copies of the PG sequence behave in a roughly additive manner. Two copies enhance transcription from the HSV-TK promoter approximately 138-fold in HCT 116 cells and 27-fold in HeLa cells (we have not yet tested HJC cells). The PG sequence also enhances, at comparable levels, expression from the heme oxygenase (HO) minimal cellular promoter in each of the three cell types. Therefore, the augmentation is not promoter-specific. However, the augmentation *is* distance-dependent. The PG sequence does not augment transcription of promoters >300 bp removed. This has a decided advantage (for some applications) over such enhancers as the β-globin LCR. One of the concerns about using enhancers such as the LCR which function at great distances is that they may inadvertently activate undesired promoters at the RVV integration site in the genome (11).

We find abundant mutant p53 in the HCT 116 (ATCC CCL 247) human colon carcinoma cells by mutant p53-specific ELISA but no detectable mutant or wild-type p53 in HeLa (ATCC CCL 2) human epithelial carcinoma or HJC glial cells (12). The levels of p53 protein in normal cells and tissues are very low, only a few thousand molecules per cell, because of the protein's very short half-life. The ready detection of p53 protein is synonymous, therefore, with mutation (13). Nevertheless, the PG sequence seems to have a very high affinity for p53 (or, less likely, some other cellular protein) which binds it and dramatically activates transcription. I should finally mention that the HJC cells were immortalized using the JC viral promoter/SV40 large T-antigen. Despite the fact that these cells produce T-antigen which presumably binds to and sequesters much of the cellular p53 (14), the PG sequence is a *strong* transcriptional augmentor in these cells.

We believe that the PG sequence interacts specifically with p53 to mediate transcription activation because 1) PG matches the p53 DNA-binding consensus sequence which has been shown to activate transcription, and 2) cotransfection of a p53 expression construct increases expression from the PG-modified promoters. Nevertheless, it is possible that the PG sequence is interacting with some other cellular factor. Regardless of the nature of the factor responsible for interacting with and mediating transcriptional up-regulation through the PG sequence, it seems to be present in a broad range of cell types and is a very powerful factor.

11

Methods

Historically, the most serious concern encountered when using retroviral vectors was that the helper genome (encoding the components of the virion particle and the reverse transcriptase) and the vector genome (encoding the protein of interest) could recombine through homologous sequences to generate replication competent virus. Dr. Dusty Miller and his colleagues, however, have used site-directed mutagenesis to generate retroviral vector genomes which, upon homologous recombination, inactivate the helper virus (15). We will employ derivatives of the Miller retroviruses to infect the cell types as stated in the Specific Objectives.

We have made derivatives of the LNSX vector (where L=LTR, N=neomycin, S=simian virus 40, X=cloned gene of interest, see Figure 1). Specifically, the simian virus 40 promoter was removed using Stu I/Bam HI, and the plasmid was religated and grown large scale (LNΔSX). Complementary oligomers of sequence 5'-CTAGGAGACATGCCTAGACATGCCTC-3' and 5'-CTAGGAGGCATGTCTAGGCATGTCTC-3' (one copy of PG, with Avr II extensions) were directly ligated into Avr II digested LNΔSX to create LNΔSX/PG$_n$ (n=2, 3, 6 or 9 depending upon copy number).The minimal HO promoter was then PCR-amplified using primers possessing Hind III extensions. The PCR amplification product was digested with Hind III and ligated to Hind III digested LNΔSX/PG$_n$ to create LNΔSX/PG$_n$/HO. Finally, the luciferase cDNA was ligated into the Cla I site downstream of the promoter/PG assembly (the promoter has no Cla I recognition sites) to create LNΔSX/PG$_n$/HO/Luc.

Transfections of cells has been performed as indicated in our accompanying publication (10).

Results

1)   We have generated RVVs in which the cellular heme oxygenase (HO) promoter regulates expression of the luciferase reporter gene. We have generated additional RVVs in which two, three, six and nine copies of the PG sequence augment transcription from the HO promoter (see Figure 1).
2) We have transiently transfected these RVV plasmids (except that which possesses nine copies of PG, we have not yet tested) into HCT 116 cells and assayed for promoter activity relative to the SV40 promoter (see Figures 2, 3, and 4).
3) We have created psi-2 cell populations stably transfected with each of these vectors.

Discussion and Future Directions

We will test the above vectors for duration of expression of integrated DNAs in a variety of tissue culture cells (neural and non-neural) by establishing populations clonal for the transgene and monitoring these as a function of time. This will involve 1) stable transduction of PA317 cells with viral vector-containing medium derived from psi-2 cells, 2) stable transduction of various cell types (neural and non-neural) with viral vector-containing medium harvested from PA317 producer cells, 3) assay of each cell type as a function of culture time.

Within the next year of this grant, we hope to have established and tested this series of RVVs and to have found that they are expressed at high levels and for prolonged periods in many cell types. We hope that this technique will be of value not only in targeting neural tissue but many other tissues *in vivo*.

Depending on the results obtained here, we will proceed to substitute for the luciferase reporter gene, functionally relevant genes such as growth and neurotrophic cDNAs.

13

References, Project 2

1. Morgenstern, J.P. and Land, H. (1991). Choice and manipulation of retroviral vectors. *Retroviral Vectors* **7,** 181-206.

2. McLachlin, J.R., Cornetta, K., Eglitis, M.A., and Anderson, W.F. (1990). Retroviral-mediated gene transfer. *Progress in Nucleic Acid Res. and Mol. Biol.* **38,** 91-135.

3. Xu, L., Yee, J.-K., Wolff, J. A., and Friedmann, T. (1989). Factors affecting long-term stability of Moloney murine leukemia virus-based vectors. *Virology* **171,** 331-341.

4. Scharfmann, R., Axelrod, J.H., and Verma, I.M. (1991). Long-term in vivo expression of retrovirus-mediated gene transfer in mouse fibroblast implants. *Proc. Natl. Acad. Sci. USA* **88,** 4626-4630.

5. Naviaux, R.K., and Verma, I.M. (1992). Retroviral vectors for persistent expression in vivo. *Biotechnology* **3,** 540-547.

6. Barbee, R.W., Stapleton, D.D., Perry, B.D., Rè, R.N., Murgo, J.P., Valentino, V.A., and Cook, J.L. (1993). Prior arterial injury enhances luciferase expression following in vivo gene transfer. *Biochem. and Biophys. Res. Comm.* **190,** 70-78.

7. El-Deiry, W.S., Kern, S.E., Pietenpol, J.A., Kinzler, K.W., and Vogelstein, B. (1992). Definition of a consensus binding site for p53. *Nature Genetics* **1,** 45-49.

8. Funk, W.D., Pak, D.T., Karas, R.H., Wright, W.E., and Shay, J.W. (1992). A transcriptionally active DNA-binding site for human p53 protein complexes. *Mol. and Cell. Biol.* **12,** 2866-2871.

9. Hupp, T.R., Meek, D.W., Midgley, C.A., and Lane, D.P. (1992). Regulation of the specific DNA binding function of p53. *Cell* **71,** 875-886.

10. Cook, J. L., Re, R.N., Giardina, J.F., Fontenot, F.E., Cheng, D.Y., and Alam, J. (1995). Distance constraints and stereospecific alignment requirements characteristic of p53 DNa-binding consensus sequence homologies. *Oncogene* **11,** 723-733.

11. Novak, U., Harris, E.A., Forrester, W., Groudine, M., and Gelinas, R. (1989). High-level β-globin expression after retroviral transfer of locus activation region-containing human β-globin gene derivatives into murine erythroleukemia cells. *Proc. Natl. Acad. Sci. USA* **87,** 3386-3390.

12. Frisque, R.J., Rifkin, D.B., and Walker, D.L. (1980). Transformation of primary hamster brain cells with JC virus and its DNA. *J. of Virol.* **35,** 265-269.

13. Lane, D.P., and Benchimol, S. (1990). p53: Oncogene or anti-oncogene? *Genes & Develop.*

4, 1-8.

14. Levine, A.J. (1992). The p53 tumour suppressor gene and product. *Cancer Surveys* **12,** 59-79.

15. Lerner, N., Brigham, S., Goff, S., and Bank, A. (1987). Human β-globin gene expression after gene transfer using retroviral vectors. *DNA* **6,** 573-582.

Figure Legend, Project 2

Figure 1. Diagrammatic illustration of construction of universal high expression RVVs.

Figure 2. LNΔSX/PG$_n$/HO/Luc clones transiently transfected into HCT 116 cells. Open bars represent cells not co-transfected with a p53-encoding construct. Diagonally-striped bars represent cells co-transfected with a p53-encoding construct. Values are standardized to a pRASCat internal control.

Figure 3. Same as 2.

Figure 4. Same as 3, replicate experiment.

LNSX

LTR   neo^R   SV40_pro   poly(A)

BamHI

StuI AvrII HindIII ClaI

digest with BamHI/StuI to remove SV40 promoter, religate

LNΔSX

LTR   neo^R   poly(A)

AvrII HindIII ClaI

digest with AvrII, introduce PG sequences with AvrII extensions

LNΔSX/PG_{2,3,6,9}

LTR   neo^R   poly(A)

PGs

HindIII ClaI

digest with HindIII, introduce minimal HO promoter

LNΔSX /PG_{2,3,6,9}/HO

LTR   neo^R   HO_pro   poly(A)

PGs

ClaI

digest with ClaI, introduce luciferase cDNA

LNΔSX /PG_{2,3,6,9}/HO/Luc

LTR   neo^R   HO_pro   Luc   poly(A)

PGs

FIGURE 1

17

Standardized Luciferase Activity
$(x10^{-5})$

FIGURE 2

Standardized Luciferase Activity
(RLU x 10^{-5})

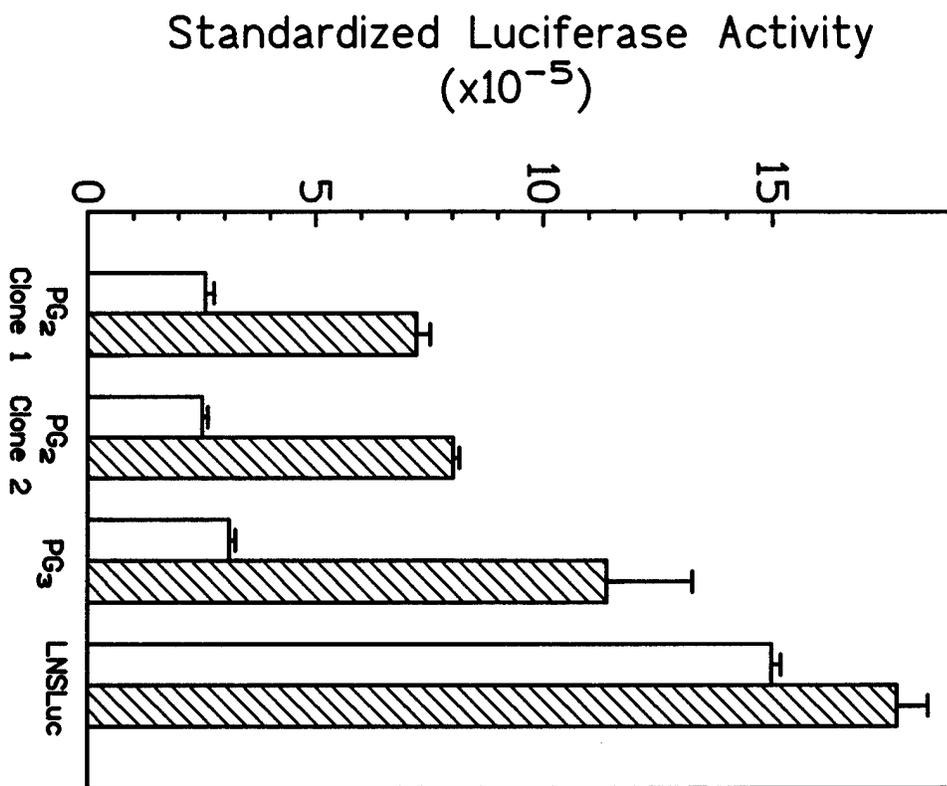**FIGURE 3**

Standardized Luciferase Values
(RLU x 10^{-5})
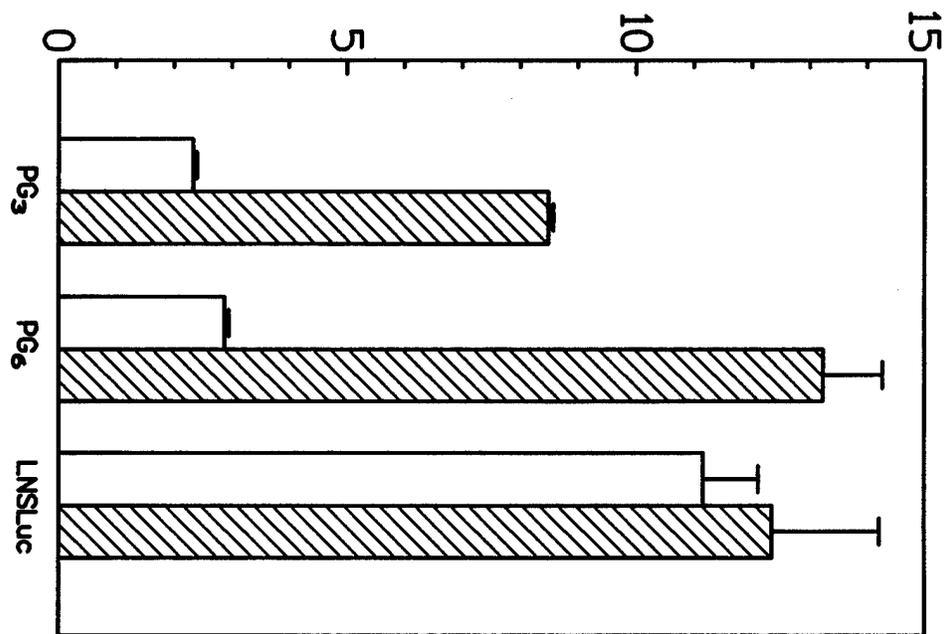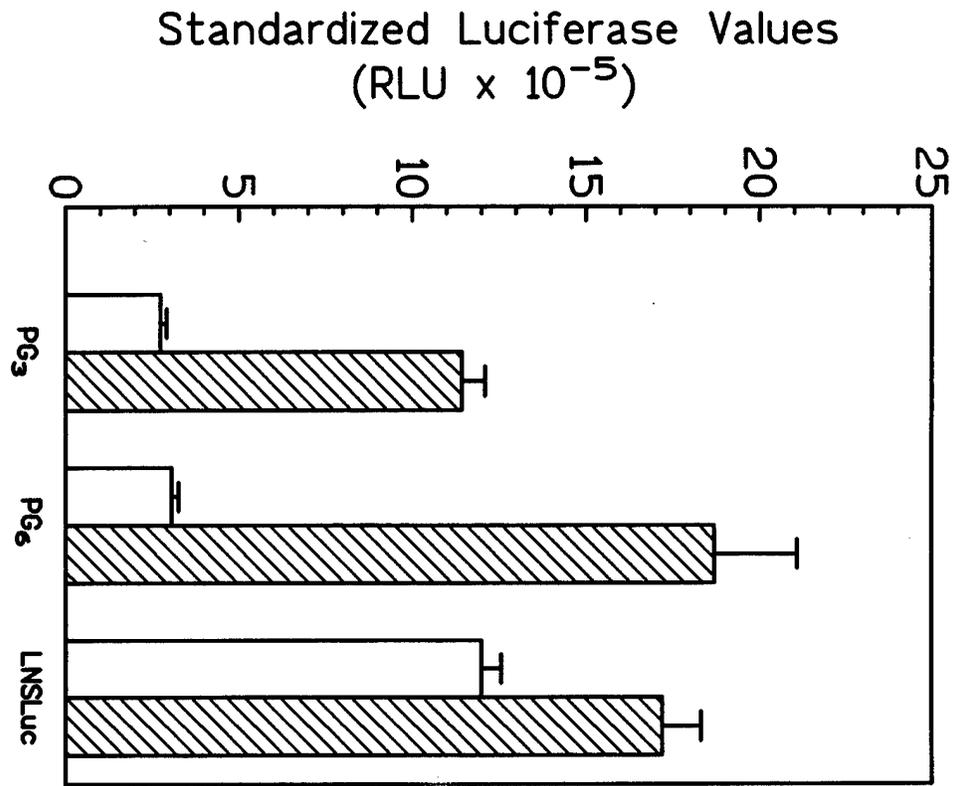
FIGURE 4

20

Distance constraints and stereospecific alignment requirements characteristic of p53 DNA-binding consensus sequence homologies

J L Cook[1], RN Ré, JF Giardina, FE Fontenot, DY Cheng and J Alam

From the Division of Research, Alton Ochsner Medical Foundation, New Orleans, Louisiana, USA 70121

We present evidence in favor of the position that *some* mutant p53 proteins retain the ability to trans-activate downstream genes through p53 DNA-binding consensus sequence (CS) homologies. We tested one cell line possessing high levels of mutant p53 and found that this mutant p53 is highly active in trans-activating one CS homology, moderately active in trans-activating a second sequence and inactive in modulating a third sequence. We tested a second cell line, also possessing high levels of mutant p53 and found the same pattern of activation. In addition we find that inter-motif distance [represented by N in RRRCWWGYYY(N)RRRCWWGYYY] is very important in determining the relative binding affinity of a given CS homology for wild-type or mutant p53. Our studies suggest that stereospecific alignment of the DNA-binding motifs within the CS may favor binding of wild-type p53 while misalignment may favor binding of mutant p53. Furthermore, we find that the maximum distances at which p53 DNA-binding CS homologies are functionally active vary for different sequences. Introduction of as few as 200 bp between one CS homology and the downstream TATA box can eliminate a 45-fold p53-mediated trans-activation. We present evidence that the composition of the DNA which flanks a p53 DNA-binding consensus sequence may also modulate trans-activation.

Keywords: p53; transcriptional regulation; stem cell leukemia gene; consensus sequence

Introduction

The p53 tumor suppressor gene encodes the protein most often found mutated in human cancers (Kern *et al.*, 1992; Vogelstein and Kinzler, 1992). Mutations and allele loss of the p53 gene have been associated with human tumors of, among other tissues, breast, lung, esophagus, liver, bladder, ovary, brain and hematopoietic tissues (Hollstein *et al.*, 1991). p53 acts directly and indirectly to block cell cycle progression and trigger programmed cell death. It blocks the cell cycle by stimulating activity of the gene *Waf1* (*Cip1, p21, Sdi1*) which encodes a protein that inhibits cyclin-dependent kinases (El-Deiry *et al.*, 1993; Harper *et al.*, 1993) and the gene *GADD45*, which encodes a protein involved in DNA repair (Kastan *et al.*, 1992; Smith *et al.*, 1994). Gadd45 stimulates DNA excision repair and inhibits cell entry into S phase.

p53 binds very tightly to a p53 DNA-binding consensus of sequence RRRCWWGYYY$(N)_{0-13}$RRRCWWGYYY in double-stranded DNA (El-Deiry *et al.*, 1992; Funk *et al.*, 1992). Wild-type p53 is believed to bind to this sequence primarily as a tetramer with each subunit recognizing 5 nt of the 20 nt long DNA site (Halazonetis and Kandil, 1993). When this sequence is placed in direct proximity to a promoter, p53 has been shown to mediate positive or negative transcriptional regulation of downstream reporter genes. For this reason, it has been hypothesized that p53 mediates transcriptional regulation of genes *in vivo* through this sequence. Homologies of this sequence are located 2.4 kb upstream of the *Waf1* gene (El-Deiry *et al.*, 1993) and in intron three of the *GADD45* gene (Kastan *et al.*, 1992). Homologies of the consensus sequence *motif* (RRRCWWGYYY) have also been found between −15 and −569 of the EGF receptor promoter, a region which also confers p53-transcriptional activation (Deb *et al.*, 1994).

p53 clearly regulates transcription of other genes through as yet unknown mechanisms. Co-transfection of a p53 expression construct with a muscle-specific creatinine kinase (*MCK*) promoter reporter gene construct indicates that a p53 responsive element lies between 2.8 and 3.3 kb upstream of the *MCK* gene (Weintraub *et al.*, 1991). p53 induces this promoter 10-to 80-fold. The responsive element has not, to our knowledge, been identified. p53 has also been shown to repress the human *IL-6* (−225 to +13), c-*fos* (−711 to +42), and β-*actin* (−3400 to +912) promoters and the porcine *MHC-1* gene promoter (−528 to −38) by unknown mechanisms (Ginsberg *et al.*, 1991; Santhanam *et al.*, 1991). In addition, wild-type p53 specifically represses the multidrug resistance (*MDR1*; Chin *et al.*, 1992) and the basic fibroblast growth factor (*bFGF*) promoters (Ueba *et al.*, 1994) while mutant p53 specifically stimulates these promoters. It has been suggested that stimulation of MDR1 and bFGF expression by mutant p53 may contribute to tumor progression. p53 DNA-binding consensus sequence (CS) homologies have not been found associated with these promoters. Furthermore, a negative element exists in the 5′-untranslated (UT) region of the *bcl-2* gene through which p53 downregulates expression. This region, once again, demonstrates no CS homology (Miyashita *et al.*, 1994). While other examples have been reported, the above are testimony to the fact that p53 can mediate transcriptional effects through means other than p53 DNA-binding CS homologies.

Our identification of a perfect p53 DNA-binding CS homology in the 3′-UT region of the stem cell leukemia gene (*SCL*) led us to investigate the potential of this sequence to enhance wild-type and mutant p53-mediated transcription. This sequence was investigated in its genomic context (3′-flanking UT region) and as a cloned

oligomeric sequence (SCL CS). Transcriptional activity of this CS homology is severely distance-constrained. Depending upon the composition of the flanking DNA sequence, an insertion of as few as 200 bp between the CS and the downstream TATA can eliminate p53-inducible transcriptional activity. The surprising characteristics of this CS homology led us to investigate and compare the properties of two additional CS homologies. Only one of the three CS homologies demonstrates activity when positioned 1.7 kb from the TATA box and downstream of a reporter gene. Each of these three CS homologies demonstrate different and unique properties of transcriptional activation by mutant *vs* wild-type p53.

Finally, the transcriptional effects of altering the length of the inter-motif region of the SCL CS were examined. Our studies suggest that stereospecific alignment of the motifs (RRRCWWGYYY) within the CS may favor binding of wild-type p53 while misalignment may favor binding of mutant p53.

Results

Mutant p53 ELISAs

We chose to investigate, initially in HCT 116 cells, the trans-activation potential of a p53 DNA-binding CS (the SCL CS) which we identified in the 3'-UT region of the SCL gene. These cells, previously employed by Vogelstein and associates (Kern *et al.*, 1992), were reported to possess only very low levels of wild-type p53. In addition, exons 5–8 of the p53 gene from HCT 116 cells were sequenced and determined to be wild-type (Kern *et al.*, 1992). Despite this, our studies indicate that (our subclone of) HCT 116 cells possess considerable amounts of mutant p53 (8.03 ng mg^{-1} protein, Table 1) as determined by mutant p53-specific ELISA. By comparison, HeLa cells have 1.75 ng mg^{-1} of protein and K562 cells have 0.27 ng mg^{-1} protein. Mutant p53 values were standardized to a background value of 0.00 for p53-null fibroblasts (cells derived from a mouse homozygous for a null mutation introduced by homologous recombination, Donehower *et al.*, 1992).

We next investigated the trans-activation potentials of the SCL CS and other CS homologies in HJC cells. These cells also possess high levels of mutant p53 as determined by mutant p53-specific ELISA (Table 1).

Trans-activation properties of the SCL consensus and flanking sequence from the SCL 3'-UT region
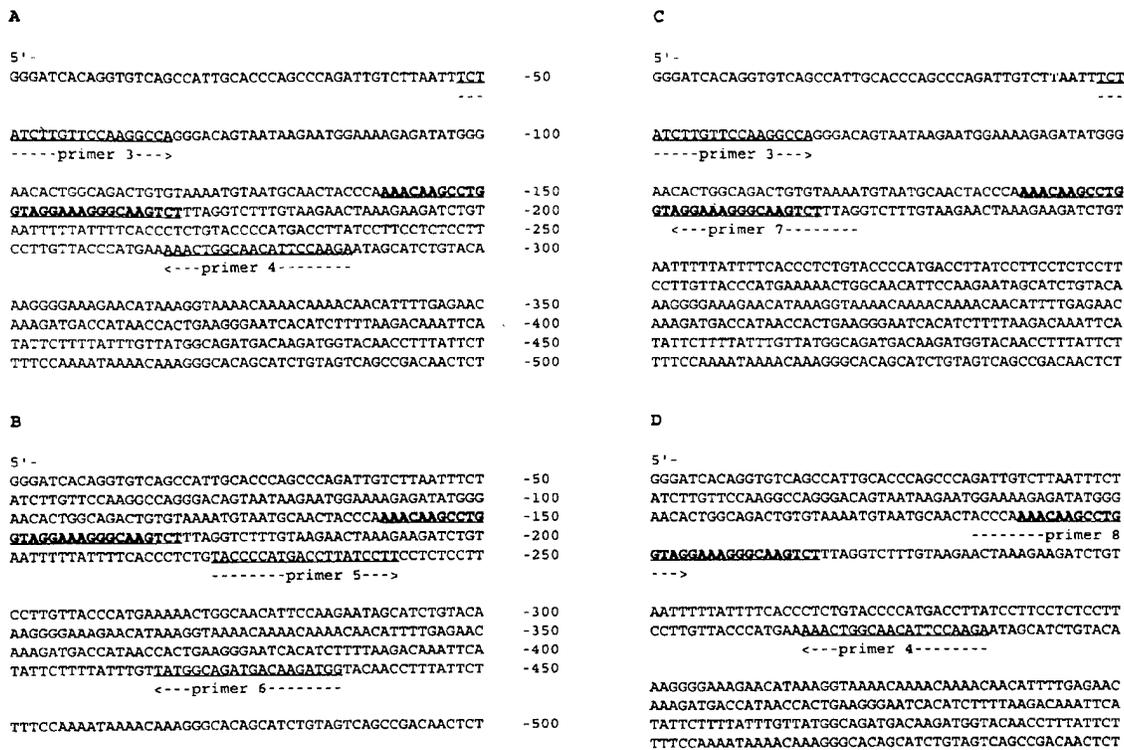
We have identified a p53 DNA-binding CS homology within the SCL gene 3'-UT region. A 238 bp fragment containing the consensus and flanking sequence was PCR amplified (SCL 34, Figure 1A). A control fragment of 213 bp, also from the SCL 3'-UT region was PCR amplified (SCL 56, Figure 1B). The latter fragment possesses no p53 DNA-binding CS homology. SCL 34 and SCL 56 were ligated upstream of the HSV-TK promoter, in both orientations, and tested for basal and p53-inducible enhancer activities. Specifically, SCL 34 was ligated upstream of the TK promoter in the pT81luc luciferase reporter vector (Nordeen, 1988) to generate SCL34+/T81luc (SCL CS is in the (+) orientation, Figure 2) and SCL34−/T81luc (SCL CS is in the (−) orientation, Figure 2). Similarly, SCL 56 was ligated upstream of the TK promoter in the pT81luc luciferase reporter vector to generate SCL 56+/T81luc (control fragment in the (+) orientation, Figure 2) and SCL56−/T81luc (control fragment in the (−) orientation, Figure 2). These reporter constructs were transfected with and without a wild-type p53 expression construct to assess basal and p53-inducible enhancer activities. Interestingly, the 213 bp control sequence does slightly increase basal and p53-inducible activity (Table 2). Our studies (data not shown) indicate that many different DNA fragments with no recognizable p53 DNA-binding CSs can elevate basal and p53-inducible activity 2–3-fold, perhaps reflecting introduction of incidental transcription factor-binding sites. The SCL p53 CS homology possesses no basal or p53-inducible activity (no activity significantly different from that observed using the control fragment) when it is positioned 251 bp (SCL 34+/T81luc) or 183 bp (SCL 34−/T81luc) upstream of the HSV-TK TATA box, in the context of the flanking SCL 3'-UT region sequence (Table 2). This suggests that either the SCL CS does not activate transcription at this distance from the HSV-TK promoter or that the flanking sequences within the SCL 3'-UT region repress transcriptional activation. To test the latter possibility, we generated two new PCR products representing SCL 34 truncations. We PCR amplified fragments corresponding to the proximal and distal portions of the SCL 34 fragment (Figure 1C and D). SCL 37, 125 bp in length, represents the proximal portion of the SCL 34 fragment and possesses the SCL CS distally. SCL 48, 152 bp in length, is the distal portion of the SCL 34 fragment and possesses the SCL CS proximally. The SCL 37 and SCL 48 amplification products are devoid, therefore, of the distal and proximal SCL 34 sequences, respectively. These products were ligated upstream of the HSV-TK promoter, in both orientations and tested for basal and wild-type p53-inducible enhancer activities. SCL 37−/T81luc (Figure 2), in which the CS is positioned 188 bp from the TATA box, demonstrates a slight increase in wild-type p53-inducible activity (Table 3). SCL 37+/T81luc (Figure 2), in which the CS is positioned 99 bp from the TATA exhibits an increase in both basal and wild-type p53-inducible activities (Table 3). This suggests that elimination of the distal sequences might influence basal and inducible expression and that orientation of the CS or distance from the TATA box might also affect transcriptional activation. SCL 48+/T81luc (Figure 2), in which the CS is positioned 212 bp from the TATA box, shows increased basal activity and SCL 48−/T81luc (Figure 2) in which the CS is positioned only 100 bp has less, but slightly enhanced basal

Table 1 Mutant p53 content of various cell types[1]

	Mutant p53 (ng mg^{-1} protein)
HCT 116[2]	8.03 ± 2.33
HJC[2]	6.50 ± 2.17
HeLa[2,3]	1.75 ± 0.88
K562[2,3]	0.27 ± 0.01
p53 Null[2]	0.00

[1]Values represent the mean ± SD. [2]$P < 0.05$ versus HCT 116 and HJC cells. [3]Values are standardized to a p53-null value of 0.00

A

```
5'-
GGGATCACAGGTGTCAGCCATTGCACCCAGCCCAGATTGTCTTAATTTCT      -50
                                                ---

ATCTTGTTCCAAGGCCAGGGACAGTAATAAGAATGGAAAAGAGATATGGG      -100
-----primer 3--->

AACACTGGCAGACTGTGTAAAATGTAATGCAACTACCCAAAACAAGCCTG      -150
GTAGGAAAGGGCAAGTCTTTAGGTCTTTGTAAGAACTAAAGAAGATCTGT      -200
AATTTTTATTTTCACCCTCTGTACCCCATGACCTTATCCTTCCTCTCCTT      -250
CCTTGTTACCCATGAAAAACTGGCAACATTCCAAGAATAGCATCTGTACA      -300
              <---primer 4--------

AAGGGGAAAGAACATAAAGGTAAAACAAAACAAAACAACATTTTGAGAAC      -350
AAAGATGACCATAACCACTGAAGGGAATCACATCTTTTAAGACAAATTCA      -400
TATTCTTTTATTTGTTATGGCAGATGACAAGATGGTACAACCTTTATTCT     -450
TTTCCAAAATAAAACAAAGGGCACAGCATCTGTAGTCAGCCGACAACTCT     -500
```

B

```
5'-
GGGATCACAGGTGTCAGCCATTGCACCCAGCCCAGATTGTCTTAATTTCT      -50
ATCTTGTTCCAAGGCCAGGGACAGTAATAAGAATGGAAAAGAGATATGGG      -100
AACACTGGCAGACTGTGTAAAATGTAATGCAACTACCCAAAACAAGCCTG      -150
GTAGGAAAGGGCAAGTCTTTAGGTCTTTGTAAGAACTAAAGAAGATCTGT      -200
AATTTTTATTTTCACCCTCTGTACCCCATGACCTTATCCTTCCTCTCCTT      -250
              --------primer 5--->

CCTTGTTACCCATGAAAAACTGGCAACATTCCAAGAATAGCATCTGTACA      -300
AAGGGGAAAGAACATAAAGGTAAAACAAAACAAAACAACATTTTGAGAAC      -350
AAAGATGACCATAACCACTGAAGGGAATCACATCTTTTAAGACAAATTCA      -400
TATTCTTTTATTTGTTATGGCAGATGACAAGATGGTACAACCTTTATTCT     -450
              <---primer 6--------

TTTCCAAAATAAAACAAAGGGCACAGCATCTGTAGTCAGCCGACAACTCT     -500
```

C

```
5'-
GGGATCACAGGTGTCAGCCATTGCACCCAGCCCAGATTGTCTTAATTTCT
                                                ---

ATCTTGTTCCAAGGCCAGGGACAGTAATAAGAATGGAAAAGAGATATGGG
-----primer 3--->

AACACTGGCAGACTGTGTAAAATGTAATGCAACTACCCAAAACAAGCCTG
GTAGGAAAGGGCAAGTCTTTAGGTCTTTGTAAGAACTAAAGAAGATCTGT
   <---primer 7--------

AATTTTTATTTTCACCCTCTGTACCCCATGACCTTATCCTTCCTCTCCTT
CCTTGTTACCCATGAAAAACTGGCAACATTCCAAGAATAGCATCTGTACA
AAGGGGAAAGAACATAAAGGTAAAACAAAACAAAACAACATTTTGAGAAC
AAAGATGACCATAACCACTGAAGGGAATCACATCTTTTAAGACAAATTCA
TATTCTTTTATTTGTTATGGCAGATGACAAGATGGTACAACCTTTATTCT
TTTCCAAAATAAAACAAAGGGCACAGCATCTGTAGTCAGCCGACAACTCT
```

D

```
5'-
GGGATCACAGGTGTCAGCCATTGCACCCAGCCCAGATTGTCTTAATTTCT
ATCTTGTTCCAAGGCCAGGGACAGTAATAAGAATGGAAAAGAGATATGGG
AACACTGGCAGACTGTGTAAAATGTAATGCAACTACCCAAAACAAGCCTG
                                 --------primer 8
GTAGGAAAGGGCAAGTCTTTAGGTCTTTGTAAGAACTAAAGAAGATCTGT
--->

AATTTTTATTTTCACCCTCTGTACCCCATGACCTTATCCTTCCTCTCCTT
CCTTGTTACCCATGAAAAACTGGCAACATTCCAAGAATAGCATCTGTACA
              <---primer 4--------

AAGGGGAAAGAACATAAAGGTAAAACAAAACAAAACAACATTTTGAGAAC
AAAGATGACCATAACCACTGAAGGGAATCACATCTTTTAAGACAAATTCA
TATTCTTTTATTTGTTATGGCAGATGACAAGATGGTACAACCTTTATTCT
TTTCCAAAATAAAACAAAGGGCACAGCATCTGTAGTCAGCCGACAACTCT
```

Figure 1 PCR amplified regions from the SCL gene 3'-UT region. (A) SCL 34, (B) SCL 56, (C) SCL 37, (D) SCL 48. Primer hybridization sites are indicated and the p53 DNA-binding CS is underlined and of bold type

activity (Table 3). The CS is in the (+) orientation relative to the promoter in both SCL 37+/T81luc and SCL 48+/T81luc, which suggests orientation could be important.

Trans-activation properties of an oligomeric SCL consensus sequence

To further test the ability of the SCL CS to function as a transcriptional enhancer, we synthesized an oligomer duplex corresponding to the SCL CS (Table 4) and ligated it upstream of the TK promoter in pT81luc at a position 92 bp from the TATA box (Figure 3). Transcriptional activation by one or three copies of the CS was assayed (Table 5). One copy exhibits no basal activity but shows approximately a 40-fold p53-mediated enhancer activity. Three copies have roughly threefold the activity of one copy. This suggests that the enhancer effect is additive in this range of copies and that p53 is not limiting in these transfections. It also suggests that the effect is CS orientation-independent since in SCL CS(3)/T81luc, two copies are in the (−) and one in the (+) orientation. More accurately, the transcriptional effect is clearly orientation-independent when the CS is present at a distance of 92 bp from the TATA.

At this point in our studies, it was clear that both distance from the TATA box and flanking sequences might influence SCL CS-mediated transcriptional enhancer activity. Consequently, we tested the ability of the SCL CS to function downstream of the chloramphenicol acetyltransferase (CAT) gene in a classic enhancer capacity. Specifically, SCL CS was ligated upstream (21 bp from the TATA box) in the HOCAT plasmid (Figure 4). This tests the ability of the

SCL CS to enhance activity from a minimal heme oxygenase (HO) promoter. The SCL CS induces approximately a 30-fold wild-type p53-mediated induction in CAT transcription from the SCL CS/HOCAT construct (Table 6). The SCL CS, however, does not stimulate p53-mediated transcriptional activation from the HO promoter when it is ligated 1.7 kb downstream of the CAT gene (HOCAT/SCL CS, Figure 4, Table 6).
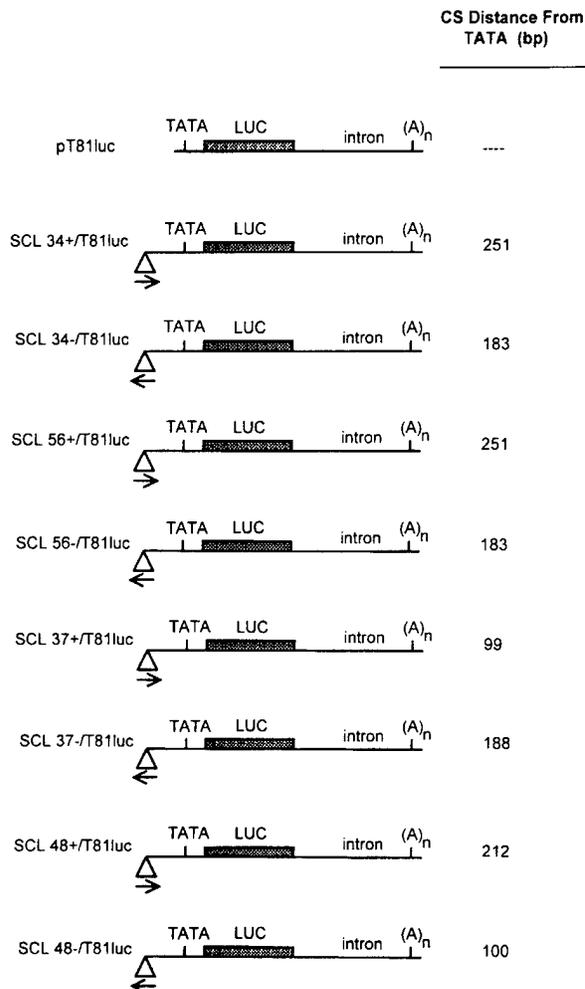
Trans-activation properties of an oligomeric PG consensus sequence

For comparison, we assayed two additional p53 DNA-binding CS homologies. Properties of the PG CS (Table 4), a synthetic oligomer first used by Vogelstein and colleagues (El-Deiry et al., 1992) to study p53 DNA-binding properties and later employed by Lane and associates (Hupp et al., 1992), were compared with those of the SCL CS. This PG sequence should not be confused with a different sequence also referred to as PG (Kern et al., 1992; Pietenpol et al., 1994) in which each copy contains a single p53-binding motif from the human nontranscribed ribosomal spacer region, previously shown to bind p53 (Kern et al., 1991). One copy or two copies of the PG CS were ligated upstream of the TK promoter in pT81luc (Figure 3) and transfected, with or without co-transfection of the wild-type p53 expression construct, into HCT 116 cells. Unlike the SCL CS, the PG CS demonstrates dramatic basal transcriptional activity in HCT 116 cells (Table 5). One copy of the PG CS enhances basal expression from the HSV-TK promoter approximately 50-fold and two copies have roughly twice the activity of one copy. p53 induction leads to an *additional* 7–10-fold increase in PG CS-mediated expression.

One copy of the PG CS was also ligated upstream and downstream of the CAT gene in the HOCAT plasmid (Figure 4). As in the pT81luc plasmid, the PG CS in PG/HOCAT induces a strong basal activity and a more modest inducible activity (Table 6). Therefore the trend is the same though the absolute values are not. PG CS induces approximately a 40-fold basal enhancer activity and a threefold *additional* p53-mediated activity when ligated upstream of the CAT gene (24 bp from the TATA box). It is noteworthy, therefore, that the PG CS, like the SCL CS, demonstrates similar trans-activation properties for both a minimal cellular promoter (heme oxygenase) and a viral promoter (HSV TK). The PG CS also

possesses basal and p53-inducible enhancer activity when ligated 1.7 kb downstream of the CAT gene in HOCAT (HOCAT/PG CS). One copy of the PG CS enhances basal transcriptional activity fivefold and wild-type p53-mediated transcription an additional 2.5-fold (Table 6).

In summary, the PG CS possesses enhancer activity when located at a distance from the promoter (classic enhancer activity) while the SCL CS is far more distance-restricted. For purposes of comparison, we also ligated the SV40 enhancer, perhaps the 'archetypal' enhancer, upstream of the heme oxygenase promoter in the HOCAT construct (SVE/HOCAT) and found it to enhance basal activity from the CAT gene 1600-fold (Table 7). Interestingly, the SV40 enhancer is minimally effective when ligated downstream of the HOCAT gene (HOCAT/SVE). This suggested to us that the SV40 enhancer might not, at a distance, strongly enhance transcription from a heterologous promoter. Therefore, we ligated the SV40 enhancer downstream of the CAT gene with the SV40 promoter upstream. In this construct, the SV40 enhancer augments transcription 25-fold. When located at a distance of > 1.7 kb from the promoter, the SV40 enhancer appears to augment transcription of the homologous promoter much more efficiently than a heterologous promoter. To our knowledge, this has not been previously reported and may represent a general feature of enhancers.

Trans-activation properties of an oligomeric WAF consensus sequence

A third synthetic oligomer, the WAF CS (Table 4), which corresponds to the p53 DNA-binding CS located 2.4 kb upstream of the WAF gene (El-Deiry *et al.*, 1993) was ligated upstream of the HSV TK promoter in the pT81luc plasmid (Figure 3). At an equivalent distance from the TATA box (92 bp), the WAF CS has basal and p53-inducible properties intermediate between those displayed by the PG and SCL CSs (Table 5). The WAF CS enhances basal activity 20-fold and wild-type p53-inducible activity 170-fold. In summary, for basal enhancer activity: PG CS > WAF CS > SCL CS.

The WAF CS was also ligated upstream and downstream of the CAT gene in the HOCAT plasmid (Figure 4). Again, in this context, the WAF CS demonstrates properties intermediate between those of the SCL CS and the PG CS (Table 6).

Effects of intermotif distance

We consider the basal:inducible activity ratio to be one of the most significant features of CS homology

	CS Distance From TATA (bp)

Figure 2 Reporter constructs used in transfections. LUC, luciferase cDNA; TATA, TATA box; Δ, inserted fragment; $(A)_n$, polyadenylation signal; CS, consensus sequence homology. Arrows indicate orientation of CS relative to the TATA box

Table 2 HCT 116 transfections[1] Fold-induction[2] of standardized luciferase values[3]

	pT81luc		SCL 34+/T81luc		SCL34-/T81luc		SCL 56+/T81luc		SCL 56-/T81luc	
p53	−	+	−	+	−	+	−	+	−	+
Exp. 1	1	3	2	5	1	3				
Exp. 2	1	3	2	5	1	2				
Exp. 3	1	3					2	3	3	4

[1]Each experimental value represents the mean of triplicate transfections rounded to the nearest whole number. [2]Fold-induction relative to pT81luc. [3]Luciferase values are standardized to a pRAScat internal control

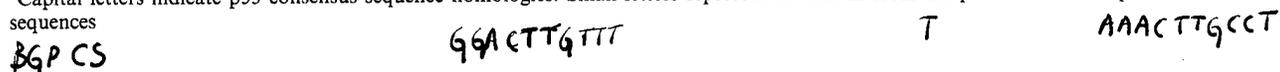**Table 3** HCT 116 transfections[1] Fold-induction[2] of standardized luciferase values[3]

	pT81luc		SCL 37+/T81luc		SCL37-/T81luc		SCL 48+/T81luc		SCL 48-/T81luc	
p53	−	+	−	+	−	+	−	+	−	+
Exp. 1	1	3	3	12	1	6				
Exp. 2	1	3	3	10	2	6				
Exp. 3	1	3					7	14	2	6
Exp. 4	1	3					8	15	2	5

[1]Each experimental value represents the mean of triplicate transfections rounded to the nearest whole number. [2]Fold-induction relative to pT81luc. [3]Luciferase values are standardized to a pRAScat internal control
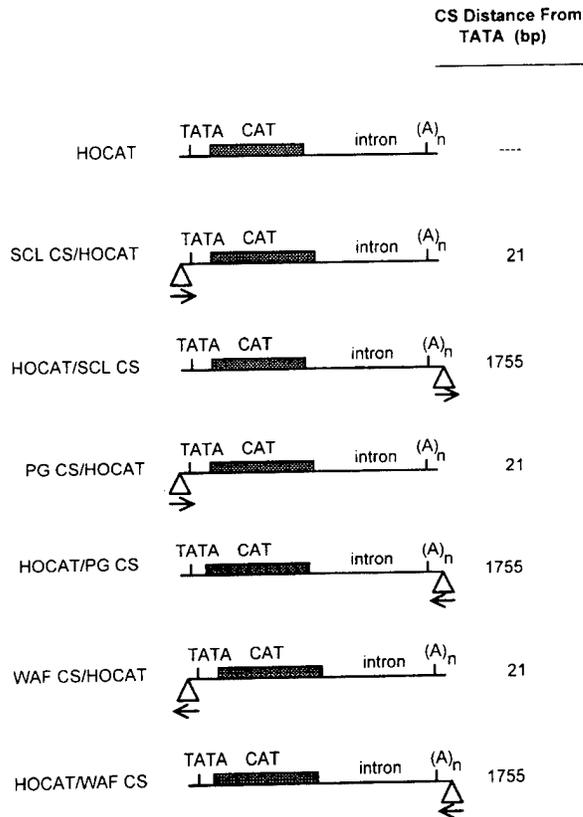
Table 4 p53 DNA-binding consensus sequence homologies[1]

	Motif 1	Inter-motif insert	Motif 2
WAF CS	GAACATGTCC	- - -	cAACATGTTg
PG CS	AGACATGCCT	- - -	AGACATGCCT
SCL CS	AAACAAGCCT	ggtaggaaa	GGGCAAGTCT
SCL CS $(N)_0$	AAACAAGCCT	- - -	GGGCAAGTCT
SCL CS $(N)_{13}$	AAACAAGCCT	ggtaggaaaacgt	GGGCAAGTCT
SCL CS $(N)_{17}$	AAACAAGCCT	ggtaggaaaacgtacgt	GGGCAAGTCT
SCL CS $(N)_{21}$	AAACAAGCCT	ggtaggaaaacgtacgtacgt	GGGCAAGTCT

[1]Capital letters indicate p53 consensus sequence homologies. Small letters represent deviations from the p53 consensus sequence or inter-motif sequences

Figure 3 Reporter constructs used in transfections. Abbreviations are as in Figure 2. Arrows and arrowheads indicate number and orientation of CS homologies

comparisons since it reflects the likelihood that a given CS homology will activate transcription under various cellular conditions. Our electrophoretic gel shift assays indicate that only wild-type or mutant p53 proteins bind *specifically* to the SCL CS, PG CS and WAF CS oligomeric duplexes (data not shown). In fact, there is no evidence to indicate that any proteins other than wild-type or mutant p53 proteins bind with specificity to any p53 DNA-binding CS homologies. This suggests that the basal activities conferred by the PG CS and WAF CS are due to mutant p53 interactions since HCT 116 cells are rich in mutant p53. Since the SCL CS confers no basal activity and the PG CS and WAF CS confer high basal activity upon downstream minimal promoters, we asked what structural features of the sequences might be responsible. One obvious feature is that the SCL CS possesses an inter-motif region of 9 bp (for purposes of this study, motif is RRRCWWGYYY). In contrast, the PG CS and WAF CS have no inter-motif inserts. In order to assess the effect of inter-motif distance upon basal and p53-inducible activities, we compared derivatives of the SCL CS which were modified only in the inter-motif region (Figure 3). Specifically, SCL CS$(N)_0$/T81luc has no inter-motif sequence. SCL CS$(N)_{13}$/T81luc, SCL CS$(N)_{17}$/T81luc, SCL CS$(N)_{21}$/T81luc possess inter-motif sequences of 13, 17 and 21 bp, respectively and reflect additions of multiples of the sequence 'AGCT' to the SCL CS inter-motif region. We find that length modifications of the inter-motif region, between 0 and 21 bp, substantially change the basal and p53-inducible activities in a disproportionate manner (Table 8, Figure 5). The SCL CS has no basal activity but displays a 43-fold p53-mediated induction. Removal of the inter-motif sequence results in a 16-fold basal activity but the p53-mediated induction is reduced from 40-fold to 10-fold. In this and other instances, the reduction in p53-mediated induction, that accompanys increased basal activity, may merely reflect cellular transcription limitations. An increase in the inter-motif region from 9 bp to 13 bp also results in an increase in basal

Table 5 HCT 116 transfections[1] Fold-induction[2] of standardized luciferase values[3]

	pT81luc		PG CS(1)/ T81luc		PG CS(2)/ T81luc		SCL CS(1)/ T81luc		SCL CS(3)/ T81luc		WAF CS(1)/ T81luc	
p53	−	+	−	+	−	+	−	+	−	+	−	+
Exp. 1	1	3	53	522	97	870						
Exp. 2	1	3	67	507	122	893						
Exp. 3	1	3					1	47	3	153		
Exp. 4	1	3					1	39	3	115		
Exp. 5	1	3									26	186
Exp. 6	1	3									20	159

[1]Each experimental value represents the mean of triplicate transfections rounded to the nearest whole number. [2]Fold-induction relative to pT81luc. [3]Luciferase values are standardized to a pRAScat internal control

CS Distance From TATA (bp)

HOCAT ----

SCL CS/HOCAT 21

HOCAT/SCL CS 1755

PG CS/HOCAT 21

HOCAT/PG CS 1755

WAF CS/HOCAT 21

HOCAT/WAF CS 1755

Figure 4 Reporter constructs used in transfections. Abbreviations are as in Figure 3. CAT, chloramphenicol acetyltransferase

activity (sevenfold) but, again, a reduction in p53-mediated induction to only 14-fold. An increase in the inter-motif region from 9 bp to 17 bp only slightly increases the basal activity and once again, results in a reduction in p53-mediated induction to only 10-fold. Finally, an increase in the inter-motif distance from 9 to 21 bp eliminates all basal activity and results in a 30-fold p53-inducible activity. Of the reporter constructs used in this study, the greatest p53-inducible activities are observed when the inter-motif distances are 9 bp and 21 bp (Figure 5). This trend is suggestive of the periodicity of α-helical DNA. The basal activity levels of SCL CS derivatives follow a very different trend. In fact, basal activity is lowest when the inter-motif distance is 9 bp or 21 bp.

The SCL CS and derivatives modified within the inter-motif region, were also tested for basal and p53-inducible activities in HJC cells (Table 9, Figure 6).

There are some differences between the activities of these sequences in HCT 116 and HJC cells, but the most striking features are conserved. In HJC cells, as in HCT 116 cells, SCL CS derivatives with inter-motif distances of 9 or 21 bp confer no basal activity upon minimal promoters while wild-type p53-inducible activities are greatest at these inter-motif distances. The primary differences in the activities displayed by the SCL CS derivatives in HCT 116 and HJC cells are (1) SCL(N)$_{17}$/T81luc displays less p53-inducible activity than SCL(N)$_{13}$/T81luc in HCT 116 cells and more p53-inducible activity than SCL(N)$_{13}$/T81luc in HJC cells and (2) SCL(N)$_{0}$/T81luc exhibits greater basal activity than SCL(N)$_{13}$/T81luc in HCT 116 cells and basal activity equal to that of SCL(N)$_{13}$/T81luc in HJC cells. These features may reflect specific characteristics of the mutant p53 proteins present in these two cell types.

Finally, the SCL CS and derivatives modified within the inter-motif region were tested for wild-type or mutant p53-inducible activities in p53-null Saos-2 cells (Table 10, Figure 7). Saos-2 cells are human osteosarcoma cells that do not produce detectable p53 because of a genomic deletion (Masuda et al., 1987; Diller et al., 1990; Deb et al., 1992). The mutant p53 expression plasmid used encodes a 141^{Cys}-to-141^{Tyr} transition and has been previously identified in human tumors (Nigro et al., 1989). Again, the most striking features of this study are conserved with those exhibited following HCT 116 and HJC cellular transfections. SCL CS derivatives with inter-motif distances of 9 or 21 bp confer no mutant p53-inducible activities upon minimal promoters while wild-type p53-inducible activities are greatest at these inter-motif distances.

Discussion

While our studies indicate that PAb240-immunoreactive p53 proteins present in both HCT 116 and HJC cells are transcriptionally active, these proteins have properties distinct from wild-type p53. This is illustrated by the fact that endogenous mutant p53 does not trans-activate the SCL CS but wild-type p53 trans-activates this sequence very strongly. These observations further suggest that the PAb240-immunoreactive p53 proteins endogenous to HCT 116 and HJC cells are not merely alternative (promoter) conformations (Milner, 1991; Rivas et al., 1992; Hainaut et al., 1994) of wild-type p53, rather are genetic mutants.

Despite many early studies which suggested that

Table 6 HCT 116 transfections[1] Fold-induction[2] of standardized CAT values[3]

	HOCAT		SCL CS/ HOCAT		HOCAT/ SCL CS		PG CS/ HOCAT		HOCAT/ PG CS		WAF CS/ HOCAT		HOCAT/ WAF CS	
p53	–	+	–	+	–	+	–	+	–	+	–	+	–	+
Exp. 1	1	3	2	62	2	2								
Exp. 2	1	3	2	63	1	4								
Exp. 3	1	3					38	138	5	13				
Exp. 4	1	3					48	140	5	12				
Exp. 5	1	3									9	125	1	5
Exp. 6	1	3									12	144	1	3

[1]Each experimental value represents the mean of triplicate transfections rounded to the nearest whole number. [2]Fold-induction relative to pT81luc. [3]CAT values are standardized to a pRASluc internal control

Table 7 HCT 116 transfections[1] Fold-induction[2] of standardized CAT values[3]

	HOCAT		SVE/HOCAT		HOCAT/SVE		SVP/CAT		SVP/CAT/SVE	
p53	–	+	–	+	–	+	–	+	–	+
Exp. 1	1	3	1617	1523	5	4				
Exp. 2	1	3	1798	2030	4	5				
Exp. 3							1	3	32	25
Exp. 4							1	3	29	22

[1]Each experimental value represents the mean of triplicate transfections rounded to the nearest whole number. [2]Fold-induction relative to pT81luc. [3]CAT values are standardized to a pRASluc internal control

Table 8 HCT 116 transfections[1] Fold-induction[2] of standardized luciferase values[3]

	pT81luc		SCL CS(1)/ T81luc		SCL CS(N)0/ T81luc		SCL CS(N)13/ T81luc		SCL CS(N)17/ T81luc		SCL CS(N)21/ T81luc	
p53	–	+	–	+	–	+	–	+	–	+	–	+
Exp. 1	1	3	1	47								
Exp. 2	1	3	1	39								
Exp. 3	1	3					7	80	4	35		
Exp. 4	1	3					6	104	3	35		
Exp. 5	1	3			18	171					1	27
Exp. 6	1	3			15	173					1	36

[1]Each experimental value represents the mean of triplicate transfections rounded to the nearest whole number. [2]Fold-induction relative to pT81luc. [3]Luciferase values are standardized to a pRAScat internal control
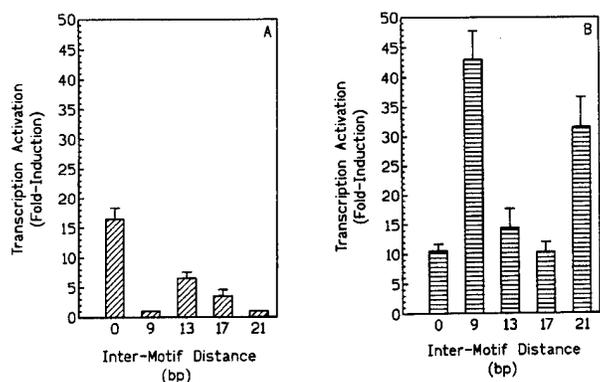
Figure 5 (A) Basal and (B) p53-inducible transcription activation, in HCT 116 cells, of SCL CS derivatives possessing inter-motif regions of varying lengths

mutant p53 proteins were unable to bind to DNA and activate transcription (El-Deiry et al., 1992; Farmer et al., 1992; Kern et al., 1992; Scharer and Iggo, 1992), recent reports argue that some mutant p53 proteins retain trans-activation properties (Fields and Jang, 1990; Unger et al., 1992; Chen et al., 1993; Chumakov et al., 1993; Zhang et al., 1993a,b; Park et al., 1994). Park and associates have shown that four of five cell

lines with homozygous p53 mutations at codon 273 (273[His]), contain p53 which has the ability to bind to p53 DNA-binding sequences and trans-activate. Furthermore, Soussi and colleagues have recently reported that several mutants at positions 175, 248 and 273 display wild-type activity, suggesting that the presence of a mutation is not strictly correlated with protein inactivation in tumors (Ory et al., 1994). In a recent study, Pietenpol and colleagues (1994) noted, upon co-transfection of plasmids encoding wild-type or mutant p53 proteins with plasmids encoding various p53 binding site-regulated reporter genes, that synthetic sequences are more likely to be trans-activated by wild-type and mutant p53 than are genomic sequences. They further demonstrated that binding site copy number and precise sequence may modify relative affinity of the artificial sites for wild-type and mutant p53 proteins. Using expression constructs encoding mutants 143[Ala], 175[His], 248[Trp] and 273[His], they showed that none of three genomic fragments containing p53 DNA-binding CSs were significantly trans-activated by these mutant p53 proteins. Various configurations of tested synthetic sequences, in contrast, were trans-activated by mutant p53 to a degree dependent on the precise sequence and copy number. Consistent with their report, we find that the synthetic PG sequence is highly activated in two cell lines possessing abundant mutant p53. In further

Table 9 HJC cells transfections[1] Fold-induction[2] of standardized luciferase values[3]

	pT81luc		$SCL\ CS(1)/$ $T81luc$		$SCL\ CS(N)_0/$ $T81luc$		$SCL\ CS(N)_{13}/$ $T81luc$		$SCL\ CS(N)_{17}/$ $T81luc$		$SCL\ CS(N)_{21}/$ $T81luc$	
p53	−	+	−	+	−	+	−	+	−	+	−	+
Exp. 1	1	3	1	52								
Exp. 2	1	3	1	58								
Exp. 3	1	3					11	102	4	100		
Exp. 4	1	3					8	95	5	117		
Exp. 5	1	3			8	112					1	50
Exp. 6	1	3			10	120					1	45

[1]Each experimental value represents the mean of triplicate transfections rounded to the nearest whole number. [2]Fold-induction relative to pT81luc. [3]Luciferase values are standardized to a pRAScat internal control
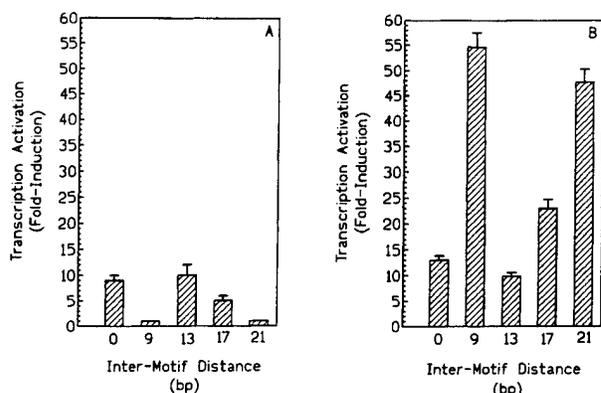
Figure 6 (A) Basal and (B) p53-inducible transcription activation, in HJC cells, of SCL CS derivatives possessing inter-motif regions of varying lengths

agreement with their findings, the genomic SCL sequence is not activated by mutant p53 proteins present in either of these cell lines or by mutant 141[Tyr] following controlled co-transfections. However, the genomic WAF sequence is trans-activated by mutant p53, though to a lesser extent than is the PG CS. One explanation for this observation is that HCT 116 and HJC cells might each possess p53 mutations with properties different than those studied by Pietenpol and associates. Alternatively, some genomic p53 DNA-binding CSs (including the WAF CS) may respond to both mutant and wild-type p53 proteins or, indeed, to mutant p53 proteins preferentially.

Our studies further indicate that the potential of p53 DNA-binding CS homologies to modify transcription from nearby minimal promoters can be stringently distance dependent and that these distance restraints may be modified by the CS homology flanking regions.

We have shown that the SCL CS exhibits similar, but not identical behaviour, when ligated 92 bp upstream of the HSV-TK promoter in SCL CS(1)/ T81luc or 24 bp upstream of the heme oxygenase promoter in SCL CS/HOCAT. Therefore, within certain distance constraints, this CS homology can similarly augment transcription from a viral or cellular promoter.

We explored the effect of inter-motif distance upon SCL CS activity. The greatest wild-type p53-inducible activities are observed when the inter-motif distances are 9 bp (wild-type SCL CS) and 21 bp. Since one complete turn of helical B DNA is represented by 10.5 bp, 9 bp places the two motifs of the p53 DNA-

binding CS homology in close proximity on one side of the helix. A 21 bp inter-motif insert places the two motifs directly adjacent on the same face of the helix. These results suggest that the interacting wild-type p53 complex functions with greatest efficiency when the two motifs are on the same face of the DNA helix. The basal activities associated with the SCL CS and its derivatives follow a very different trend. In fact, the basal activities are lowest when the inter-motif distances are 9 bp or 21 bp. One possibility consistent with this data is that mutant p53 binds poorly to stereospecifically aligned motifs yet binds well to and stimulates transcription from out-of-phase motifs (0, 13 and 17 bp inter-motif inserts). Alternatively, an endogenous cellular protein other than mutant p53 might bind to and stimulate transcription from misaligned motifs. The fact that our electrophoretic mobility shift assays demonstrate that only a single protein from the HCT 116 and HJC extracts binds to the PG, WAF and SCL CSs and that these bands can be supershifted by PAb421 (data not shown), suggests that the former is more likely. While the latter is a formal possibility, to our collective knowledge, there is no evidence that any proteins other than wild-type or mutant p53 bind to the PG CS or any other p53 DNA-binding CS homologies.

The observation that the inter-motif spacing within the SCL CS and consequently, helical positioning of the motifs, is related to the transcriptional functionality, is reminiscent of other repeated protein-binding sites in DNA. Most well known of these are the λ repressor sites (Hochschild and Ptashne, 1986), the SV40 early promoter elements (Takahashi et al., 1986) and the elements of the E. coli arabinose operon (Dunn et al., 1984). Each of these systems possess multiple elements whose members interact co-operatively when positioned on the same side of the helix.

Our data suggest that the p53 DNA-binding CS homology inter-motif distance may stereospecifically modify DNA transcription augmentation by modifying the ability of p53 to interact with the palindrome. As of yet, however, we have no data regarding the importance of stereospecific alignment of the CS and the TATA box. Our experiments were not methodically designed to test that parameter. However, an examination of the data that we do have (analysis not presented) does not support such a model.

Several comments are now in order regarding the limitation of these investigations. The majority of these studies were conducted in HCT 116 and HJC cells, cell lines rich in mutant p53. However, a corroborating experiment was performed in p53-null cells, which

Table 10 SAOS-2 116 transfections[1] Fold-induction[2] of standardized luciferase values[3]

	pT81luc		SCL CS(1)/ T81luc		SCL CS(N)0/ T81luc		SCL CS(N)13/ T81luc		SCL CS(N)17/ T81luc		SCL CS(N)21/ T81luc	
p53	–	+	–	+	–	+	–	+	–	+	–	+
Exp. 1	1	3	1	28								
Exp. 2	1	3	1	32								
Exp. 3	1	3					5	45	4	30		
Exp. 4	1	3					4	40	5	35		
Exp. 5	1	3			9	120					1	15
Exp. 6	1	3			11	128					1	18

[1]Each experimental value represents the mean of triplicate transfections rounded to the nearest whole number. [2]Fold-induction relative to pT81luc. [3]Luciferase values are standardized to a pRAScat internal control
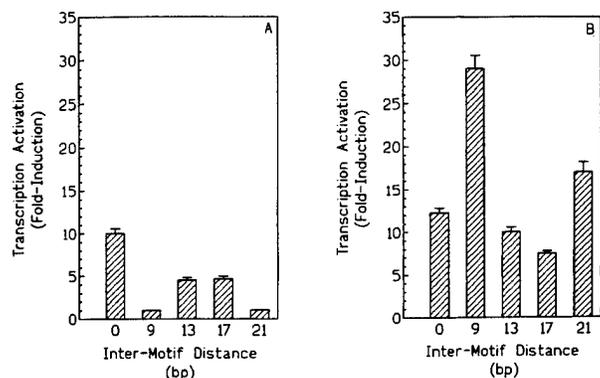
Figure 7 (**A**) Mutant and (**B**) p53-inducible transcription activation, in Saos-2 cells, of SCL CS derivatives possessing inter-motif regions of varying lengths

demonstrates the same pattern of trans-activation of SCL CS derivatives by mutant and wild-type p53 as that observed in HCT 116 cells. In order to further corroborate our hypotheses, assays should be performed folowing co-transfections of reporter constructs possessing the spectrum of SCL CS derivatives with expression constructs encoding *various* mutant p53 proteins (possessing variable properties).

Furthermore, we should comment on the significance of the p53 DNA-binding CS in the 3′-UT region of the SCL gene. The SCL gene was discovered because of its involvement in a chromosomal translocation associated with the occurrence of stem cell leukemia manifesting myeloid and lymphoid differentiation capabilities (Begley *et al.*, 1989; Aplan *et al.*, 1990). In these leukemic cells, an aberrant fusion mRNA is transcribed which differs in the 3′-UT region from the wild-type SCL cDNA. Despite the fact that the SCL coding sequence is preserved intact, the quantitative expression of the altered mRNA is increased over that of the wild-type allele. Kirsch and colleagues speculated that this gene might be relevant to the interesting multipotential phenotype of this leukemic cell line. For this reason, our identification of a p53 DNA-binding CS within the 3′-UT region of the SCL gene and the possibility that this gene might be regulated by p53, is intriguing. Our investigations to date suggest that (1) the sequences that flank the p53 DNA-binding CS within the SCL 3′-UT region may actually silence the trans-activation potential of the CS homology and/or (2) that the trans-activation potential of the SCL CS is severely distance constrained.

However, we have not yet tested the SCL CS in more extensive contexts of the SCL gene or together with the SCL promoter.

Materials and methods

Mutant p53 ELISAs

Intracellular pAb240-immunoreactive mutant p53 levels were determined using the p53 mutant selective quantitative ELISA from Oncogene Science Inc. (Manhasset NY) with their protocol. Extract preparations were also performed according to the recommendations of Oncogene Science.

Cells and culture conditions

HCT 116 (ATCC CCL 247) and Saos-2 (ATCC HTB-85) cells were maintained in McCoy's 5a medium (Irvine Scientific, Santa Ana CA) with 10% fetal bovine serum (FBS, Irvine Scientific) or 15% FBS, respectively. The HJC cells (HJC15, clone 8) were a gift of Dr Richard Frisque (Pennsylvania State University, Walker *et al.*, 1973) and were maintained in DMEM (Gibco/BRL, Grand Island NY) with 10% FBS. HeLa cells (ATCC CCL 2 were maintained in EMEM (Gibco/BRL) with 10% FBS. p53-Null cells (secondary fibroblasts) obtained from a homozygous p53-null mouse (GenPharm Intn., Mountain View CA) skin explant, were maintained in DMEM, high glucose with 25% FBS. All cells were maintained at 37°C in 5% CO_2.

PCR amplifications and vector constructions

PCR primers were synthesized on a Milligen 8750 DNA synthesizer using phosphoramidite chemistry by LSUMC Core Laboratories (New Orleans). Fragment SCL34 was generated by PCR amplification of the sequence, within the SCL 3′-UT region, which possesses the p53 DNA-binding CS, using primers 3 (5′-TCTATCTTGTTCCAAGGCCA-3′) and 4 (5′-TCTTGGAATGTTGCCAGTTT-3′). Fragment SCL 56 was generated by PCR amplification of a separate region within the SCL 3′-UT region using primer 5 (5′-TACCCCATGACCTTATCCTT-3′) and primer 6 (5′-CCATCTTGTCATCTGCCATA-3′). Fragments SCL 37 and SCL 48 were generated using PCR primers 3 and 7 (5′-CTAAAGACTTGCCCTTTCCT-3′) and 4 and 8 (5′-ACCCAAAACAAGCCTGGTAG-3′), respectively. PCR amplifications were performed using clone 2117 (a gift of Dr Ilan Kirsch, NCI, Bethesda MD, Begley *et al.*, 1989; Aplan *et al.*, 1990) as a template. Clone 2117 possesses the entire 3′-UT region of the SCL gene. The resulting PCR products were ligated into the pCR II TA cloning vector

(Invitrogen Corp., San Diego CA) and subsequently recloned into reporter constructs. All clones were sequenced in order to confirm the integrity and orientation of the PCR products.

Wild-type p53 was expressed from plasmid pSVL (Pharmacia Biotech, Piscataway NJ), in which expression is regulated by the SV40 late promoter. Mutant 141^{Tyr} was generated from wild-type p53 using the Transformer Kit from Clontech (Palo Alto CA) according to their recommendations and sequenced to confirm mutagenesis.

Oligomer ligations and vector constructions

Plasmid SVPCAT (Alam and Zhining, 1992) contains the SV40 early gene promoter upstream of the *E. coli* chloramphenicol acetyltransferase (CAT) reporter gene. Plasmid HOCAT (Alam and Zhining, 1992) possesses the CAT gene under control of the minimal mouse heme oxygenase-1 gene promoter (residues −33 to +73). Plasmid pT81luc (Nordeen, 1988) contains the Herpes simplex virus thymidine kinase gene minimal promoter upstream of the firefly luciferase gene. The luciferase expression vector, pRASluc and the CAT expression vector pRAScat (Barbee *et al.*, 1993), which were used as internal controls in these experiments, possess the human Harvey *ras* proto-oncogene promoter upstream of the luciferase and CAT genes, respectively. This promoter is not regulated by p53 (Chin *et al.*, 1992).

For SCL, WAF and PG oligomeric clones, complementary oligonucleotides were synthesized with *Hind*III extensions, annealed and cloned into the *Hind*III site of pT81luc upstream of the TK gene promoter. The same double-stranded oligonucleotides were blunt-end repaired and cloned into the *Spe*I (blunted) site of HOCAT upstream of the HO-1 promoter or cloned into the *Xho*I (blunted) site of HOCAT downstream of the CAT gene. The 216 bp *Pvu*II/*Nco*I fragment from plasmid pSV2cat containing the SV40 early gene enhancer, was blunted and cloned upstream of the HO-1 promoter or downstream of the CAT gene in plasmid HOCAT as described above to generate plasmids SVE/HOCAT and HOCAT/SVE, respectively. Plasmid SVP/CAT/SVE was constructed in a manner analogous to HOCAT/SVE. All constructs were sequenced to confirm oligomer or DNA insert fragment copy number and orientation.

Transfections

Cells were plated in 60 mm diameter tissue culture dishes at 10^6 cells per dish and permitted to attach overnight. The following day, cells were transfected with various combinations of: experimental reporter gene construct, 1.7 µg per dish; p53 expression construct, 5 µg per dish; internal control, 0.25 µg per dish. Internal controls, either pRASluc or pRAScat, depending upon the experimental reporter construct, were included in all transfections. DNAs were transfected using lipofectin (Gibco/BRL, Grand Island NY) at 30 µg per dish and Opti-MEM I low serum medium (Gibco/BRL) for an overnight incubation. Cells were harvested 48 h after the start of the transfection period and the extracts were assayed for luciferase and CAT expression.

In order to optimize transfection efficiency, lipofectamine (Gibco/BRL) was used instead of lipofectin for Saos-2 cells. Optimum transfection efficiency was obtained using 10 µl of lipofectamine per 60 mm dish.

Transfection Assays

Cells were harvested from 60 mm dishes and washed twice with PBS. Cells were resuspended in 40 µl of TM (10 mM Tris pH 7.5, 4 mM MgCl$_2$) containing 0.1% PMSF. After resuspension, an additional 40 µl of TT (20 mM Tris pH 7.5, 0.2% Triton X-100) was added. Luciferase assays were performed in duplicate using 25µl of plate lysate, by the method of Brasier *et al.* (1989). Relative light units (RLUs) of luciferase activity were determined using a Monolight 2010 luminometer (Analytical Luminescence Laboratories, San Diego CA). Purified luciferase and luciferin were also obtained from Analytical Luminescence Laboratories. The assay background level was determined by combining all components except cell extract. In order to compensate for variation in transfection efficiency, all luciferase values were standardized using CAT internal control values. Following luciferase assay, the remainder of each cell extract was heated to 60°C for 10 min and immediately placed on ice for 1 min. CAT levels were determined by incorporation of [³H]acetate into [³H]acetyl chloramphenicol (Nordeen *et al.*, 1987). Samples were counted for 0.3 min per sample using a Beckman LS 5000CE scintillation counter. In order to compensate for variations in transfection efficiencies, all experimental CAT values were standardized using luciferase internal control values.

In order to optimize transfection assays of Saos-2 cells, which transfect with lower efficiency than HCT 116 or HJC cells, the Luciferase Assay System with Coenzyme A (Promega Corp., Madison WI) was employed.

References

Alam J and Zhining D. (1992). *J. Biol. Chem.*, **267**, 21894−21900.

Aplan PD, *et al.* (1990). *Mol. Cell. Biol.*, **10**, 6426−6435.

Barbee RW, *et al.* (1993). *Biochem. Biophys. Res. Comm.*, **190**, 70−78.

Begley CG, *et al.* (1989). *Proc. Natl. Acad. Sci. USA*, **86**, 10128−10132.

Brasier AR, Tate JE and Habener JF. (1989). *BioTechniques*, **7**, 1116−1122.

Chen JY, *et al.* (1993). *Oncogene*, **8**, 2159−2166.

Chin K-V, Ueda K, Pastan I and Gottesman MM. (1992). *Science*, **255**, 459−462.

Chumakov AM, Miller CW, Chen DL and Koeffler HP. (1993). *Oncogene*, **8**, 3005−3011.

Deb S, Jackson CT, Subler MA and Martin DW. (1992). *J. Virol.*, **66**, 6164−6170.

Deb SP, *et al.* (1994). *Oncogene*, **9**, 1341−1349.

Diller L, *et al.* (1990). *Mol. Cell. Biol.*, **10**, 5772−5781.

Donehower LA, *et al.* (1992). *Nature*, **356**, 215−221.

Dunn TM, Hahn S, Ogden S and Schleif RF. (1984). *Proc. Natl. Acad. Sci. USA*, **81**, 5017−5020.

El-Deiry WS, *et al.* (1992). *Nature Genetics*, **1**, 45−49.

El-Deiry WS, *et al.* (1993). *Cell*, **75**, 817−825.

Farmer G, *et al.* (1992). *Nature*, **358**, 83−86.

Fields S and Jang SK. (1990). *Science*, **249**, 1046−1049.

Funk WD, *et al.* (1992). *Mol. Cell. Biol.*, **12**, 2866−2871.

Ginsberg D, Mechta F, Yaniv M and Oren M. (1991). *Proc. Natl. Acad. Sci. USA*, **88**, 9979−9983.

Hainaut P, Hall A and Milner J. (1994). *Oncogene*, **9**, 299−303.

Halazonetis TD and Kandil AN. (1993). *EMBO J.*, **12**, 5057−5064.

Harper JW, et al. (1993). Cell, 75, 805–816.

Hochschild A and Ptashne M. (1986). Cell, 44, 681–687.

Hollstein M, Sidransky D, Vogelstein B and Harris CC. (1991). Science, 253, 49–53.

Hupp TR, Meek DW, Midgley CA and Lane DP. (1992). Cell, 71, 875–886.

Kastan MB, et al. (1992). Cell, 71, 587–597.

Kern SE, et al. (1991). Science, 252, 1708–1711.

Kern SE, et al. (1992). Science, 256, 827–830.

Masuda J, et al. (1987). Proc. Natl. Acad. Sci. USA, 84, 7716–7719.

Milner J. (1991). Proc. R. Soc. Lond., 245, 139–145.

Miyashita T, Harigai M, Hanada M and Reed JC. (1994). Cancer Res., 54, 3131–3135.

Nigro JM, et al. (1989). Nature, 342, 705–708.

Nordeen SK. (1988). BioTechniques, 6, 454–457.

Nordeen SK, Green III PP and Fowlkes DM. (1987). DNA, 6, 173–178.

Ory K, Legros Y, Auguin C and Soussi T. (1994). EMBO J., 13, 3496–3504.

Park DJ, et al. (1994). Oncogene, 9, 1899–1906.

Pietenpol JA, et al. (1994). Proc. Natl. Acad. Sci. USA, 91, 1998–2002.

Rivas CI, et al. (1992). Blood, 79, 1982–1986.

Santhanam U, Ray A and Sehgal PB. (1991). Proc. Natl. Acad. Sci. USA, 88, 7605–7609.

Schärer E and Iggo R. (1992). Nucleic Acids Res., 20, 1539–1545.

Smith ML, et al. (1994). Science, 266, 1376–1380.

Takahashi K, et al. (1986). Nature, 319, 121–126.

Ueba T, et al. (1994). Proc. Natl. Acad. Sci. USA, 91, 9009–9013.

Unger T, Nau MM, Segal S and Minna JD. (1992). EMBO J., 11, 1383–1390.

Vogelstein B and Kinzler KW. (1992). Cell, 70, 523–526.

Walker DL, et al. (1973). Science, 181, 674–676.

Weintraub H, Hauschka S and Tapscott SJ. (1991). Proc. Natl. Acad. Sci. USA, 88, 4570–4571.

Zhang W, et al. (1993a). Oncogene, 8, 2555–2559.

Zhang W, Shay JW and Deisseroth A. (1993b). Cancer Res., 53, 4772–4775.

PATHOPHYSIOLOGICAL EVENTS TRIGGERED DURING LIGHT-INDUCED DAMAGE TO THE RETINA

INTRODUCTION

The present grant period has proved very productive. The following information is novel and does not represent previously published data. The main, critical point is that, while studying a series of events triggered by bright light and leading to photoreceptor cell death (apoptosis), we have found a point within this sequence that can be targeted by an experimental drug to reduce photoreceptor cell damage.

Exposure to intense illumination damages photoreceptor cells, triggering a sequence of events that, ultimately, causes cell death (Rapp 1995). As this progresses, sight is impaired, with blindness eventually resulting. Such intense light can exist naturally: sand, snow, and water have very high reflectance, and prolonged exposure will produce retinal damage and possibly blindness. In addition, accidental exposure to nearby explosions and laser-based technology can produce severe retinal damage, both acute and long-term.

Generally, a sequence of events precedes cell death, with the initial insult triggering the activation of immediate early genes. Activation of transcription factor(s) allows the formation and release of the mRNAs coding for cyclooxygenases. These enzymes permit the metabolism of arachidonic acid to form the precursor for prostaglandins.

Several forms of cyclooxygenase exist in cells. COX-1, the constituitive cyclooxygenase, appears to be present at all times, and is used as a standard by

which to compare the amounts of the inducible form, COX-2. COX-2, however, is normally absent, or present only in very low quantities, unless the cells have undergone some form of trauma; soon after the stimulus, COX-2 is induced and tissue levels increase sharply (Breder et al., 1992, 1995). COX-2, therefore, can serve as an indicator of the degree of stress associated with a particular stimulus and a specific cell type.

Analysis of tissues for cell damage and loss will reveal the extent to which light treatment affects the retina. Apoptosis is the process of programmed cell death whereby specific endonucleases induce DNA fragmentation (White, 1996). The study of the processes leading up to this form of cell death has become extremely important since specific genes have now been characterized that trigger and regulate the initiation, timing, and extent of apoptosis. New, very sensitive techniques are now available to label the fragmented DNA within apoptotic nuclei in tissue sections, and, when used in retina in conjunction with light treatment, can demonstrate which photoreceptor cells have undergone irreversible trauma.

We have monitored this pathway in retina, following the administration of 2 hours of damaging light, to determine the degree of retinal damage. Also, we have demonstrated the time course for the induction of COX-2, retinal photoreceptor apoptosis, and photoreceptor cell loss. Additionally, we have administered an inhibitor (BN-50730) of platelet activating factor (PAF) prior to light exposure, and have observed a reduced amount of damage. Analysis has been by Western blotting and immunohistochemistry. We present the results of

this exciting study in this report.

We have monitored this pathway in retina, following the administration of 2 hours of damaging light, to determine the degree of retinal damage. We have also demonstrated the time course for the induction of COX-2, retinal photoreceptor apoptosis, and photoreceptor cell loss. Additionally, we have administered an inhibitor (BN-50730) of platelet activating factor (PAF) prior to light exposure and have observed a reduced amount of damage. Analysis has been by Western blotting and immunohistochemistry. We present the results of this exciting study in this report.

METHODS

General protocol.

Young, male albino rats (150 g) were dark adapted overnight and then placed within a 10"-high white plastic bin. Measures were taken to isolate each of the animals to prevent stacking and shielding of the eyes. Animals were then subjected to 2 hours of white fluorescent light and then placed in a darkened cabinet for up to 8 days (Remè et al., 1995; Szczesny et al., 1995). At the appropriate times, they were killed and the eyes collected. Some animals were injected intravitreally with the PAF inhibitor BN-50730 or the carrier solution alone, DMSO. A complete parallel set of animals was maintained in darkness.

General description of the photostimulator.

A bank of 6 fluorescent lights (33 Watts each, 24" long, G.E. cool white) situated above supplied 7000 lux at the bottom of the bin. The bin, in turn, was placed within a 21° C incubator with an inside fan to maintain a constant, cool temperature.

General histological procedures.

It has been shown previously that under these stimulus conditions (i.e., light presented from above in a normally posturing animal), the inferior-temporal quadrant of the retina demonstrates the first response to intense illumination. Additionally, time studies show that, while the damage can begin to spread toward

the superior-nasal quadrant, little or no structural damage is apparent there, even after 8 days. Therefore, when retinas were collected, the superior-nasal quadrant was always used in comparison with the damaged inferior-temporal quadrant.

After the eyes were obtained, fronts were removed and an eyecup formed. These were cut in half diagonally through the optic nerve to bisect the inferior-temporal (light damaged) region. Each half was placed in fixative and prepared for histological sectioning. At other times, retina were cut into 4 quadrants; the superior-nasal and the inferior temporal quarters were saved and the others discarded. Quadrants formed in this manner were used for Western blot analysis.

Retinal tissue samples to be studied immunohistochemically for the presence of COX-1 and COX-2, and tissue to be used for analysis of photoreceptor cell death by apoptosis, were placed in cold 4% formaldehyde in PBS for 3 days. They were then dehydrated through ethanol, embedded in paraffin, and sectioned at 10 μm thickness. Sections were dryed onto subbed slides prior to immunohistochemical reactions.

Samples intended for structural analysis were fixed in 2% glutaraldehyde and 2% formaldehyde, and post fixed in 1% OsO_4. Sodium cacodylate buffer (0.135 M, pH 7.3) was used throughout fixation. Dehydration through ethanol and acetone, embedding in Epon-Araldite epoxy, and sectioning at 1 μm thickness followed. After drying onto glass slides, sections were contrasted with 1% toluidine blue.

Apoptosis.

The evaluation of DNA fragmentation and apoptotic cell death was achieved by analysis of TUNEL stained sections. The Promega G-3250 Apoptosis Detection Kit was utilized as specified by directions contained within. Nuclei containing labeled DNA fragments appeared as bright yellow-green globes after fluorescein tagging. All other nuclei appeared red following a general background stain with propidium iodide (Sigma).

Immunohistochemical localization of retinal COX-1 and COX-2.

Sections were deparaffinized and brought to water through an ethanol series, then fixed in ether, treated to block endogenous peroxidases, and then blocked with BSA and normal goat serum. Avidin D followed by biotin were blocked by specific kit (Vector). Incubation with primary antibodies to COX-1 (rabbit, anti-COX-1) and COX-2 (rabbit, anti-COX-2) was followed by treatments with biotinylated goat anti-rabbit IgG H+L (Vector), and then with the ABC-Elite-HRP reagent (Vector). DAB (Vector) was finally reacted with the complex to form a brown reaction product.

Western blot analysis.

Retinal quadrants were collected and homogenized, and then treated with protease inhibitors. After protein concentration and addition of bromphenol blue, samples were loaded onto an SDS-polyacrylamide gel and electrophoresed.

Transfer was made to nitrocellulose membranes, which were then soaked in buffer. Next, membranes were incubated with primary antibody (mouse anti-COX-1 or mouse anti-COX-2), washed, and then treated with secondary antibody (goat anti-mouse or goat anti-rabbit IgG-conjugated alkalin phosphatase), followed by equilibration in buffer, and incubation in assay buffer (Western-light Tropix). Finally, membranes were exposed to x-ray film or a phosphor-imaging plate.

Time course of COX-2 induction.

At 0, 3, 6, 12, 24, and 48 hours after the initial 2 hours of light treatment, inferior-temporal retinal quadrants and superior-nasal quadrants were collected and prepared for Western blot analysis. These were compared with dark controls and BN-52730-injected retinas.

RESULTS

Photoreceptor cell dropout - background information.

We have previously shown in long term studies that light damaged regions of the retina exhibit photoreceptor cell dropout. By 4 days post stimulus, as many as 50-70% of the photoreceptors have died and been removed, leaving a much thinner inferior-temporal retina (Figure 1). Throughout our histological evaluation of control, damaged, and treated retinas, we have compared the light-sensitive inferior-temporal region with the less affected superior-nasal region. This technique, coupled with time courses and the 12 hour COX and 24 hour apoptosis analysis, has allowed us to monitor the protective effects of the PAF inhibitor, BN-50730.

Time course of COX-2 induction.

The amount of COX-2 induced in retinal quadrants by light treatment was compared with amounts of the constituitive COX-1 in the same regions (COX-2/COX-1). The superior-nasal quadrant demonstrated a slow increase in COX-2 induction, with a slight peak at 12 hours post-treatment at a ratio of about 0.2, but continued to slowly rise through 48 hours. The inferior-temporal quadrant, however, peaked at 12 hours with a ratio of 0.5, and then began to slowly decline (Figure 2).

Immunohistochemical localization of COX-1 and COX-2.

Following 2 hours of light stimulation plus 12 hours of darkness, retinas were prepared for immunohistochemistry. Within regions where light damage had been induced, antibodies to COX-2 accumulated within the photoreceptor inner segment as a dense brown band (Figure 3). However, the noninducible (constituative) COX-1 was present under both conditions. In both cases, a light background reaction was apparent, but the dense brown immunoreaction appeared only in photoreceptors and at the base of the retina near the vitreal interface (figure 4).

In experiments where some retinas were pretreated with BN-50730 by intravitreal injection just prior to light treatment, only untreated retinas could be light damaged. When COX-2 (PGHS-2) was compared with COX-1 (PGHS-1) (COX-2/COX-1) by Western blot analysis in these untreated retinas, only the lower quadrants showed an increased ratio (from about 0.5 in control lower and upper quadrants to about 1.5 in light-treated lower quadrants) (Figure 5). Pretreatment with BN-50730 produced a constant ratio of COX-2/COX-1; no increase in COX-2 was observed under these conditions.

Time course of DNA fragmentation.

Early in this project it was learned that the peak of cell death occurred 24-30 hours following the 2 hour light stimulus. This was demonstrated in two ways. Detection of fragmented DNA was determined by the use of an ELISA assay,

scanning at 405 nm, over a time course. Fragmented DNA peaked at 30 hours post stimulation (Figure 6). Also, over the same time course, nuclei were isolated from exposed retinas and the DNA obtained. This was run on a gel along with DNA fragment standards to demonstrate DNA laddering. The most intense laddering was seen at plus 24-30 hours.

Immunohistochemical visualization of apoptosis by TUNEL.

Rats were subjected to 2 hours of light followed by 24 hours in darkness, and retinal tissues were then prepared for visualization of nicked DNA by the TUNEL protocol. In inferior-temporal regions, where light damage had occurred, labeled nuclei appeared (Figures 7 and 8). These nuclei first took on a ringed appearance as the induced endonucleases first contacted the outer edges of the nucleus (Figure 9), but with time, labeled nuclei became globe-like in their brilliance. At the edges of the light damaged regions, nicked DNA-labeled nuclei declined sharply in numbers until no fluorescence could be observed at the edges of the retina (Figure 10), whereas, at the periphery on the same sections, no damaged nuclei were found (Figure 11). When animals had been placed in darkness and not stimulated, only occasionally were labeled photoreceptor nuclei observed within the retina (Figure 12).

DISCUSSION

To summarize:

<u>Light treatment</u>:

Overhead, white fluorescent light triggers photoreceptor cell death within the inferior-temporal retinal quadrant in normally posturing animals.

<u>8-12 hours after light treatment</u>:

Within 8-12 hours COX-2 has been induced and reaches maximum expression within retina, while COX-1 remains constant.

COX-1 is concentrated within photoreceptor cell inner segments following light damage plus 12 hours, and in dark controls.

COX-2 is concentrated within photoreceptor cell inner segments following light damage plus 12 hours, but not in dark controls.

Pretreatment with the PAF inhibitor BN-50730 abolishes the light damaging effect, and no COX-2 induction occurs.

<u>24 hours after light treatment</u>:

Precise boarders delimit the region of light damage and are apparent within the tissue sections.

TUNEL labeling of apoptotic nuclei peaks at 24 hours post-treatment. This peak occurs 12 hours after COX-2 light induction.

BN-50730-pretreated eyes show reduced levels of TUNEL labeling.

<u>48 hours after light treatment</u>:

The maximum rate of cell loss occurs 24 hours after COX-2 peaks within

42

the light treated retina.

4 days after light treatment:

Photoreceptor cell dropout reaches 50-70%.

BN-50730-pretreated eyes show reduced levels of photoreceptor cell dropout.

To conclude:

Light triggers the induction of COX-2 (+12 hours), followed by initiation and peaking of apoptosis (+24 hours), and photoreceptor cell dropout (greater than 60% by +8 days). Pretreatment with the PAF antagonist BN-50730 prevents the induction of COX-2, as well as supressing apoptosis and photoreceptor cell loss. Thus, the occurrance of COX-2 is linked with PAF activity in retinas undergoing photoreceptor cell loss by light damage.

REFERENCES

Breder CD, DeWitt D, Kraig RP 1995 Characterization of inducible cyclooxygenase in rat brain. J Comp Neurol 355:296-315.

Rapp LM 1995 Retinal phototoxicity. In: Handbook of Neurotoxicology. (Chang LW, Dyer RS eds) Marcel Dekker: New York. Pp 963-1003.

Szczesny PJ, Munz K, Remé CE 1995 Light damage in the rat retina: Patterns of acute lesions and recovery. In: New Strategies in Prevention and Therapy (Schmidt K ed); from: Cell and Tissue Protection in Ophthalmology (Pleyer U, Schmidt K, Thiel H-J eds) Hippokrates Verlag: Stuttgart. Pp 163-175.

Remé CE, Weller M, Szczesny P, Munz K, Hafezi F, Reinboth J-J, Clausen M 1995 Light-induced apoptosis in the rat retina in vivo: Morphological features, threshold and time course. In: Degenerative Diseases of the Retina. (Anderson RE, LaVail MM, Hollyfield JG eds) Plenum: New York. Pp 19-25.

White E 1996 Life, death, and the pursuit of apoptosis. Genes & Dev 10:1-15.

LIST OF FIGURES

Figure 11
TUNEL analysis with fluorescein tag for photoreceptor apoptotic nuclei outside the light damaged region of the retina.

Figure 12
TUNEL analysis with fluorescein tag for photoreceptor apoptotic nuclei within a dark treated control retina.

Figure 1

Photoreceptor cell loss following 2 hours of light treatment. The upper graph compares the number of photoreceptor nuclei within the upper quadrant control region with those in the lower quadrant light damaged region in typical light damaged retinas. Notice that by 4 days post-treatment only about 30% of photoreceptors remain. Microscopy reveals most of these to be cone photorecepter nuclei. The lower graph demonstrates the survival ratio of the lower quadrant damaged (d) region to the upper quadrant control (c) area (open circles). A plot of the change in survival ratio is represented by the closed circles. The highest rate of nuclei loss occurs at day 2 post-treatment, indicating that apoptosis had to have occured 24 hours previously (at light treatment plus 24 hours).
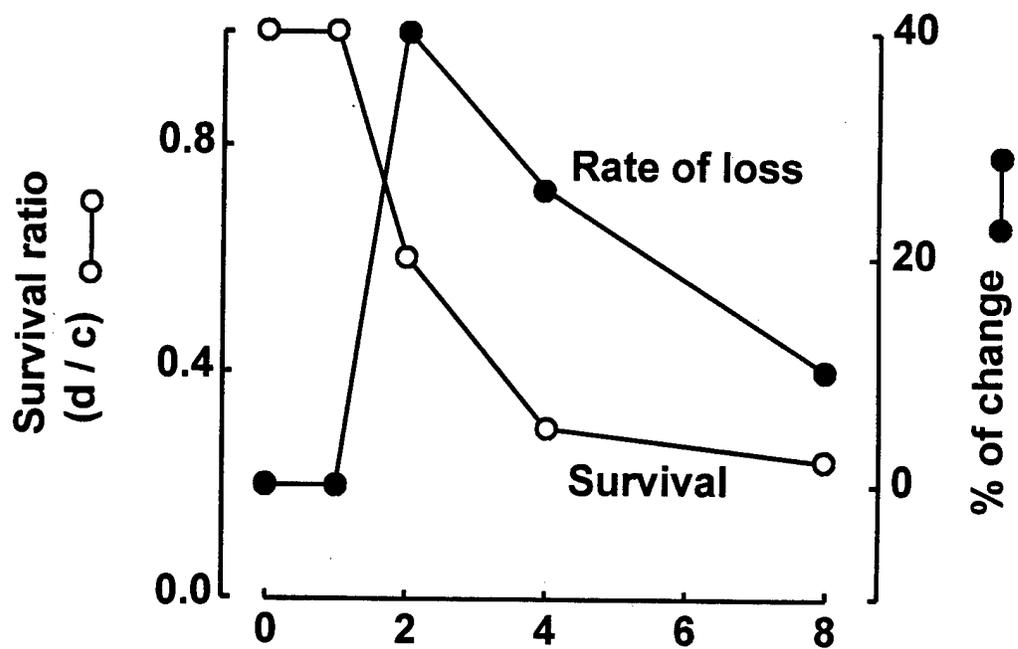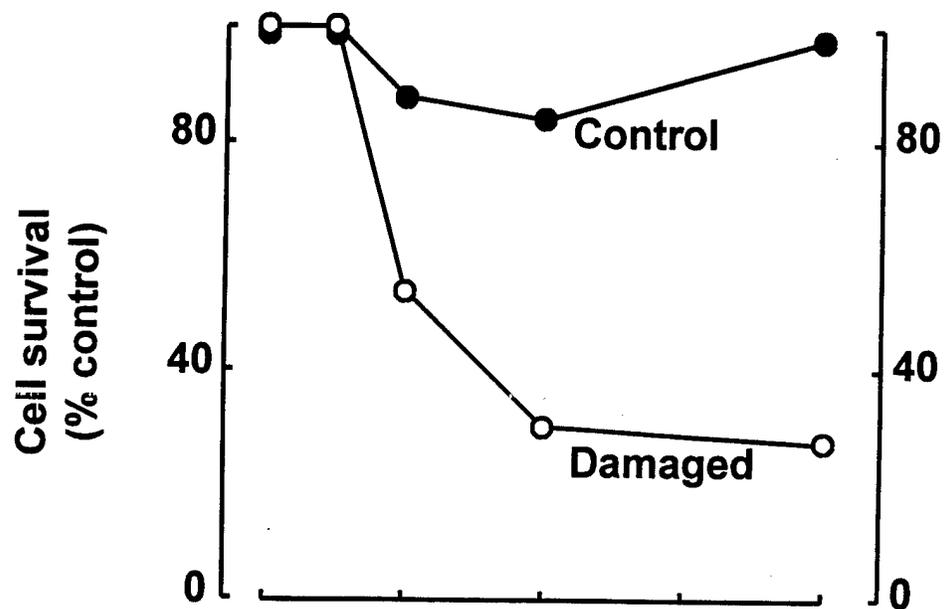
Figure 2
A time course comparing COX-2 induction within upper and lower quadrants of the rat retina following light treatment. Western blot analysis of 8 animals in two separate experiments demonstrates only a slight rise in the upper control quadrant, while the lower light damaged quadrant had a peak of COX-2 induction after 12 hours, followed by a slight, slow decline. This indicates that COX-2 induction precedes the peak of apoptosis by about 12 hours.

UPPER QUADRANT OF THE RETINA

HOURS AFTER LIGHT DAMAGE
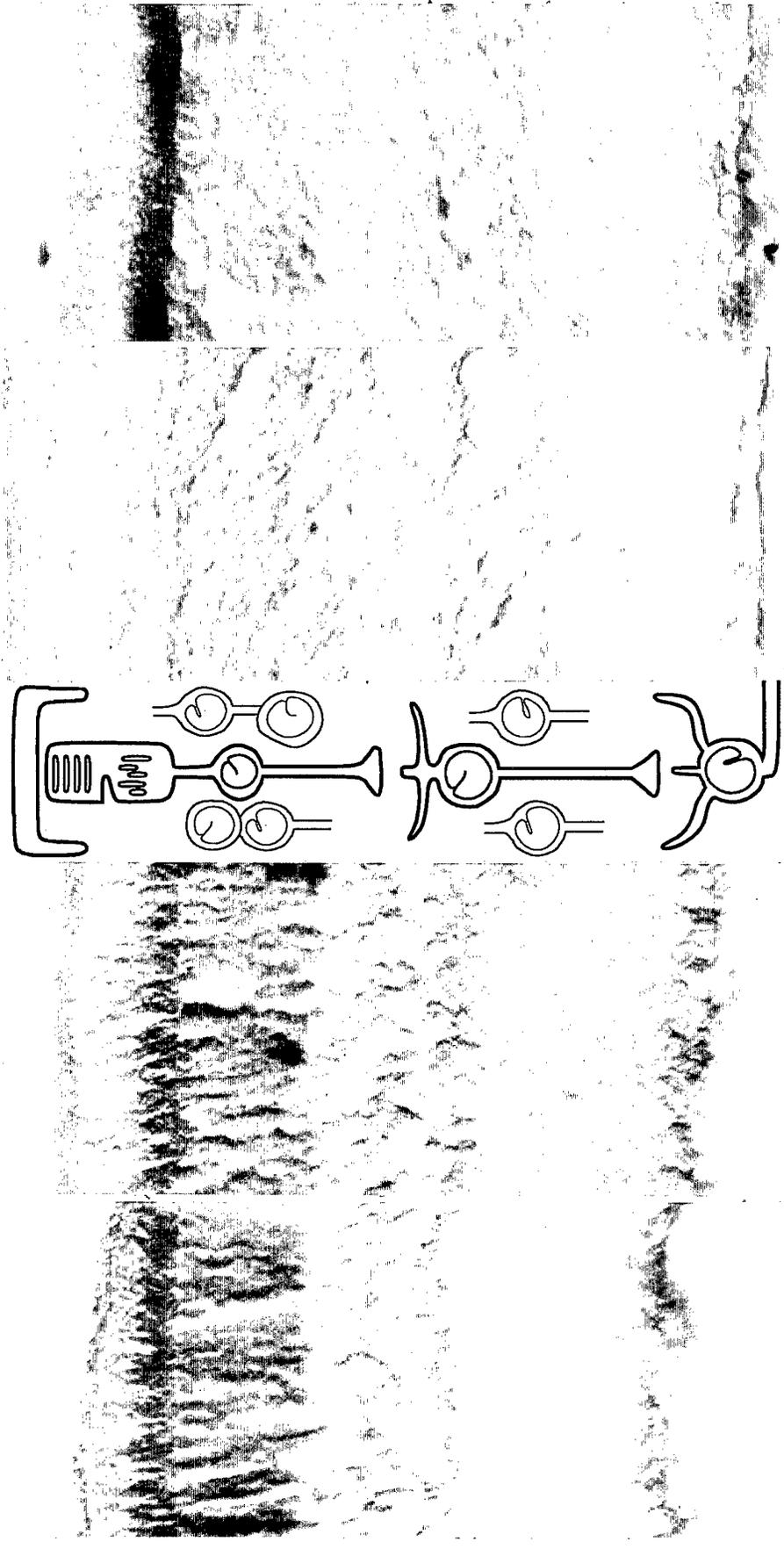
LOWER QUADRANT OF THE RETINA

HOURS AFTER LIGHT DAMAGE
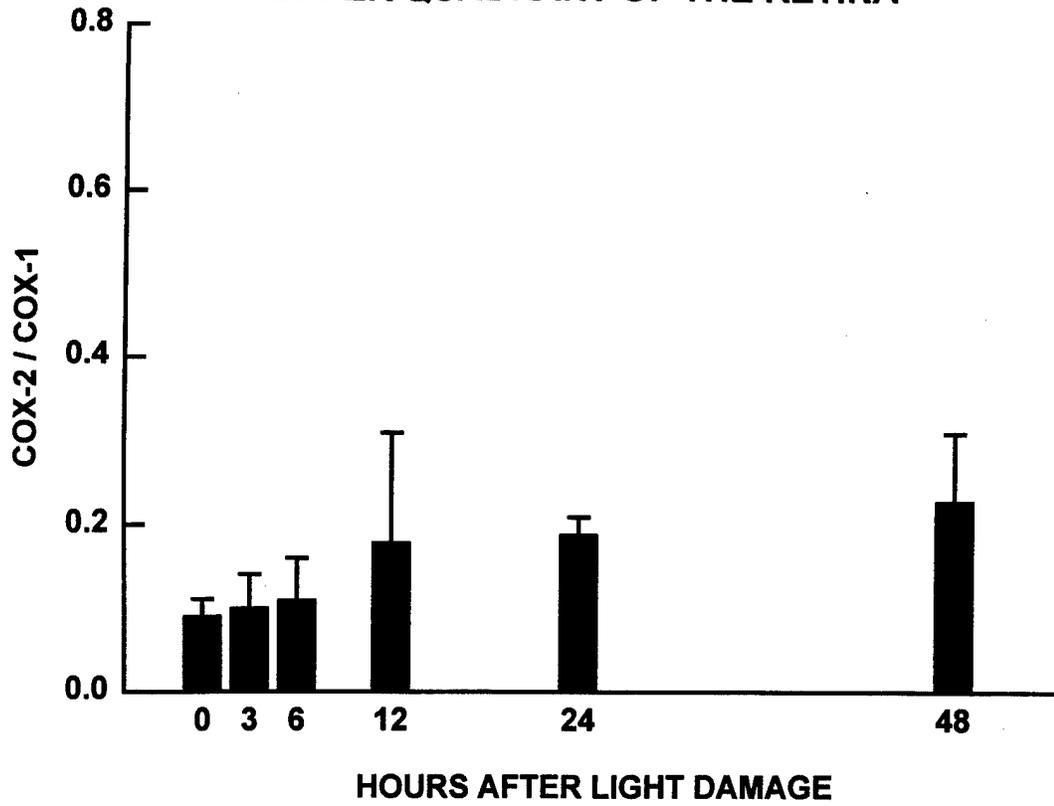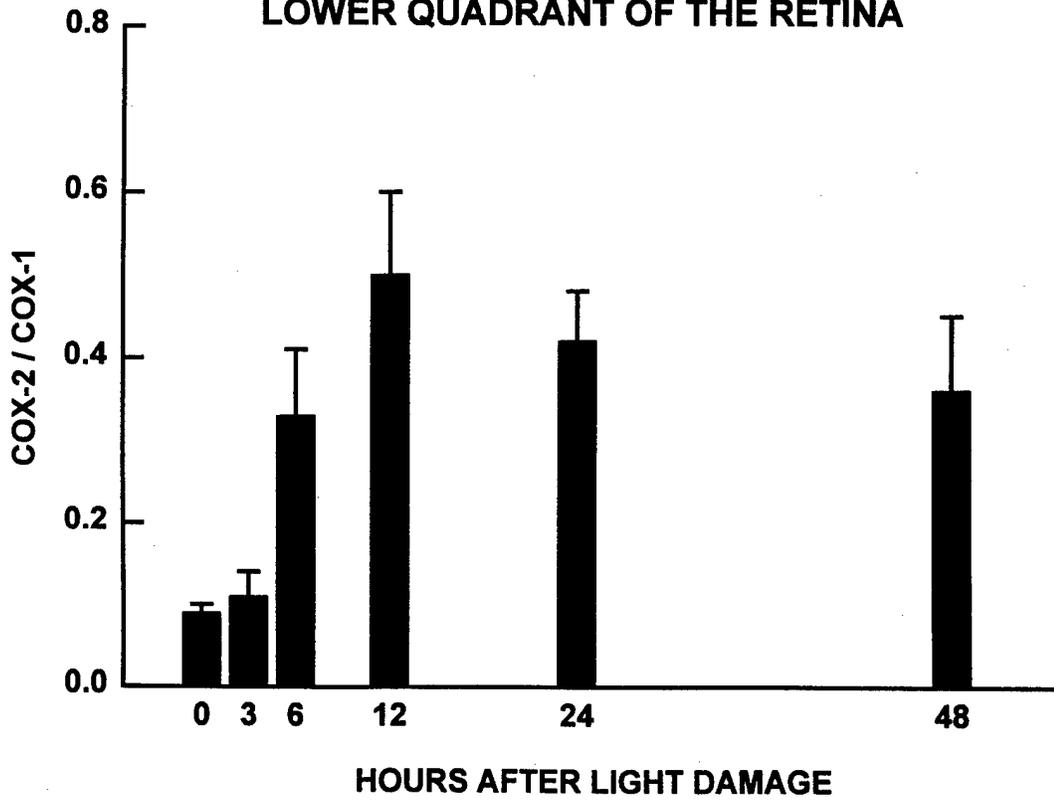
Figure 3

Immunohistochemistry of rat retina demonstrating the localization of antibodies to COX-1 and COX-2 within the inner segments of photoreceptor cells under dark and light conditions. The central figure illustrates the layers of the retina and some of the cell types associated with each. Photoreceptors, located at the top, accumulate antibody reaction product within the inner segment. COX-1 is present but does not increase, while COX-2 is very low or absent in dark controls, but accumulates within 12 hours following light treatment. Notice also, a similar labeling pattern at the base of the retina near the retina-vitreous interface.

LIGHT-INDUCED ROD PHOTORECEPTOR CELL APOPTOSIS

COX-2
LIGHT DAMAGE

DARK

COX-1
LIGHT DAMAGE

DARK

Figure 4
Immunohistochemistry of photoreceptors demonstrating the localization of antibodies to COX-1 and COX-2 within the inner segments of photoreceptor cells under dark and light conditions. These sections are from the same tissue shown in Figure 3, but have been magnified to better illustrate the inner segment labeling patterns. In these albino animals, the small "lumps" probably represent mitochondria.
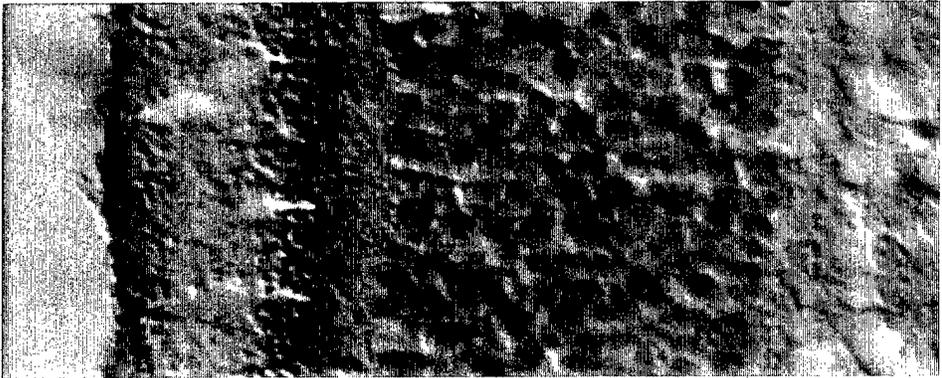
LIGHT-INDUCED ROD PHOTORECEPTOR CELL APOPTOSIS

COX-1
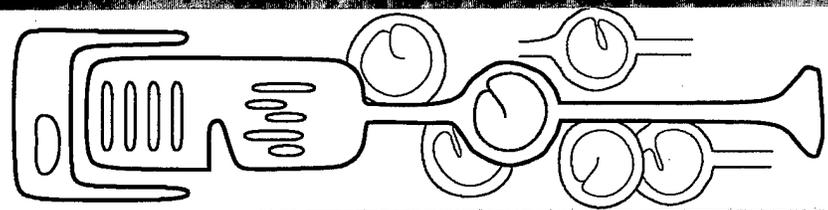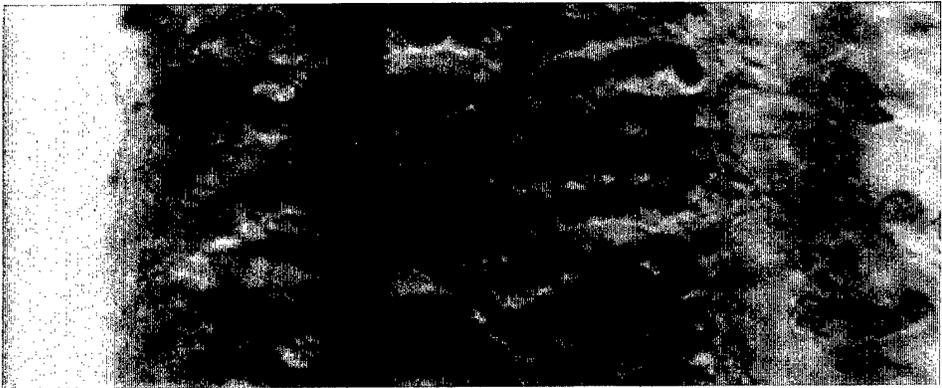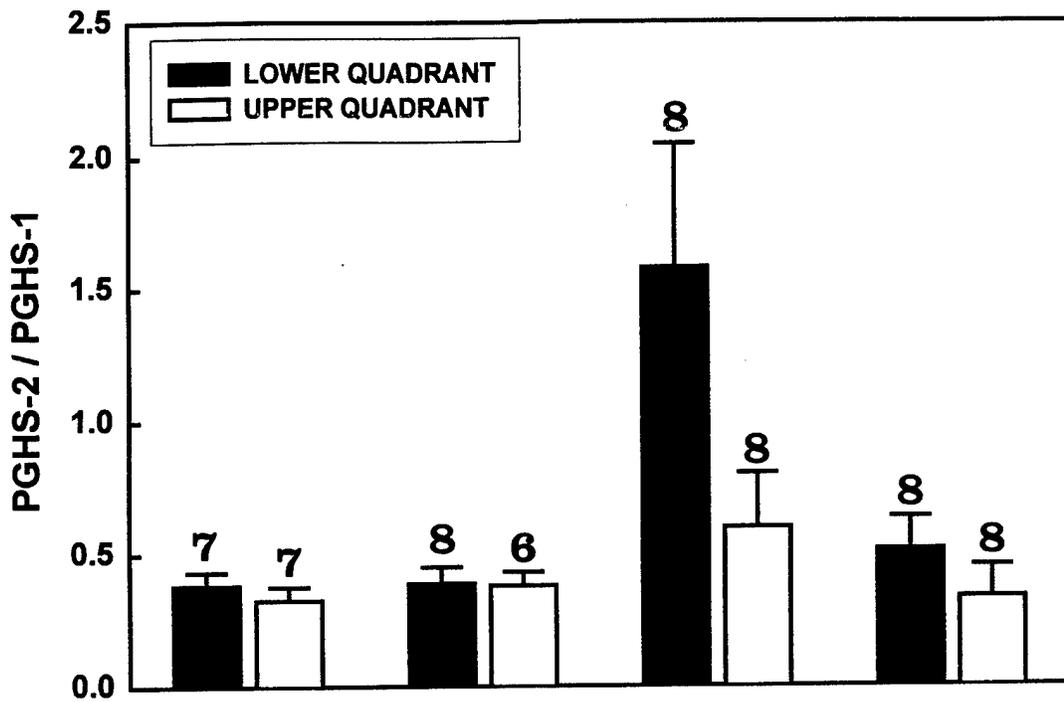DARK   LIGHT DAMAGE
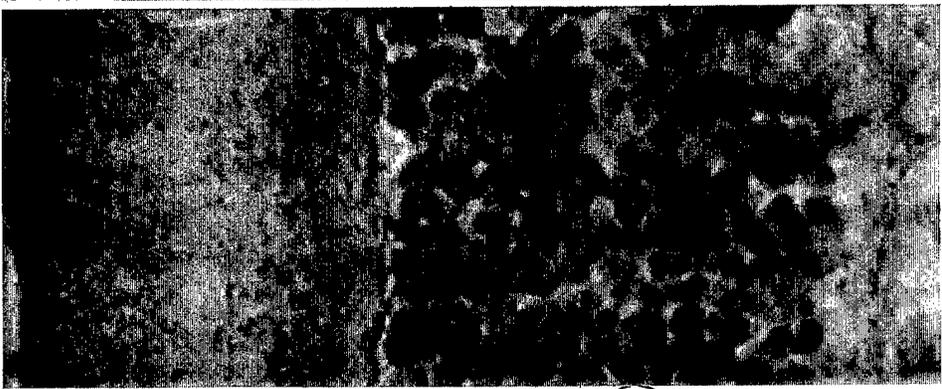
COX-2
DARK   LIGHT DAMAGE

Figure 5

The regional effects of light treatment on COX-2/COX-1 relative protein levels within the rat retina in control, light treated, and BN-50730 treated animals. Under all conditions, upper quadrant control regions remain constant, while light treatment induces COX-2 accumulation. However, pretreatment with the PAF inhibitor BN-50730 prevents the induction of COX-2 in the light treated quadrants. The numbers above each bar represent the number of animals examined by Western blot analysis at each point. Retinas from each animal were run separately. This is the average of two separate experiments.

REGIONAL EFFECT OF LIGHT DAMAGE ON PGHS-2 / PGHS-1 RELATIVE PROTEIN LEVELS IN THE RAT RETINA

Figure 6
Assay for retinal DNA fragmentation following 2 hours of light treatment. Analysis of retinal sample absorbances (405 nm) show an increase in fragmentation after light damage, peaking at about 30 hours. This suggests a peak in nuclei damage that could be from apoptotic processes.
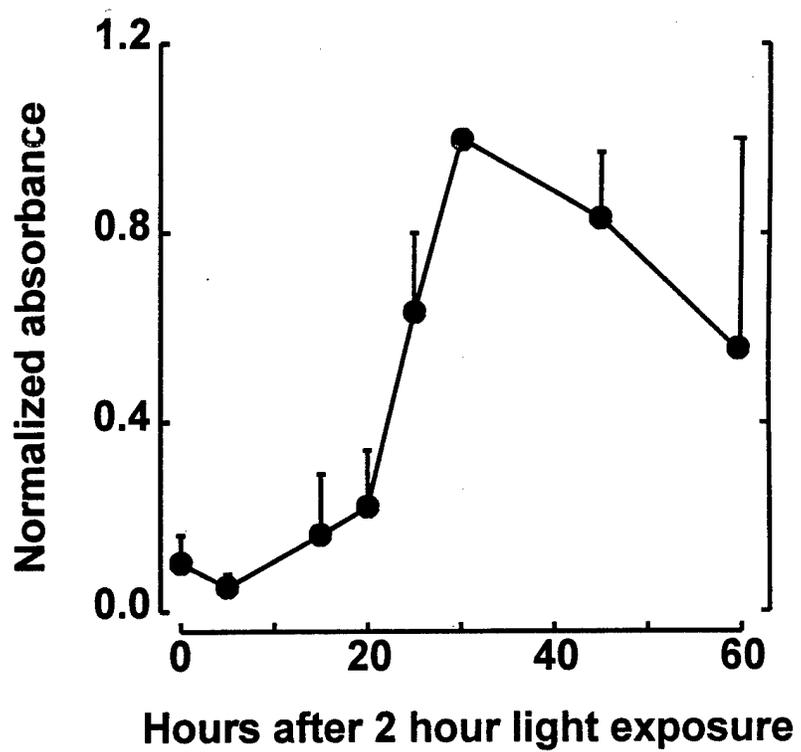
Hours after 2 hour light exposure

Figure 7
TUNEL analysis with fluorescein tag for photoreceptor apoptotic nuclei within the light damaged region of the retina. The yellow globes are labeled apoptotic photoreceptor nuclei. Hollow spheres are probably more recently damaged, while the small points are probably the oldest damaged nuclei that have already begun the process of nuclear and cell blebbing. Tissue was taken 24 hours after light treatment.
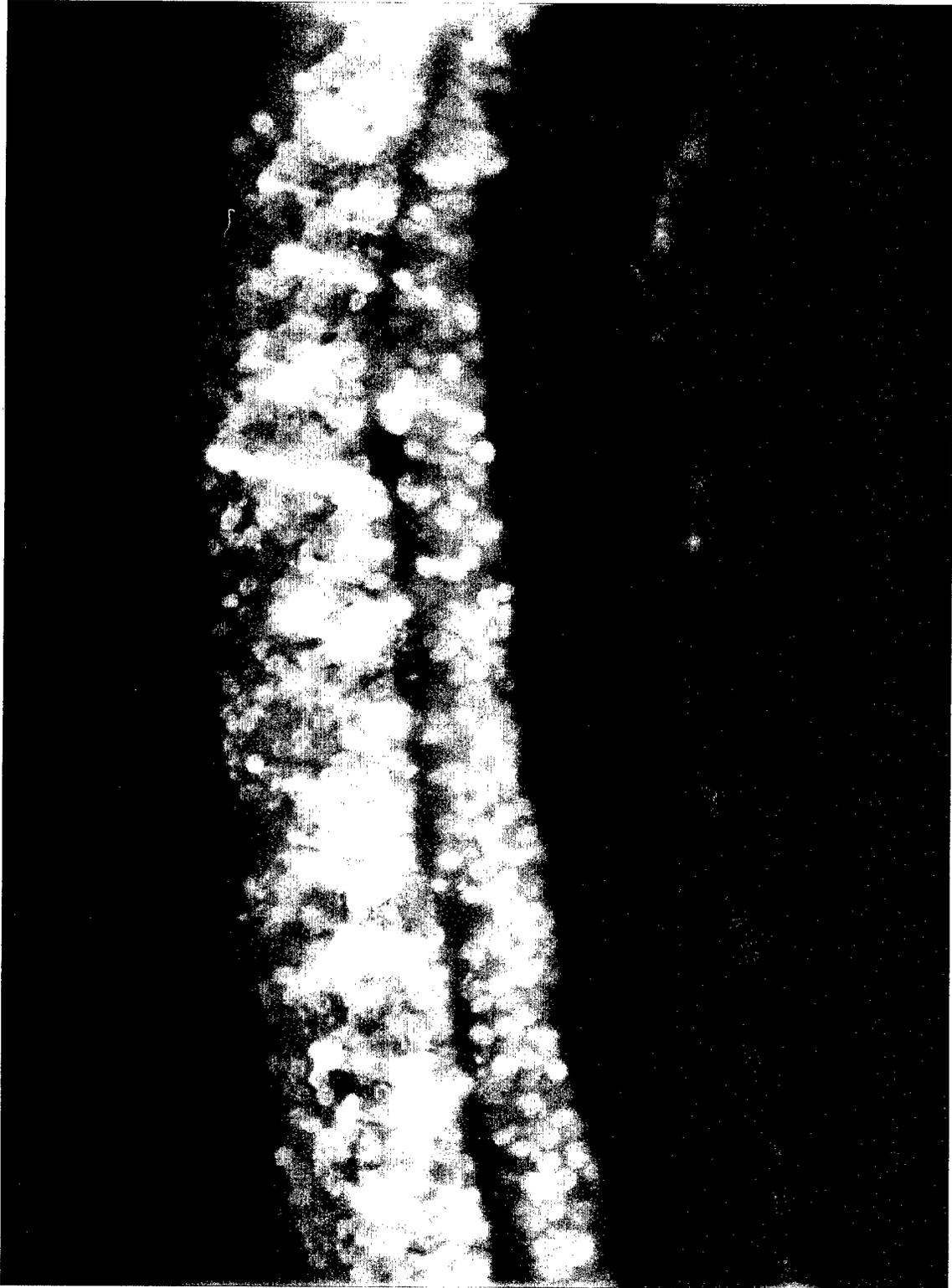
Figure 8
TUNEL analysis with fluorescein tag for photoreceptor apoptotic nuclei within the light damaged region of the retina. This is another section similar to Figure 7 demonstrating similar results.
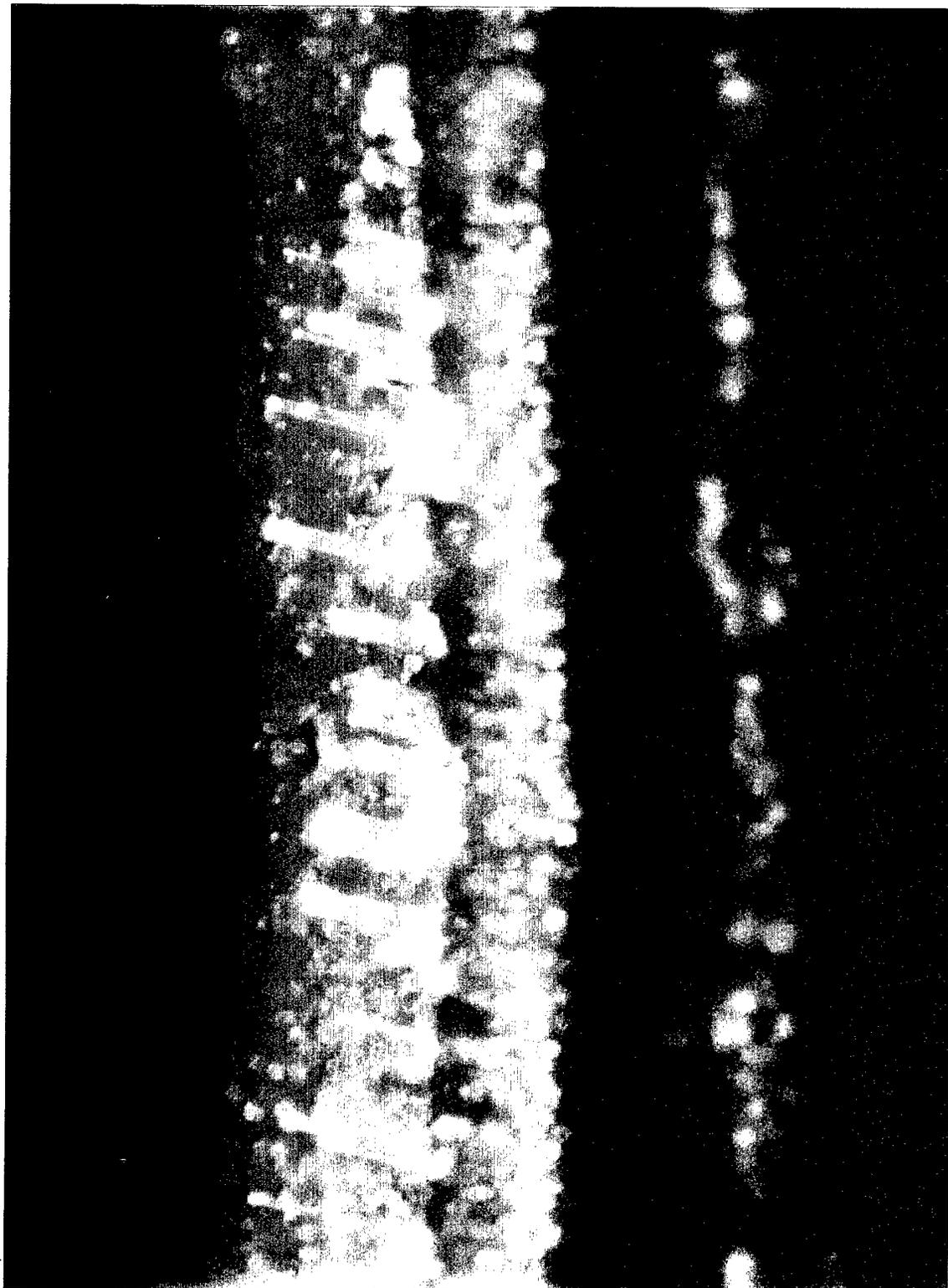
Figure 9
Higher magnification of TUNEL analysis with fluorescein tag for photoreceptor apoptotic nuclei within the light damaged region of the retina. This picture better illustrates the beginning hollow spheres and some of the later blebs associated with apoptosis.

Figure 10
TUNEL analysis with fluorescein tag for photoreceptor apoptotic nuclei at the periphery of the light damaged region. Notice that the number of labeled nuclei diminishes to the right as the undamaged peripheral region is first encountered.
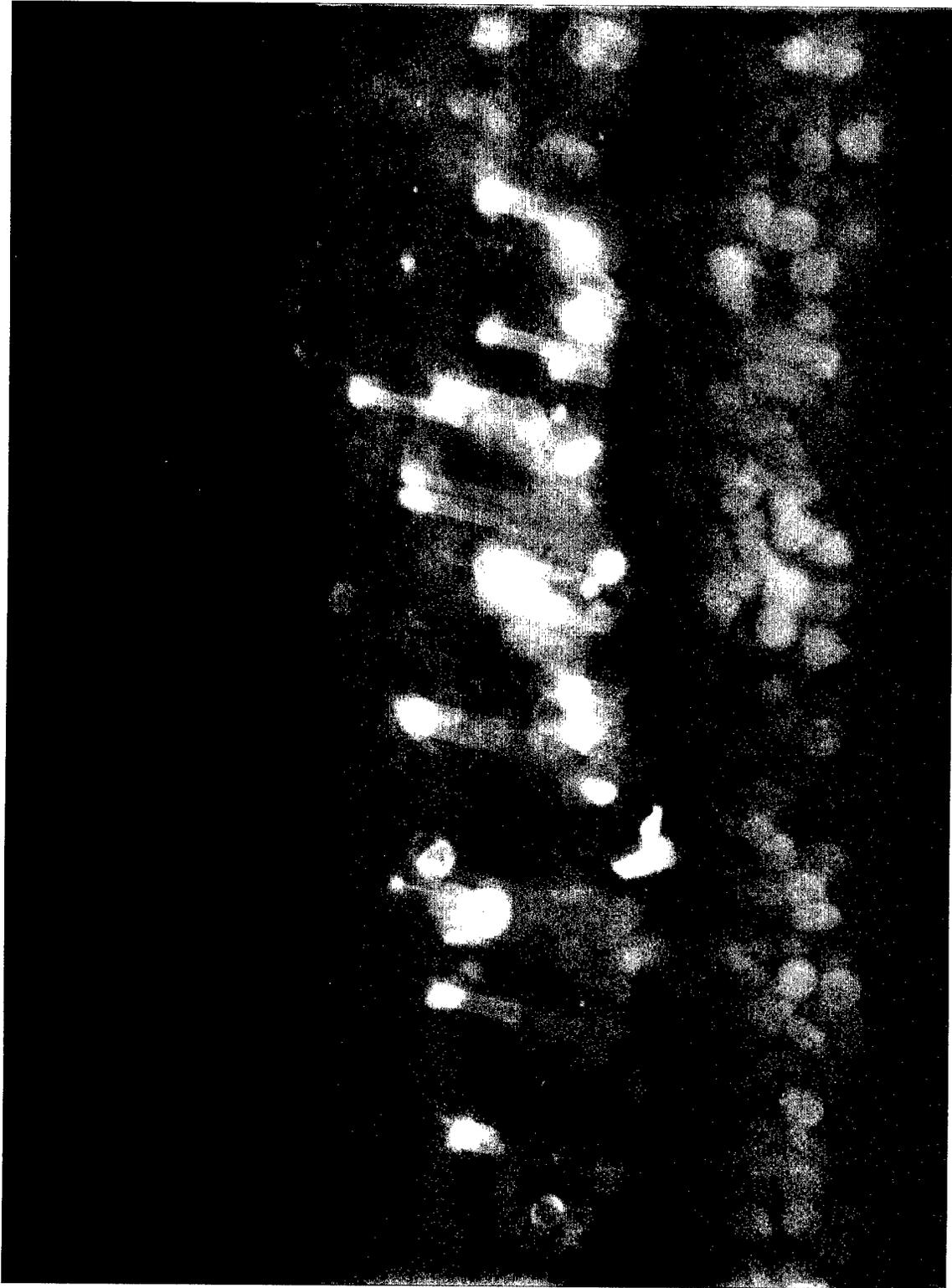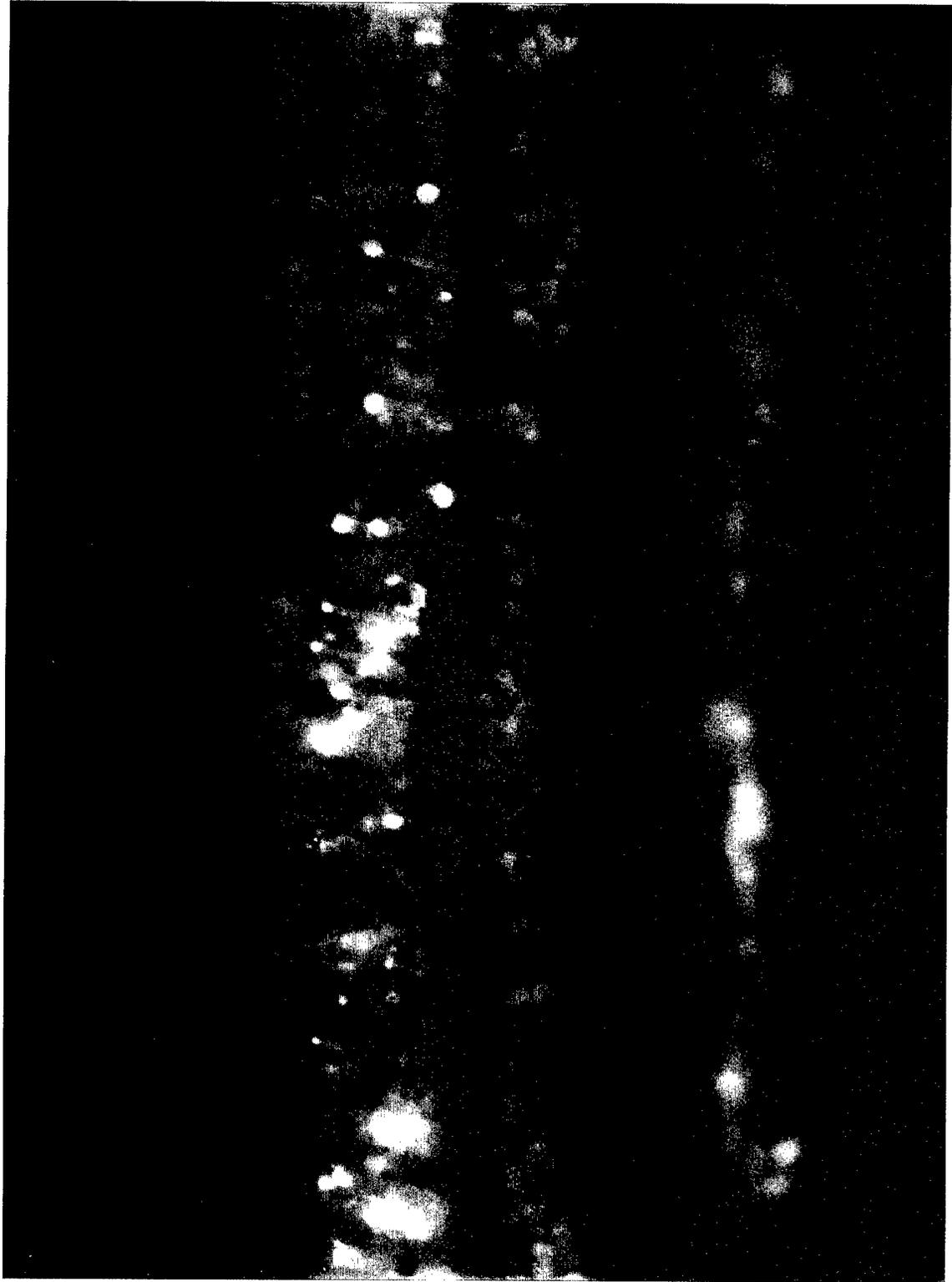
Figure 11
TUNEL analysis with fluorescein tag for photoreceptor apoptotic nuclei outside the light damaged region of the retina. This is the same section as shown in Figure 10. Notice the complete absence of apoptotic nuclei here.
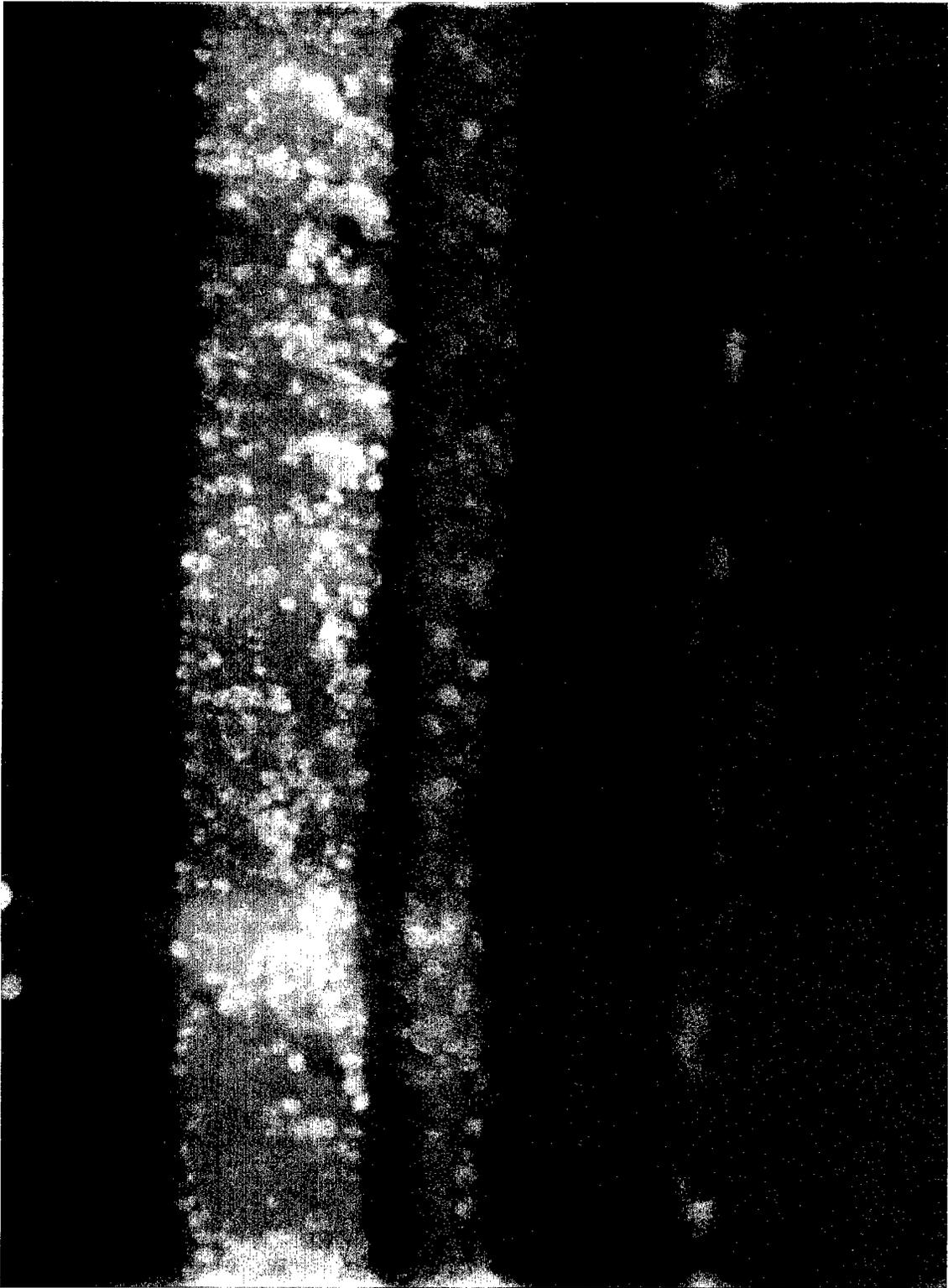
Figure 12
TUNEL analysis with fluorescein tag for photoreceptor apoptotic nuclei within a dark treated control retina. This region is similar to that shown in Figures 7 and 8, but has never been exposed to bright light.

POST-GOLGI VESICLES COTRANSPORT DOCOSAHEXAENOYL-PHOSPHOLIPIDS AND RHODOPSIN DURING FROG PHOTORECEPTOR MEMBRANE BIOGENESIS.

Elena B. Rodriguez de Turco[1]; Dusanka Deretic[2]; Nicolas G. Bazan[1]; and David S. Papermaster[3]

[1]LSU Neuroscience Center
Louisiana State University Medical Center,
School of Medicine, New Orleans, Louisiana

[2]University of Michigan
Departments of Ophthalmology and Anatomy
Ann Arbor, Michigan

[3]Univeristy of Texas
Health Science Center
Department of Pathology
San Antonio, Texas

Corresponding Author:
Nicolas G. Bazan
LSU Neuroscience Center
2020 Gravier Street, Suite B
New Orleans, LA 70112
Tel   (504) 568-6700 ext 321
Fax   (504) 568-5801
email nbazan@lsumc.edu

1

Running Title:

Co-transport of DHA-phospholipids and rhodopsin in retina

SUMMARY

Post-Golgi vesicles budding from the trans-Golgi network (TGN) are involved in the vectorial transport and delivery of rhodopsin to photoreceptor rod outer segments (ROS). We report here that newly synthesized docosahexaenoyl (DHA) phospholipids are sequestered and cotransported by rhodopsin-bearing post-Golgi vesicles to ROS. Frog retinas were pulse labeled with [^{35}S]methionine/cysteine and [^{3}H]DHA prior to ROS isolation and subcellular fractionation of retinas. After a one hour pulse, relatively uniform [^{3}H]DHA-lipid labeling (DPM/µg protein) was observed in all fractions enriched in post-Golgi vesicles, TGN, Golgi, and endoplasmic reticulum (ER) membranes. During the subsequent two hour chase translocation of free [^{3}H]DHA from ROS to the photoreceptor inner segment contributed to an additional overall increase in labeling of lipids. The specific activity (DPM/nmole of DHA) in ER-enriched fraction 14 was similar or higher than in other subcellular fractions after both the pulse and the chase, indicating that the bulk of [^{3}H]DHA-lipids was synthesized in the ER. After the chase a 2-fold increase in labeling of lipids in the ER and Golgi and a 2.6-fold in lighter TGN enriched fractions 7-8 was observed. The highest labeling was in the post-Golgi vesicle fraction 5 (4-fold increase), with [^{3}H]DHA-phosphatidylcholine and [^{3}H]DHA-phosphatidylethanolamine showing the greatest increase. At the same time, newly synthesized [^{35}S]rhodopsin shifted from the ER and Golgi towards TGN and post-Golgi fractions 4-6. Therefore, sequestration and association of [^{35}S]rhodopsin and [^{3}H]DHA-lipids in a TGN membrane domain occurs prior to their exit and subsequent vectorial cotransport on post-Golgi vesicles to ROS. Labeling ROS lipids was very low, with

3

phosphatidylinositol and diacylglycerols displaying the highest labeling. This indicates that other mechanisms by-passing Golgi, i.e., facilitated by lipid carrier proteins, may also contribute to molecular replacement of disc membrane DHA-phospholipids, particularly phosphatidylinositol.

INTRODUCTION

Vertebrate photoreceptors are polarized and compartmentalized cells, with a photosensitive outer segment and a synaptic terminal domain at opposite ends of the cell. These domains are attached through a connecting cilium and a short axon, respectively, to a central region, the inner segment. The inner segment is the site where lipid and protein synthesis, polarized sorting of molecules and initiation of membrane biogenesis for both the outer segment and synaptic terminals takes place. Disc membranes in rod outer segments (ROS)[1] display a unique lipid-protein composition. The visual pigment rhodopsin, which accounts for more than 85% of disc membrane proteins (1), is embedded within a highly fluid lipid bilayer comprised of phospholipids (PLs) enriched in docosahexaenoic acid (DHA, 22:6n-3) (2-5). DHA esterified at the *sn*-1 carbon in hexanoic molecular species and at the *sn*-1 and *sn*-2 carbons of the glycerol backbone in dipolyunsaturated or *supraenoic* species, contributes to more than 50% of phosphatidylcholine (PC), phosphatidylethanolamine (PE), and phosphatidylserine (PS) acyl groups (6, 2, 3, 5-8).

Amphibian photoreceptor cells are a useful experimental model to study protein and lipid trafficking in a polarized cell. Photoreceptors actively synthesize proteins (mainly rhodopsin), and DHA-PLs to support the dynamic daily renewal of 50-80 large disc membranes in each rod cell that results in the addition of membrane at ≈3 μm^2/min (9-10). ROS lack the capacity for *de novo* synthesis of the major structural lipids, i. e. PC, PE, PS (4), and for phosphatidylinositol (PI) (11). Therefore, they depend entirely on a external supply of PLs from the inner segment where

5

they are synthesized mainly in the rough endoplasmic reticulum (ER) (12). How these highly unsaturated lipids become components of ROS membranes and at which stage of membrane biosynthesis and disc morphogenesis they become associated with rhodopsin is not yet clear.

Newly synthesized rhodopsin is vectorially transported from its site of synthesis in the rough ER to ROS by vesicles that bud from the trans-Golgi network (TGN), cluster beneath the connecting cilium and fuse with the inner segment plasma membrane within the periciliary ridge complex (13, 14). A very low buoyant density ($\rho = 1.09$ g/ml) post-Golgi vesicular subcellular fraction carrying newly synthesized rhodopsin has been isolated and characterized from frog retinal photoreceptor cells (14-17). While rhodopsin and the bulk of DHA-PLs are synthesized in the rough ER, and both can follow a vesicle-mediated traffic through the biosynthetic pathway, other mechanisms can contribute to trafficking and selective delivery of PLs to intracellular organelles (18-20). For example, the rapid monomer transport of PLs is facilitated by transfer proteins (TP) through the cytosol (21). A transfer protein that with high affinity transfers PC to ROS membranes has also been described (22), and immunohistochemical analysis of chicken retinas at hatching revealed the presence of phosphatidylinositol (PI)-TP in retinal cells including the inner segment of photoreceptors (23).

Phospholipid renewal of ROS membranes involves both membrane replacement (as new disc membranes are assembled at the base of the ROS) and molecular replacement (i. e. PL-TP mediated and remodeling of disc PLs by turnover) (24-25). Using various radiolabeled lipid precursors under experimental conditions that inhibit protein synthesis or vesicle-mediated

transport, lipids can be transported to ROS by-passing the Golgi, suggesting that there are Golgi independent pathways for transport of lipids to ROS (26-30). However sorting of DHA-PLs, vectorial transport to ROS, and the contribution of alternative pathways to their trafficking has not been experimentally addressed. This question is especially intriguing because biochemical and autoradiographic studies of [^{3}H]DHA trafficking in frog photoreceptors after *in vitro* (31-32) and *in vivo* (33-34) labeling, have disclosed that newly synthesized [^{3}H]DHA-PLs display a polarized delivery to ROS, where they are incorporated at the base as new discs are formed, in a pattern paralleling incorporation of radiolabeled amino acids into disk membrane proteins.

The aim of the current study was to investigate if newly synthesized DHA-lipids could be, at least in part, segregated and cotransported with rhodopsin in vesicles budding from the TGN and then enter the ROS as new membranes are formed (membrane replacement). To address this question, we pulse-labeled frog retinas for one hour in the presence of [^{3}H]DHA and [^{35}S]methionine/cysteine, followed by a two hour chase in a cold buffer prior to subcellular fractionation (14, 35). [^{3}H]DHA was chosen because this precursor is actively esterified into photoreceptor PLs which are then vectorially transported to the ellipsoid region at the base of ROS and also to synaptic terminals (31-32). Moreover, an active synthesis of poly- and dipolyunsaturated species of DHA-PLs, either involving incorporation of DHA via *de novo* synthesis, turnover, and/or a combination of both, occurs in the inner segment prior to their vectorial delivery to ROS (7, 36-39). Our results demonstrate that newly synthesized [^{3}H]DHA-PLs, especially the main components of disc membranes (i. e. DHA-PC and DHA-PE), are

7

segregated and loaded together with newly synthesized [^{35}S]rhodopsin in post-Golgi vesicles.

Some lipids, i. e. [^{3}H]DHA-PI and [^{3}H]DHA-diacylglycerols (DAG) are very rapidly synthesized

and delivered to ROS probably by alternative pathways that by-pass the Golgi, and may be

facilitated by carrier proteins (40).

EXPERIMENTAL PROCEDURES

Frogs, *Rana berlandieri* (100-250g) were purchased from Rana Co. (Brownsville, TX), maintained in a 12h light/12 h dark cycle, and fed crickets for a week prior to the experiment. [4, 5- ^{3}H]DHA (specific activity 17 Ci/mmol) and [^{35}S]Express protein labeling mixture (1,000 Ci/mmol) were from New England Nuclear (Boston, MA). High performance thin layer chromatographic (HPTLC) plates (10x10cm, 150 μm thickness) were from Analtech (Newark, Delaware). Lipids and fatty acid methyl ester standards and protease inhibitors were from Sigma Chemical Co. (St. Louis, MO). HPLC grade solvents were from EM Science (Gibbstown, New Jersey). All other reagents used were of the highest purity available.

In vitro **labeling of retinal lipids and proteins with [^{3}H]DHA and [^{35}S]methionine/cysteine.**

Retinas recovered from frog eyecups two hours before the time of light offset, were dissected and subsequently incubated under dim red light. Two sets of twenty one retinas were incubated in 30 ml of an oxygenated medium as described (14, 35) at 22^{0}C in the presence of [^{3}H]DHA (5.7 μCi/retina), and [^{35}S]Express protein labeling mixture (25 μCi/retina) for 1 hour. One set of retinas was further incubated for two hours in cold buffer containing unlabeled amino acids (pulse-chase samples) prior to subcellular fractionation.

Rod outer segments isolation and retinal subcellular fractionation.

All the procedures followed for the isolation of ROS and subcellular fractionation have been described in detail elsewhere (14, 35). Briefly, following the pulse and pulse-chase labeling, retinas were sheared through a 14-gauge needle and ROS were separated by flotation on 34%

sucrose. Retinal pellets were rehomogenized in 0.25M sucrose in 10 mM Tris acetate, pH 7.4,

containing 1 mM $MgCl_2$ and centrifuged for 4 min at 4,000 rpm (1250 g_{av}, JA20 rotor, Beckman

Instruments, Inc., Palo Alto, CA). The post-nuclear supernatant (3 ml) recovered after this

centrifugation (PNS) is enriched in photoreceptor biosynthetic membranes and organelles

involved in rhodopsin transport (14, 35). To isolate post-Golgi vesicles from TGN, Golgi, and

ER membranes, the PNS was overlaid on a 10 ml linear 20-39% (w/w) sucrose gradient in 10 mM

Tris acetate buffer, pH 7.4, containing protease inhibitors and 1mM $MgCl_2$, above a 0.5 ml

cushion of 49% (w/w) sucrose in the same buffer. Gradients were centrifuged for 13 hours at 4^0C

in a SW40 rotor (Beckman) at 28,000 rpm (100000 g_{av}). Fourteen fractions (0.9 ml each) were

reproducibly collected from the top of the gradient. A Buchler Auto Densi-Flow fractionator was

used to prepare the gradient and to collect the fractions. The subcellular fractions were diluted

four fold with 10 mM Tris-HCl and pelleted at 50,000rpm (240,000 g_{av}) for 40 min in a SW50

rotor. The pellets were resuspended in 210 µl of Tris-acetate, pH 7.4 and divided into two

aliquots: one third for protein analysis and two thirds for lipid analysis.

Protein analysis.

SDS-polyacrylamide gel electrophoresis was performed as described previously (14). [^{35}S]

labelled rhodopsin was determined in subcellular fractions by exposure of dried SDS gels to

storage phosphor screens, and the intensity of luminescence associated with the rhodopsin band

measured and analyzed by a PhosphorImager densitometer (Molecular Dynamics). Total proteins

were quantified according to Fanger (41), using BSA as a standard.

Lipid extraction and analysis.

Lipids were extracted from the fractions by adding 3 ml of chloroform:methanol (2:1, v/v) followed by sonication under nitrogen for 15 min at room temperature and subsequent centrifugation (1000 g_{av}) for 10 min. The organic phase was washed with upper theoretical phase (42), evaporated to dryness under nitrogen, and then resuspended in a known volume of chloroform:methanol (2:1, v/v). Individual phospholipids and neutral lipids were isolated in the same TLC plate following a two-dimensional, 3- step TLC procedure (8) as follows: an aliquot of the labeled lipid extract containing phospholipid and neutral lipid standards as a carriers, was applied on the lower right corner (1.5 cm from each border) of 10 x 10cm HPTLC plates previously sprayed with 3% Mg Acetate and activated for at least 1 hour at 100 ^{0}C. The plate was developed in the first dimension twice using the Rouser I chromatographic system (chloroform:methanol:ammonia 65:25:5, v/v) until the solvent front reached 2 cm from the top of the plate. After drying with cold air, the plate was turned to the right 90^0, neutral lipid standards (cholesterol ester, triacylglycerol, diacylglycerol, and monoacylglycerol) were spotted 1.5 cm from the bottom and 0.5 cm from the right border. Plates were then developed in Hexane:ether (60:40, v/v) to isolate individual neutral lipids that had accumulated at the front of the first chromatographic system. The silica gel was cut with a vertical line to isolate neutral lipid (right) from phospholipid (left) areas of the plate (approximately 3 cm from the right border) and the silica was scraped off from the bottom right corner prior to running the plates in the Rouser II system (chloroform:acetone: methanol:acetic acid 30:40:10:10:5, v/v). This third

chromatographic step, run in the same direction as the second step, allows the isolation of individual phospholipid classes and free fatty acids that run with the solvent front above PE. Lipid spots were visualized by iodine staining and scraped into scintillation vials containing 1 ml of water. Vials were kept in a oven at 60 °C for at least 4 hours, then 10 ml of Ready Gel (Beckman, Fullertone, CA) cocktail was added and the radioactivity was determined in a Beckman scintillation counter.

Aliquots of lipid extracts were taken for gas-liquid chromatography (GLC) analysis of endogenous fatty acid content and composition. Fatty acid methyl esters (FAME) were prepared in glass tubes by transmethylation with 2 ml toluene:methanol:sulfuric acid (100:100:4, v/v) for 4 hr at 65 °C, after flushing the tubes with nitrogen and capping with a Teflon-lined cap. The tubes were cooled at room temperature, and 1 ml of water, 3 ml of hexane, and a mixture of two internal standards (17:0 and 21:0 methyl esters) were added. FAME resuspended in hexane were separated onto a SP-2330 column (30 m, 0.25 mm i.d., 0.2 μm film thickness, Suppelco, Bellefonte, PA) by using helium as a carrier gas, in a Varian Vista 401 gas chromatograph (Palo Alto, CA). The injector and detector temperatures were 220 and 250°C, respectively, and the column temperature was programmed from 70 to 230 °C (43). The peaks were detected by flame ionization, identified by comparison with the retention times of authentic FAME standard, and quantified using the internal standards.

Statistical analysis.

Values for [³H]DHA lipid labelling and [³⁵S]rhodopsin are presented as a mean ± S.E.M. for n=4 individual experiments. Data were compared using Student's *t* test for pair samples. A p value of < 0.05 was considered statistically significant.

RESULTS

Post-Golgi vesicles are enriched with newly synthesized [^{35}S]rhodopsin and [^{3}H]DHA-lipids.

Subcellular fractionation on sucrose density gradients of the frog retinal PNS enriched in

photoreceptor inner segment membranes, allows the isolation of membrane compartments

involved in protein and lipid synthesis (i.e. rough ER) and transport (i. e. Golgi, TGN) from post-

Golgi vesicles involved in the vectorial transport of rhodopsin to ROS (14, 35). To determine

whether newly synthesized [^{3}H]DHA-PLs and [^{35}S]rhodopsin are transported together in the same

population of post-Golgi vesicles that bud from the TGN and, therefore, can be recovered in post-

Golgi fraction 5 of the sucrose gradient, retinas were pulse labeled for one hour in the presence of

both precursors and further incubated for two hours (chase) in cold buffer prior to subcellular

fractionation. Since the rapid *in vitro* incorporation of nM concentrations of [^{3}H]DHA into

retinal lipids is very similar to that obtained *in vivo* after injecting the precursor systemically and is

altered at μM DHA concentrations (31-32, 44), cold DHA was not added during the chase. For

this reason, only unlabeled methionine/cysteine replaced the labeled precursor in the chase media.

Since excess cold DHA was not added, this chase period will hereafter be identified as "chase" to

reflect this condition. While the total [^{35}S]rhodopsin labeling recovered from the combined 14

fractions was similar for pulse and chase samples (data not shown), total [^{3}H]DHA found

esterified into lipids was increased by 2.6 ± 0.2 -fold after a two hour cold "chase" (from 1.2 x 10^{6}

DPM/21 retinas after a one hour pulse to 3.2 x 10^{6} DPM after a two hour "chase"), indicating its

continuous and active esterification from free [^{3}H]DHA. After one hour of pulse labeling, 58% of

14

total [^{35}S]rhodopsin was recovered in TGN (fractions 7 to 10) and Golgi (fraction 11) (Figure 1) as expected (14). After a two hour cold "chase", a shift towards post-Golgi fractions 4 to 6 was observed, with fraction 5 displaying the greatest increase (ratio chase / pulse: 2.4 ± 0.5).

The profile of total esterified [^{3}H]DHA among subcellular fractions was similar to that of [^{35}S]rhodopsin, with the highest percent values observed in those fractions that also accumulated the largest proportion of membranes (Figure 1). In Figure 2-D, fractions enriched in TGN (fractions 8-10), Golgi (fraction 11-12) and ER (fraction 13) are shown to contribute to more than 60 % of the protein recovered from the 14 fractions while each of the post-Golgi vesicle fractions 4 to 6 accounted for only 5% of the total. The profile of [^{3}H]DHA labeling of subcellular fractions after the two hour "chase" was similar to the profile after an one hour pulse; TGN fractions 8 to 10 had the highest labeling (Figure 1). Remarkably only post-Golgi fraction 5 displayed significantly higher [^{3}H]DHA percent labeling after the chase (ratio chase / pulse: 1.7 ± 0.2) at the time when newly synthesized [^{35}S]rhodopsin accumulated in this fraction. Moreover, the ratio of percent [^{35}S]rhodopsin to percent [^{3}H]DHA-lipids in fraction 5 was the same after the pulse (1.2 ± 0.3) and the chase (1.2 ± 0.1) labeling, suggesting that newly synthesized [^{35}S]rhodopsin exits the TGN together and/or in close association with newly synthesized [^{3}H]DHA-lipids, and is probably cotransported in the same population of vesicles.

Labeling recovered from individual subcellular fractions based upon protein content is shown in Figure 2 and reveals four features: First, after a one hour pulse, all fractions displayed similar labeling of esterified [^{3}H]DHA (Figure 2B). This indicates that newly synthesized DHA-

15

lipids were rapidly transported throughout the multiple compartments of the biosynthetic pathway either by vesicle budding and fusion, by carrier proteins, and/or by lateral diffusion through intermembrane bridges (19-20). Incorporation of [^{3}H]DHA by turnover in lipids trafficking along the transport pathway could also contribute to the uniform labeling distribution observed among subcellular fractions. Second, after the subsequent two hours incubation in cold media, labeling of DHA-lipids increased at least 2-fold in the heavy fractions that correspond to the density of ER (13-14), Golgi (11-12), and TGN (10), by 2.6-fold in lighter TGN fractions 7-9, and peaking at 4-fold higher labeling in post-Golgi vesicles recovered in fraction 5 as compared to pulse-labeled values (Figure 2B-2C). It is noteworthy that the homogeneous [^{3}H]DHA labeling of subcellular fractions observed after a one hour pulse was greatly altered after the two hour "chase", coincident with the displacement of newly synthesized rhodopsin toward post-Golgi vesicles recovered in fractions 4-6 (Figure 1). Third, no significant difference between pulse and chase labeling was observed in the free [^{3}H]DHA pool, indicating an equilibrium between the arrival of the precursor to these membrane compartments and its esterification into lipids either by *de novo* synthesis and/or turnover (Figure 2A). The peak of labeling observed in fraction 8 may be the result of free [^{3}H]DHA contributed by a small proportion of heavily labeled ROS cosedimenting between fractions 7 and 9 at a buoyant density of 1.13 g/ml (14). Fourth, most of the label recovered from ROS after pulse and chase labeling was found as free DHA (92 ± 1% and 76 ± 1%, respectively) (Figure 2A). This contrasted with the very low labeling of ROS lipids, the lowest among all subcellular fractions analyzed (Figure 2B). The decrease observed in ROS

16

free [³H]DHA after the chase (from 2600 to 1160 DPM/µg protein) was paralleled by a 2.5-fold

increase in [³H]DHA-lipids (from 138 ± 25 to 350 ± 40 DPM/µg protein). Assuming that the

labeling of ROS lipids was mainly due to acyl group turnover, the increase in [³H]DHA-lipids can

be accounted for by the concommitant loss of 15% of free [³H]DHA. Therefore free [³H]DHA

found in ROS after a one hour pulse appears to be actively incorporated into lipids in the inner

segment after its translocation during the two hour "chase" towards the inner segment leading to

the observed increase in esterified [³H]DHA in the ER and in other membrane compartments of

the biosynthetic pathway (Figure 2B).

The specific activity of total [³H]DHA-lipids (DPM/nmole of endogenous DHA content)

showed that fraction 14 (ER) displayed, after both the pulse (2790 ± 245 DPM/nmole DHA) and

the "chase" (5060 ± 840 DPM/nmole DHA) labeling, similar or higher values than other fractions.

After the pulse labeling, the specific activity of fraction 5 (1990 ± 115 DPM/nmole DHA) was

significantly lower than that of fraction 14 (p<0.05). After the chase, the specific activity of

fraction 5 increased 3-fold (6580 ± 550 DPM/nmole DHA) but was not significantly different

from the specific activity of fraction 14 (p>0.19). These results indicate that [³H]DHA is

incorporated into lipids mainly in the ER membranes and then reaches a rapid equilibrium among

membranes of the biosynthetic pathway.

Phosphatidylcholine, phosphatidylethanolamine, and phosphatidylinositol are highly labeled

in all subcellular fractions; [³H]DHA-PC and [³H]DHA-PE preferentially shift toward post-

Golgi vesicles (Fraction 5) after the chase.

17

The two most abundant PLs in retinal membranes, PC and PE, reveal a similar labeling profile after a two hour "chase" (Figure 3). [³H]DHA-PC and [³H]DHA-PE gradually increased from fractions enriched in ER to heavy fractions of the TGN, with a sharp peak in post-Golgi fraction 5 reaching a 5.2-fold and 4.6-fold increase, respectively, above pulse labeling. The profile of [³H]DHA-PI was very similar to that of diacylglycerol (DAG) labeling. In contrast to PC and PE, PI and DAG labeling was significantly increased only in the lightest TGN fractions 7-9, with the highest increase in post-Golgi fraction 5 (3.9 and 2.5-fold, respectively). PS was the only phospholipid that did not show a peak of labeling in fraction 5 but rather, displayed 3-fold increase between fractions 5 to 7. Phosphatidic acid (PA) gradually increased in labeling from ER fractions to post-Golgi fraction 5 with no significant differences from the one hour pulse labeling.

[³H]DHA-PL labeling in ROS was very low (Figure 3, insets) with a different pattern of distribution than all other subcellular fractions (Figure 4). Although the small amount of ROS that are recovered in the gradient between fraction 7 and 9 may contribute to the highly free [³H]DHA labelling of these factors (Figure 2), it cannot contribute to, but rather results in an underestimation of lipid labeling in these fractions that arise from inner segment membranes. [³H]DHA-PI displayed, by far, the highest labeling in ROS, with a 7.9-fold increase after a two hour "chase", followed by DAG (4.8-fold), PC and PS (3-fold each). No differences were observed between a one hour pulse and two hour "chase" labeling in [³H]DHA-PE and [³H]DHA-PA (Figure 3, insets). This short-term incubation, may reflect the labeling of disc membrane lipids by molecular replacement including: a) [³H]DHA incorporation by turnover; b) the fast transport

18

from the inner segment of a portion of newly synthesized [³H]DHA-lipids (i. e. [³H]DHA-PI)

and/or c) further metabolism of newly incorporated [³H]DHA-PLs into ROS such as N-

methylation of [³H]DHA-PE to [³H]DHA-PC (4, 44).

The percent distribution of esterified [³H]DHA displayed high values for PI, PC, and PE in

all fractions except for ROS (Figure 4). PI displayed the highest percent labeling after a one hour

pulse and remained unchanged after the two hour "chase", while PC and PE values increased

concommitantly with a lower percent labeling of neutral lipids: TAG, DAG, and MAG. Only in

fraction 5 did the percent labeling of PI, PC, and PE reach a similar value (28 %), while in other

fractions, PI labeling alone prevailed. The highest percent labeling of PI was observed in fraction

1 (48 %) and to a lesser extent in fraction 2 (34 %), probably associated with cytosolic proteins

recovered at the top of the gradient that may sediment after the 40K centrifugation (14). This

could reflect an active synthesis and transport of [³H]DHA-PI facilitated by PI-TP leading to a

very rapid labeling of intracellular membranes, including Golgi, TGN, and ROS. The ratio PI to

PC labeling was higher in TGN fractions as compared to post Golgi fractions 4-6, showing the

highest value in fraction 8 of the TGN after both pulse and "chase" labeling (Figure 5).

The content of endogenous fatty acyl chains of lipids from post-Golgi vesicular fractions.

Total fatty-acyl-group content, reflecting mainly membrane phospholipids, increased

gradually from the heaviest, ER-enriched fractions (2 nmole/μg protein) to the post-Golgi light

vesicular fractions 4-5 (4 nmole/μg protein) (Figure 6). The density of fraction 5 membranes in

the sucrose gradient (ρ= 1.09 g/ml) was much lower than that of membranes recovered in

19

fractions 7- 8 and ROS (ρ = 1.12-1.13 g/ml); however, their total lipid-acyl group content was similar. An increased content of cholesterol and/or other sterols, synthesized at the ER level and displaying higher concentration towards the Golgi-trans Golgi membrane compartments of the secretory pathway (18,19, 45), may contribute to lowering the density of post-Golgi vesicles recovered in fraction 4 to 6.

The DHA content for all fractions, from those enriched in ER membranes to those containing post-Golgi vesicles, was very similar (approx. 20% of total acyl groups) except for TGN fractions 7 to 9 where ROS, not completely removed prior to subcellular fractionation, cosedimented. In ROS, DHA accounted for 50 % of total acyl groups. The lower % DHA content in fraction 5 as compared to ROS suggests that either the lipids from the vesicles bearing rhodopsin are less enriched in DHA-lipid and/or that lipids contributed by other vesicles with a lower degree of unsaturation are recovered in this fraction. The latter possibility is unlikely since immunoisolation of rhodopsin-bearing post-Golgi vesicles with anti-rhodopsin antibody indicated that they constitute >85% of the vesicles sedimenting in fraction 5 of the gradient (14). The net amount of DHA per protein in ROS (1.93 nmole/μg) was twice that of lipids from fraction 5 vesicles (0.85 nmole/μg protein). Although rhodopsin is the most abundant protein recovered in fraction 5, its contribution to the total proteins in the fraction is less than 50 %, while rhodopsin accounts for 85-90 % of total ROS proteins (14). Therefore, the net amount of DHA-PLs with respect to rhodopsin protein in these post-Golgi vesicles, may reach values similar to that of ROS.

DISCUSSION

This study provides the first available information about the closely coordinated

trafficking, sorting and association of newly synthesized [^{3}H]DHA-PLs with [^{35}S]rhodopsin in

frog photoreceptors as the two major membrane components initiate their journey from the rough

ER, where they are synthesized, move through the Golgi, and leave the TGN on post-Golgi

vesicles vectorially driven to ROS for the assembly of new disc membranes. Our results also yield

several other important findings: **a)** free [^{3}H]DHA may be incorporated by turnover in disc PLs

although much less efficiently than when utilized in the inner segment for [^{3}H]DHA-PLs synthesis;

b) some [^{3}H]DHA-PLs, mainly [^{3}H]DHA-PI, are actively synthesized in the inner segment, rapidly

transported to ROS and incorporated into disc membranes; **c)** during short period of *in vitro*

labeling (1-3 hours), the fast labeling of all disc membranes by molecular replacement (i. e. protein

mediated transport of [^{3}H]DHA-PLs and/or [^{3}H]DHA incorporation by turnover) as compared to

the labeling of a few discs at the base by membrane replacement, makes it difficult to assess the

contribution of the latter mechanism to the overall labeling of ROS lipids. Moreover, the study of

DHA-lipids in rhodopsin-bearing post-Golgi vesicles is a useful experimental approach to further

explore lipid classes and molecular species selectively delivered to ROS together with rhodopsin

as new disk membranes are assembled.

[^{3}H]DHA incorporation into lipids reached similar values in all subcellular fractions

within the first hour of pulse labeling. This rapid equilibrium of DHA-lipids among all fractions

was also reflected in a similar mole percent content of endogenous DHA (20%). The [^{3}H]DHA-

lipids recovered in Golgi and TGN enriched fractions at any time represent newly synthesized

lipids that become constitutive components of the membranes as well as the different[³H] DHA-

lipids pools that are in transit through these compartments to different destinations.

Autoradiography of [³H]DHA trafficking in frog retinas labeled *in vitro* reveals that [³H]DHA-PL

accumulates in the ellipsoid region at the base of ROS with labeling also in synaptic terminals

(31). These results parallel the vesicle-mediated vectorial transport of rhodopsin to ROS (13-15)

and synaptic terminal proteins (12). Thus, different [³H]DHA-PL pools must be segregated and

sorted at the TGN (46) prior to their incorporation into post-Golgi vesicles tagged for delivery to

membranes localized at opposite ends of photoreceptors.

Lipid movement through membranes of the biosynthetic pathway involves various

mechanisms (19) and may contribute to the rapid labeling distribution we observed. Newly

synthesized PLs in the rough ER are necessary to support vesicule-mediated protein (i. e.

rhodopsin) traffic leading to an anterograde membrane flow. Cytosolic PL transfer proteins (PL-

TPs) (21), may also catalyze the rapid transport of lipid monomers from the ER to Golgi

membranes. A retrograde transport from Golgi to the ER, mediated by vesicles and PL-TPs has

been suggested, the former for the recycling of integral membrane proteins (47) and the latter for

the retrieval of PL to support the rate of membrane flow from the ER (48). Selective retrieval of

PLs from Golgi membranes may also contribute to the increase of cholesterol concentration in

these membranes (48). Cholesterol is found in very low concentrations in the ER, accumulates

gradually from cis- to trans-Golgi cisternae and displays the highest content in the plasma

membrane (19,20, 45). These changes in membrane lipid composition may be a key factor, as we

will discuss later, for the sequestration of newly synthesized DHA-lipids and rhodopsin prior to

their exit from the TGN.

Frog and primate retinas labeled *in vitro* with [^{3}H]DHA display an early high level of

labeling of PI, reaching values similar to that of PC and PE (31, 49). Furthermore, a similar

profile is observed in frog retinas after *in vivo* labeling (32), indicating that this preferential PI

labeling is not an artifact due to *in vitro* incubation. In the present study, we confirm and further

extend our previous observation to show that [^{3}H]DHA-PI preferentially accumulates in the

lightest fractions 1-3 of the gradient where cytosolic proteins are recovered (14), and also in ROS

and in TGN fraction 8. Several PLs-TPs have been characterized such as a PI/PC-TP with high

affinity for PI that also binds PC (21). Moreover **a)** PI/PC-TP is associated with the Golgi

complex as a peripheral membrane protein in yeast (21), in 3T3 fibroblasts (50) and in mammalian

cells (52); **b)** PI/PC-TP is identical to the protein encoded in yeast by the SEC14 gene (52) which

plays an essential role in stimulating the budding of vesicles at the exit from the Golgi (21, 53-54);

c) PI/PC-TP controls the PC content in yeast Golgi membranes by modulating its synthesis which,

in turn, may result in a high PI/PC ratio necessary for Golgi function (21, 55-56); **d)** PI/PC-TP

plays an active role in mammalian brain, transferring PI to those membranes with high inositol

lipid turnover (57), promoting PIP$_2$ synthesis and regulating the rate of IP$_3$ production in HL60

cells (58); **e)** two isoforms of PI/PC-TP were reported in Swiss mouse 3T3 fibroblasts (50) and

in the cytosol from bovine brain (59), which differ in their isoelectric point. The more acidic form

(pI 5.4) was found preferentially associated with the Golgi system and also displayed in brain a high transfer activity towards sphingomyelin (59); and finally, f) PI-TP has been identified as a cytosolic factor that stimulates the formation of secretory vesicles from the TGN in PC12 cells (60).

Little information is available about PI/PC-TP in the retina, except for a retinal PC-TP activity in isolated ROS (22) and the immunohistochemical detection of PI-TP in the inner segment photoreceptors and other chick retinal cells (23). The high ratio [³H]DHA-PI to [³H]DHA-PC found in TGN fractions 7-9 of frog retinas, is the first evidence indicating a relative enrichment with newly synthesized [³H]DHA-PI of membranes located at the exit from the Golgi compartment. As previously shown in yeast (21) and on PC12 cells (60), the high PI/PC ratio may also be essential for budding off rhodopsin-bearing vesicles from TGN and further suggests the involvement of PI/PC-TP in the dynamics of Golgi function in photoreceptors. Moreover, the high PI/PC ratio appears to be a characteristic of TGN membranes but not of post-Golgi vesicles recovered in fraction 5, since they displayed a ratio PI/PC =1. Since membranes recovered in TGN enriched fractions 6-11 also contain synaptophysin, a synaptic membrane protein (14), further studies are necessary to evaluate the possible contribution of [³H]DHA-PI, in transit together with synaptophysin towards synaptic terminals, to the high [³H]DHA-PI in TGN fractions 7-9. The overall contribution of synaptic protein biosynthesis in this fraction must be relatively minor, however, since rhodopsin synthesis greatly exceeds the rate of synthesis of all other retinal membrane proteins (61).

We also observed that [^{3}H]DHA-PI displayed by far the highest labeling in ROS. DHA

can be incorporated into PI by turnover when isolated ROS are incubated *in vitro* with [^{14}C]DHA

(62). However the highest [^{14}C]DHA-PI labeling was attained only when the whole retina was

incubated with the precursor prior to ROS isolation (38). Several lines of experimental evidence

appear to indicate that PI, synthesized *de novo* in the inner segment of photoreceptors, can

actively be transferred to the outer segment probably by a protein facilitated transport (63) which

is not blocked by drugs that disrupt vesicle-mediated transport of rhodopsin (26, 30). The high

[^{3}H]DHA-PI observed in ROS correlates with the highest reported *de novo* synthesis, and

preferential translocation to ROS of 16:0-DHA-PI, which also is the more abundant PI molecular

species in frog ROS (8). ROS isolated from frog retinas do not contain the enzymes necessary for

the conversion of phosphatidic acid (PA) to PI (11). However after PI is translocated to ROS, it

can be further phosphorylated to PIP and PIP$_2$ (11, 64). Because ROS contain a light-stimulated

phosphoinositide-specific phospholipase C (65, 66), the presence of a photoreceptor cytosolic PI-

TP, possibly similar to the one found in rat brain cytosol (57), could contribute to sustain and

modulate the inositol lipid-derived signals triggered by light.

After the two hour "chase" labeling in cold buffer, it became apparent that the high

labeling of free [^{3}H]DHA in ROS was not paralleled by an efficient esterification into disc

membrane phospholipids, but rather by a translocation to the inner segment where it was actively

esterified. Along this line, the enzyme DHA-CoA synthetase that activates DHA prior to its

esterification into lipids, displays the highest activity in microsomes from frog retinas and very low

activity in ROS (67). Although free DHA can be incorporated in disc membrane PLs by turnover of their acyl groups (62, 68, 69), our present results support the notion that the bulk of DHA is incorporated into lipids in the inner segment prior to their delivery to ROS (70). Furthermore, our data provide clues to further investigate whether the rough ER is the main location where DHA is activated and esterified into lipids involving either the *de novo* pathway and/or subsequent turnover to generate mono and dipolyunsaturated species of phospholipids. Indeed, the similar or higher specific activity of total [³H]DHA-lipids observed in the ER enriched fractions as compared to other fractions enriched in membranes of the Golgi and post-Golgi, support this notion.

An interesting observation after the 2 hour cold "chase" incubation was that the increase in [³H]DHA-lipids labeling was highest in post-Golgi vesicles (gradient fraction 5) and in the lightest TGN fractions 7-9. Because these fractions also became heavily labeled with newly synthesized [³⁵S]rhodopsin after the chase, it appears that some lipids of newly synthesized DHA-PLs are sorted, along with newly synthesized [³⁵S]rhodopsin in transit towards the TGN exit, and are subsequently sequestered in post-Golgi vesicles. Moreover, the similar [³H]DHA-lipid labeling observed after one hour among all subcellular fractions also suggests an early association between newly synthesized DHA-lipids and newly synthesized rhodopsin rather than with older rhodopsin molecules already moving ahead in transit through the Golgi.

Several factors may contribute to the formation of microdomains enriched in DHA-rhodopsin such as the low miscibility between saturated and unsaturated species of phospholipids and/or between cholesterol and phospholipids and the affinity of proteins for certain lipids (71-

26

73). Rhodopsin is synthesized in a highly fluid environment within ER membranes displaying a

high content of DHA-PLs (Figure 6) and poor in cholesterol (45). In fact, rhodopsin shows a

preference for association with more fluid lipids (74) and in ROS, PLs with high DHA content are

in closer association with rhodopsin than less unsaturated ones (75). As vesicles containing

DHA-PLs and rhodopsin exit the ER and initiate their passage through the transport pathway,

vesicles may sequentially bud and fuse with adjacent compartments displaying increasing

concentrations of sterols (45) which prefer to interact with less fluid lipids (i. e. SPH). This will

facilitate a closer association of rhodopsin and DHA-PL within the membranes, moving from the

ER to the TGN in a domain laterally segregated by more saturated lipids and cholesterol rich

membrane domains. Indeed, after the "chase," [^{3}H]DHA-PLs and [^{35}S]rhodopsin accumulated in

the lightest fraction of the TGN, where proteins and lipids are sorted for their subsequent

vectorial transport to different cellular compartments (46). Moreover, [^{35}S]rhodopsin-bearing

post-Golgi vesicles displayed the highest increase in [^{3}H]DHA-PLs, suggesting that they budded

from microdomains in TGN enriched in both [^{35}S]rhodopsin and [^{3}H]DHA-PLs. Similar

cholesterol-modulated association of proteins with glycosphingolipids, as they are in transit

through the Golgi apparatus in polarized epithelial cells, has been previously reported (72, 73).

Post-Golgi vesicles recovered from the gradient fraction 5 (ρ = 1.09 g/ml) display lower

density than ROS which sediment in fractions 7-8 (ρ = 1.12-1.13) and therefore must have a

higher lipid to protein ratio (14). This is also supported by freeze-fracture EM studies (76)

showing that vesicles clustered around the conecting cilium display half the density of the

27

intramembranous particle (IMP) of ROS disks. Since in post-Golgi vesicles the total acyl group content, derived mainly from PLs (4.2 nmole/µg protein), was similar to that of the ROS (3.9 nmole/µg protein), other lipids such as sterols presumably contribute to their lower density. In frog retinas, the non saponifiable lipid product squalene is the main product generated from the precursor [³H]acetate with only minor synthesis of lanosterol and cholesterol and their delivery to ROS occurs by a mechanism different from that of rhodopsin (27). Therefore, the bulk of cholesterol necessary for disk membrane formation must be provided from lipoproteins circulating in plasma and their delivery to ROS must be accomplished either together with rhodopsin and DHA-lipid-containing post-Golgi vesicles and/or by a pathway(s) independent from that followed by integral plasma membrane proteins (20, 77). Nevertheless, sterols incorporated in rhodopsin-bearing vesicles could generate, as vesicles fuse with the plasma membrane adjacent to the base of the connecting cilium, the cholesterol-enriched domains surrounding the periciliary ridge complex observed in frog photoreceptors (78, 79) and also in nascent discs at the base of the ROS (80). These authors also suggest that cholesterol could play a role favoring the sequestration of rhodopsin in the periciliary region. Taken together, these observations suggest that a high miscibility of rhodopsin in membrane domains enriched with DHA-PLs combined with their poor association with surrounding sterol-rich membrane domains contributes to modulate rhodopsin-DHA-PLs trafficking through the biosynthetic pathway, packaging and sequestration into post-Golgi vesicles budding off the TGN, and their efficient delivery to ROS for nascent disc membrane biogenesis.

Further studies are necessary and are currently in progress to evaluate [³H]DHA labeling

of molecular species of PLs, especially those recovered in post-Golgi vesicles from fraction 5 of

the gradient to define which molecular species containing DHA are selectively cotransported with

newly synthesized rhodopsin. Moreover, the use of drugs that perturb rhodopsin trafficking

provides valuable information about DHA-lipids associated with rhodopsin-bearing vesicles which

will be incorporated in ROS by membrane replacement. Our preliminary studies using Brefeldin

A show that [³H]DHA-PL transfer into fraction 5 was successfully blocked and also that ROS

lipid labeling was reduced[2].

A further question for the future is the issue of DHA supply to photoreceptors (81),

particularly, deficient supply and its effects on vesicle-mediated delivery of rhodopsin to ROS. In

this connection, the rate of new disc assembly is significantly lower in frogs with a diet restricted

to very low levels of DHA which lead to low DHA content in liver and plasma, as compared to

controls (82). The rate increases as frogs are systemically treated with DHA. Therefore, it

appears that the early association of newly synthesized PLs and rhodopsin in transit through the

biosynthetic pathway may play an active role in determining the rate of photoreceptor membrane

renewal. Also in newborn rat retinal cells in culture, DHA supplementation is essential for

photoreceptor survival and differentiation suggesting that this specific fatty acid may be a trophic

factor for photoreceptors (83).

In summary, newly synthesized DHA-PLs are vectorially cotransported to ROS by

rhodopsin-bearing post-Golgi vesicles highly enriched with small G-proteins of the rab family (10,

15) and chaperone proteins (i. e. αA and αB crystallin) (16). These proteins are involved in budding, sorting, and targeting of post-Golgi vesicles to the plasma membrane of the inner segment at the base of the connecting cilium. The COOH-terminal cytoplasmic domain of rhodopsin plays a key role not only in the polarized sorting of rhodopsin upon its exit from the TGN, but also in sorting other proteins such as transducin and cGMP phosphodiesterase involved in phototransduction (84). Therefore rhodopsin-bearing vesicles play a leading role in the transport and delivery of proteins and DHA-PLs that selectively become components of ROS. Moreover, in the complex process of membrane biogenesis, addition of rhodopsin and DHA-PLs at the base of ROS could be "the driving force" for the incorporation of other PLs that do not contain DHA (approx. 40-50% of total PLs in disc membranes) possibly reaching the periciliary region by independent pathways. Current studies aim to delineate the mechanism(s) that contribute to the complex polarized trafficking of DHA-PLs either by vesicular and/or by transfer protein-mediated transport to ROS.

30

FIGURE LEGENDS

Figure 1. **Newly synthesized [³H]DHA-lipids and [³⁵S]rhodopsin exit the TGN in very low buoyant density vesicles recovered in the sucrose density gradient fraction 5.** Twenty one frog retinas were incubated for one hour with [³H]DHA and [³⁵S]methionine/cysteine followed by a two hour "chase" in cold buffer containing unlabeled amino acids. Aliquots were taken from each fraction recovered after pulse and chase labeling for lipid and protein analysis. Lipids were extracted and isolated by TLC. Esterified [³H]DHA was estimated after subtraction of the free [³H]DHA from total labeling. Proteins were separated by SDS-gel electrophoresis and the radioactivity incorporated into [³⁵S]rhodopsin was determined by a PhosphorImager densitometer. Mean values ± SEM from n = 4 separate experiments are shown and represent the percent distribution of total labeling recovered from the 14 fractions of the gradient. SEM are shown when the range is larger than the symbol. Asterisk denotes values that are significantly different from pulse labeling (p<0.05, Student's *t* test). C, cytosol; PG, post-Golgi vesicles; TGN, trans Golgi network; G, Golgi; ER, endoplasmic reticulum.

Figure 2. **[³H]DHA-lipids attain a relatively uniform labeling in all fractions after a one hour pulse. After a two hour "chase" newly synthesized lipids accumulate in fractions containing post-Golgi vesicles recovered in fraction 5.** Lipid labeling was normalized to protein content of individual subcellular fractions and shown as a mean value in DPM/μg protein ± SEM (n = 4). Panel A: Free [³H]DHA was isolated from phospholipids and neutral lipids by a

31

2 dimensional-three step TLC as detailed in Methods. Panel B: total esterified [^{3}H]DHA is the

sum of [^{3}H]DHA found esterified into phospholipids and neutral lipids. Panel C: the ratio of

chase / pulse labeling of total [^{3}H]DHA esterified into lipids. Panel D: protein content of

individual subcellular fractions. Mean values ± SEM from n = 8 determinations including all the

pulse and chase samples are shown. Other details as in Figure 1 legend.

Figure 3. **[^{3}H]DHA-PC and [^{3}H]DHA-PE are the phospholipids that display the highest**

increase of labeling in rhodopsin bearing post-Golgi vesicles after the "chase". Total DPM

recovered in individual lipids per μg protein are shown. Insets: labeling of ROS lipids after pulse

(open bars) and "chase" (closed bars). Other details as in Figure 1 legend.

Figure 4. **[^{3}H]DHA-PI, [^{3}H]DHA-PC, and [^{3}H]DHA-PE display the highest percent**

labeling in all retinal subcellular fractions except for ROS which show the highest labeling

in [^{3}H]DHA-PI and [^{3}H]DHA-DAG. Values represent percent labeling of individual lipids with

respect to total [^{3}H]DHA recovered esterified into lipids. Other details as Figure 1 legend.

Figure 5. **Lipids from TGN fraction 8 display the highest [^{3}H]DHA-PI / [^{3}H]DHA-PC ratio.**

Upper panel: values represent percent labeling of PI and PC with respect to total esterified

[^{3}H]DHA recovered in lipids from individual subcellular fractions. Lower panel: ratios of percent

[^{3}H]DHA-PI / [^{3}H]DHA-PC after pulse and "chase" labeling. Other details as Figure 1 legend.

Figure 6. **Lipids from post-Golgi vesicle fraction 5 display a similar content of lipid-acyl groups but a lower content of DHA as compared to ROS membranes.** An aliquot of lipid extracts was derivatized to fatty acid methyl esters and their content and acyl-group composition analyzed by GLC as detailed in Methods. Mean values ± SEM from n= 8-10 individual determinations are shown and expressed as nmole of fatty acids/µg protein. Inset: mole percent content of DHA in subcellular fractions.

REFERENCES

1.   Papermaster, D. S. and Dreyer, W. J. (1974). *Biochemistry*, **13**: 2438-2444.

2.   Aveldaño de Caldironi, M. I. and Bazan, N. G. (1980). *Neurochem. Internat.* **1**: 381-392.

3.   Aveldaño, M. I. and Bazan, N. G. (1983). *J. Lipid Res.* **24**: 620-627.

4.   Fliesler, S. J. and Anderson, R. E. (1983). In *Progress in Lipid Research*, Vol. 22, pp. 79-131, Perganom Press Ltd., London, UK.

5.   Wiegan, R. D., and Anderson, R. E. (1983). *Exp. Eye Res.* **37**: 150-173.

6.   Aveldaño de Caldironi, M. I. and Bazan, N. G. (1977). In: *Function and Biosynthesis of Lipids*, Plenum Press, New York, pp. 397-404.

7.   Louie, K., Wiegand, R. D., and Anderson, R. E. (1988). *Biochem.* **27**: 9014-9020.

8.   Choe, H-G., and Anderson, R. E. (1990). *Exp. Eye Res.* **51**: 159-165.

9.   Besharse, J. C. (1986). In *The Retina: A Model for Cell Biological Studies*. Academic Press, Inc., New York. 297-352.

10.   Deretic, D., and Papermaster, D. S. (1995). In *Progress in Retinal and Eye Research* Vol. 14, pp. 249-265, Pergamon Press, New York.

11.   Choe, H-G., Ghalayini,A. J., and Anderson, R. E. (1990). *Exp. Eye Res.* 51: 167-176.

12.   Mercurio, A. M., and Holtzman, E. (1982). *J. Neurocytol.* **11**: 295-322.

13.   Papermaster, D. S., Schneider, B. G., Defoe, D., and Besharse, J. C. (1986). *J. Histochem. and Cytochem.* **34**: 5-16.

14.   Deretic, D., and Papermaster, D. S. (1991). *J. Cell Biol.* **113**: 1281-1293.

15.   Deretic, D., and Papermaster, D. S. (1993). *J. Cell Science* **106**: 803-813.

16.   Deretic, D., Aebersold, R. H., Morrison, H. D., and Papermaster, D. S. (1994). *J. Biol. Chem.* **24**: 16853-16861.

17.   Deretic, D., Huber, L. A., Ransom, N., Mancini, M., Simons, K., and Papermaster, D. S. (1995). *J. Cell Sci.* **108** (Pt 1): 215-224.

18.   Bishop, W. R., and Bell, R. M. (1988). *Ann. Rev. Cell Biol.* **4**:579-610.

19.   Pagano, R. E. (1990). *Curr. Opin. Cell Biol.* **2**: 652-663.

20.   Voelker, D. R. (1991). *Microbiol. Rev.* **55:** 543-560.

21.   Cleves, A., McGee, T., and Bankaitis, V. (1991). *Trends in Cell Biol.* **1**: 30-34.

22.   Dudley, P. A., and Anderson, R. E. (1978). *FEBS Lett.* **95**: 57-60.

23.   Sellner, P. A., Dalton, T. P., and Helmkamp, G. M. (1991). *Invest. Ophthalmol. Vis. Sci.* **32**(ARVO suppl): 1149.

24.   Bibb, C., and Young, R. W. (1974). *J. Cell Biol.* **61**: 327- 343.

25.   Young, R. W. (1976). *Invest. Ophthalmol.* **15**: 700-725.

26.   Fliesler, S. J., and Basinger, S. F. (1987). *J. Biol. Chem.* **262**: 17516-17523.

27.   Fliesler, S. J., Florman, R., and Keller, R. K. (1995). *Exp. Eye Res.* **60**: 57-69.

28.   Matheke, M. L., Fliesler, S. J., Basinger, S. F., and Holtzman, E. (1984). *J. Neuroscience* **4**: 1086-1093.

29.   Matheke, M. L., and Holtzman, E. (1984). *J. Neuroscience* **4**: 1093-1103.

30. Wetzel, M. G., Bendala-Tufanisco, E., and Besharse, J. C. (1993). *J. Neurocytology* **22**: 397-412.

31. Rodriguez de Turco, E. B., Gordon, W. C., and Bazan, N. G. (1991). *J. Neurosci.* **11**: 3667-3678.

32. Rodriguez de Turco, E. B., Gordon, W. C., and Bazan, N. G. (1993). *Curr. Eye Res.* **13**: 21-28.

33. Gordon, W. C. and Bazan, N. G. (1990). *J. Neurosci.* **10**: 2190-2202.

34. Gordon, W. C. and Bazan, N. G. (1993). *Invest. Ophthalmol. Vis. Sci.* **34**: 2402-2411.

35. Deretic, D., and Papermaster, D. S. (1993). In *Methods for the Study of Photoreceptor Cells* Vol. 15, pp 108-120. Rockefeller University Press, New York.

36. Bazan, N. G. (1982). In *Phospoholipids in the Nervous System*. Horrocks, L. A., Ansell, G. B., and Porcellati, G. (eds). pp. 49-62.

37. Bazan, N. G., Reddy, T. S., Bazan H. E. P. and Birkle D. L. (1986). *Prog. Lipid. Res.* **25**:595-606.

38. Rotstein, N. P., and Aveldaño, M. I. (1987a). *Biochim. Biophys. Acta.* **921**: 221-234.

39. Rotstein, N. P., and Aveldaño, M. I. (1987b). *Biochim. Biophys. Acta* **921**: 235-244.

40. Fanger, B. O. (1987). *Anal. Biochem.* **162**: 11-17.

41. Folch, J., Lees, M., and Sloane-Stanley, G. H. (1957). *J. Biol. Chem.* **226**: 497-509.

42. Marcheselli, V. L., and Bazan, N. G. (1990). *J. Nutr. Biochem.* **1**: 231-237.

43. Rodriguez de Turco, E. B., Gordon, W. C., and Bazan, N. G. (1992). *Invest. Ophthalmol. Vis. Sci.* **32**(ARVO suppl.): 702.

44.   Roque, M. E., and Giusto, N. M. (1995). *Exp. Eye. Res.* **60**:631-643.

45.   Reinhart, M. P. (1990). *Experientia* **46**: 599-611.

46.   Griffiths, G., and Simons, K. (1986). *Science* **234**: 438-443.

47.   Rothman, J. E., and Warren, G. (1994). *Current Biol.* **4**: 220-233.

48.   Wieland, F. T., Gleason, M. L., Serafini, T. A., and Rothman, J. E. (1987). *Cell* **50**: 289-300.

49.   Rodriguez de Turco, E. B., Gordon, W. C., Peyman, G. A., and Bazan, N. G. (1990). *J. Neurosci. Res.* **27**: 522-532.

50.   deVries, K. J., Momchilova-Pankova, A., Snoek, G. T., and Wirtz, K. W. (1994). *Exp. Cell Res.* **215**: 109-113

51.   Snoek, G. T., de Wit, I. S. C., van Mourik, J. H. G., and Wirtz, K. W. A. (1992). *J. Cell Biochem.* **49**: 339-348.

52.   Bankaitis, V. A., Aitken, J. F., Cleves, A. E., and Dowhan, W. (1990). *Nature (Lond.).* **347**: 561-562.

53.   Bankaitis, V. A., Malehorn, D. E., Emr, S. D., and Greene, R. (1989). *J. Cell Biol.* **108**: 1271-1281.

54.   Salama, S. R., Clevesa, A. E., Malehorn, D. E., Whitters, E. A., and Bankaitis, V. A. (1990). *J. Bacteriol.* **172**: 4510-4521.

55.   McGee, T. P., Skinner, H. B., Whitters, E. A., Henry, S. A., and Bankaitis, V. A. (1994). *J. Cell Biol.* **124**: 273-287.

56. Skinner, H. B., McGee, T. P., McMaster, C. R., Fry, M. R., Bell, R. M., and Bankaitis, V. A. (1995). *Proc. Natl. Acad. Sci.* **92**: 112-116.

57. Thomas, G. M. H., Cunningham, E., Fensome, A., Ball, A., Totty, N. F., Troung, O., et al.(1993) *Cell* **74**: 919-928

58. Cunningham, E., Thomas, G. M. H., Ball, A., Hiles, I., and Cockcroft, S. (1995). *Current Biol.* **5**: 775-783

59. de Vries, K. J., Heinrichs, A. A., Cunningham, E. Brunink, F., Westerman, J., Somerharju, P. J., Cockcroft, S., Wirtz, K. W., and Snoek, G. T. (1995). *Biochem. J.* **310**: 643-649

60. Ohashi, M., de Vries, K. J., Frank, R., Snoek, G., Bankaitis, V., Wirtz, K., and Hutter, W. B. (1995). *Nature* **377**: 544-547.

61. Papermaster, D. S., Converse, C. A., and Siu, J. (1975). *Biochemistry* **14**: 1343-1352.

62. Giusto, N. M.; Boschero, M. I.; Sprecher, H., and Aveldaño, M. I. (1986). *Biochim. Biophys. Acta* **860**: 137-148.

63. Bazan, N. G. and Rodriguez de Turco, E. B. (1994) *J. Ocular. Pharm.* **10**:591-604.

64. Giusto, N. M., and Ilincheta de Boschero, M. G. (1986). *Biochim. Biophys. Acta* **877**:440-446.

65. Ghalayini, A. J., and Anderson, R. E. (1984). *Biochem. Biophys. Res. Commun.* **124**: 503-506.

66. Ghalayini, A. J., and Anderson, R. E. (1992). *J. Biol. Chem.* **267**: 1-6.

67. Reddy, T. S., and Bazan, N. G. (1984). *Curr. Eye Res.* **3**: 1225-1232.

68.   Zimmerman, W. F., and Keys, S. (1988). *Exp. Eye Res.* 47: 247-260.

69.   Louie, K., Zimmerman, W. F., Keys,S., and Anderson, R. E. (1991). *Exp. Eye Res.* **53**: 309-316.

70.   Bazan, N. G. (1990). In *Nutrition and the Brain.* Raven Press Ltd, New York pp. 1-24.

71.   Stubbs, C. D., and Smith, A. D. (1984). *Biochim. Biophys. Acta* 779: 89-137.

72.   Hoekstra, D., and Kok, J. W. (1992). *Biochim. Biophys. Acta* 1113: 277-294.

73.   Glaser, M. (1993). *Cur. Opin. Struct. Biol.* **3**: 475-481.

74.   Chen, Y. S., and Hubbel, W. L. (1973). *Exp. Eye Res.* **17**: 517-532.

75.   Aveldaño, M. I. (1988). *Biochem.* **27**: 1229-1239.

76.   Besharse, J. C., and Pfenninger, K. H. (1980). *J. Cell Biol.* **87**:451-463.

77.   Urbani, L., and Simoni, R. D. (1990). *J. Biol. Chem.* **265**: 1919-1923.

78.   Andrews, L. D., and Cohen, A. I. (1981). *Exp. Eye Res.* **33**: 1-10.

79.   Andrews, L. D., and Cohen, A. I. (1983). *J. Cell Biol.* **97**: 749-755.

80.   Andrews, L. D., and Cohen, A. I. (1979). *J. Cell Biol.* **81**:215-228.

81.   Scott, B.L. and Bazan, N.G. (1989). *Proc. Nat. Acad. Sci.* USA, **86**:2903-2907.

82.   Gordon, W. C., Rodriguez de Turco, E. B., and Bazan, N. G. (1995). *Invest. Ophthalmol. Vis. Sci.* **36** (ARVO suppl): S917.

83.   Rotstein, N. P., and Aveldaño, M. I., Barrantes, F. J., and Politi, L. E. (1996). *J. Neurochem.* **66**: 1851- 1859.

84. Deretic, D., Puleo-Scheppke, B., and Trippe, C. (1996). *J. Biol. Chem.* **271**: 2279-2286.
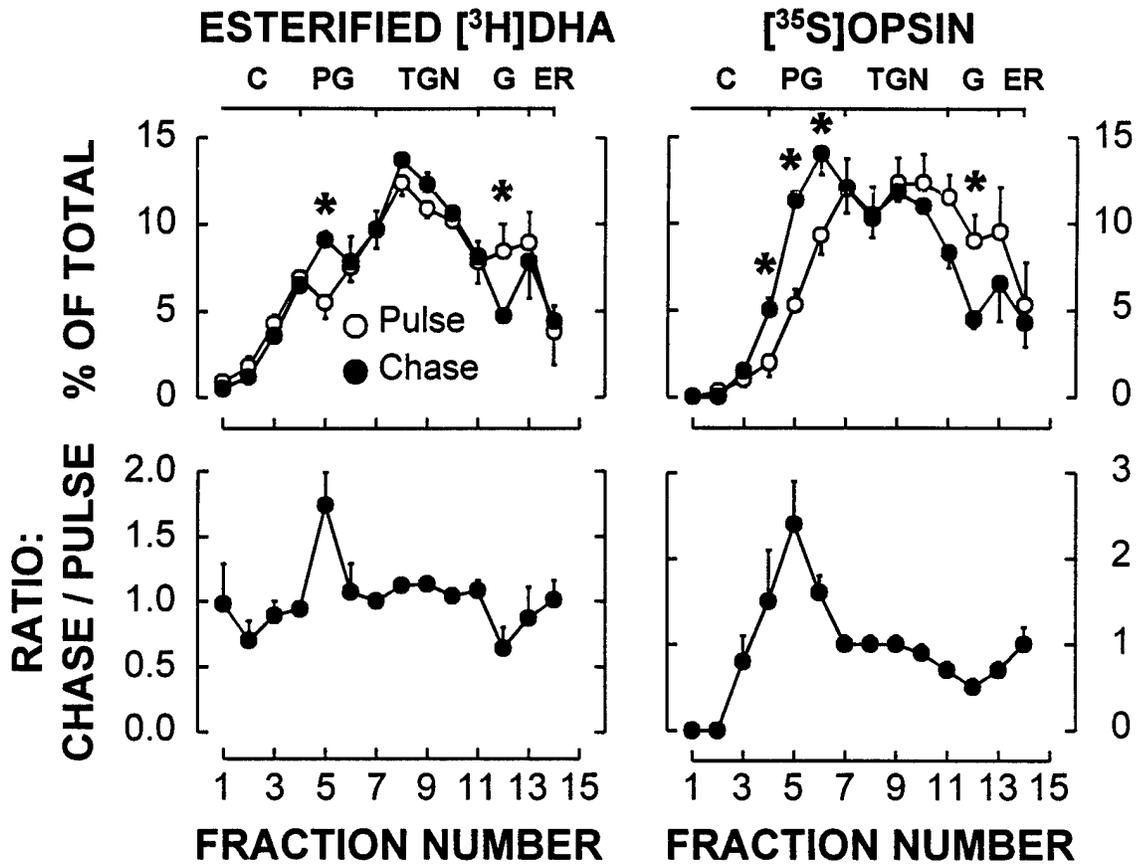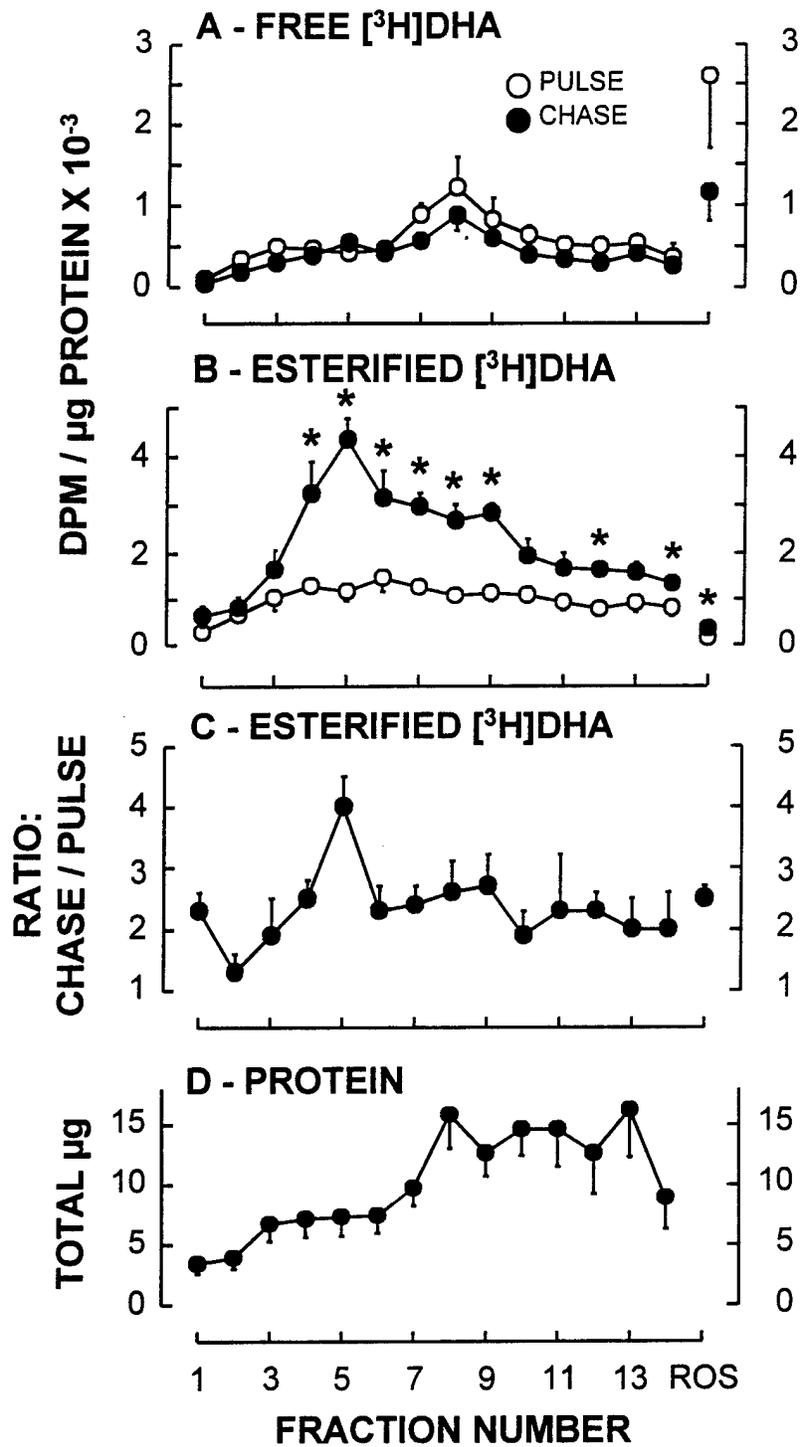
FOOTNOTES

[1]The abbreviations used are: ROS, rod outer segments; PLs, phospholipids; DHA 22:6n-3, docosahexaenoic acid; PA, phosphatidic acid; PC, phosphatidylcholine; PE, phosphatidylethanolamine; PS, phosphatidylserine; PI, phosphatidylinositol; TAG, triacylglycerol; DAG, diacylglycerol; MAG, monoacylglycerol; ER, endoplasmic reticulum; HPTLC, high performance thin layer chromatography; PNS, post-nuclear supernatant; TGN, trans-Golgi network; FAME, fatty acid methyl esters; PL-TP, PL transfer protein; IMP, intramembranous particle.
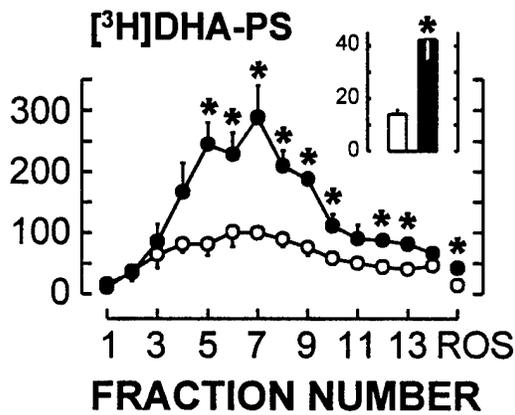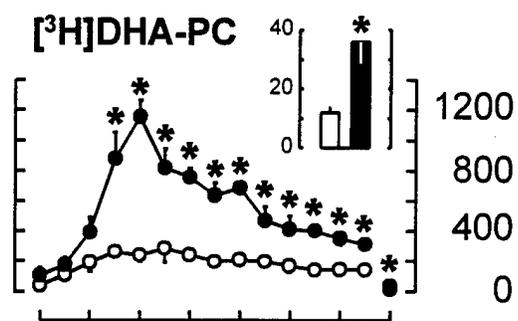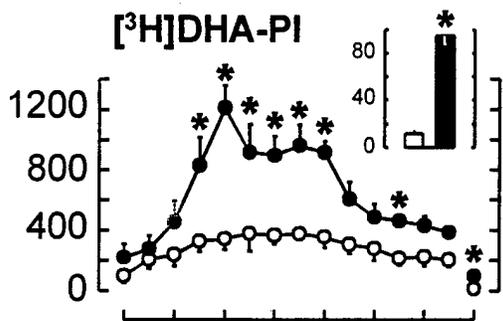
[2]Deretic et al., manuscript in preparation.

ACKNOWLEDGEMENTS.

A - FREE [³H]DHA

○ PULSE
● CHASE

B - ESTERIFIED [³H]DHA

C - ESTERIFIED [³H]DHA

D - PROTEIN

FRACTION NUMBER

DPM / µg PROTEIN X 10⁻³

RATIO: CHASE / PULSE

TOTAL µg

[³H]DHA-PA

[³H]DHA-DAG

[³H]DHA-PI

[³H]DHA-PC

[³H]DHA-PS

[³H]DHA-PE

○ Pulse
● Chase

DPM / μg PROTEIN

FRACTION NUMBER

FRACTION NUMBER

FRACTION 1

FRACTION 5
(Post-Golgi Vesicles)

□ Pulse
■ Chase

FRACTION 8
(TGN)

FRACTION 11
(Golgi)

FRACTION 14
(ER)

ROS

% LABELING

PA PS PI PC PE TAG DAG MAG
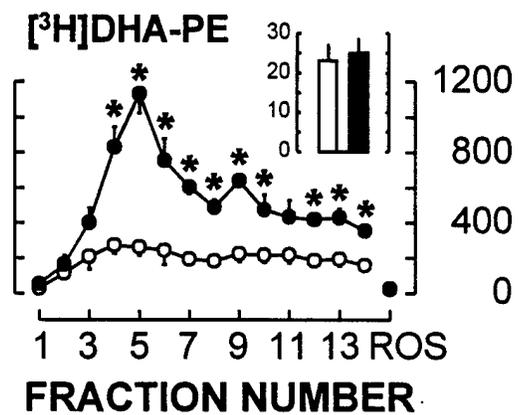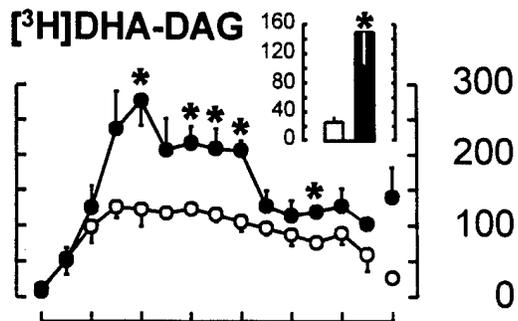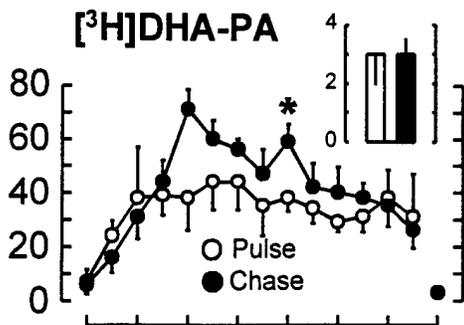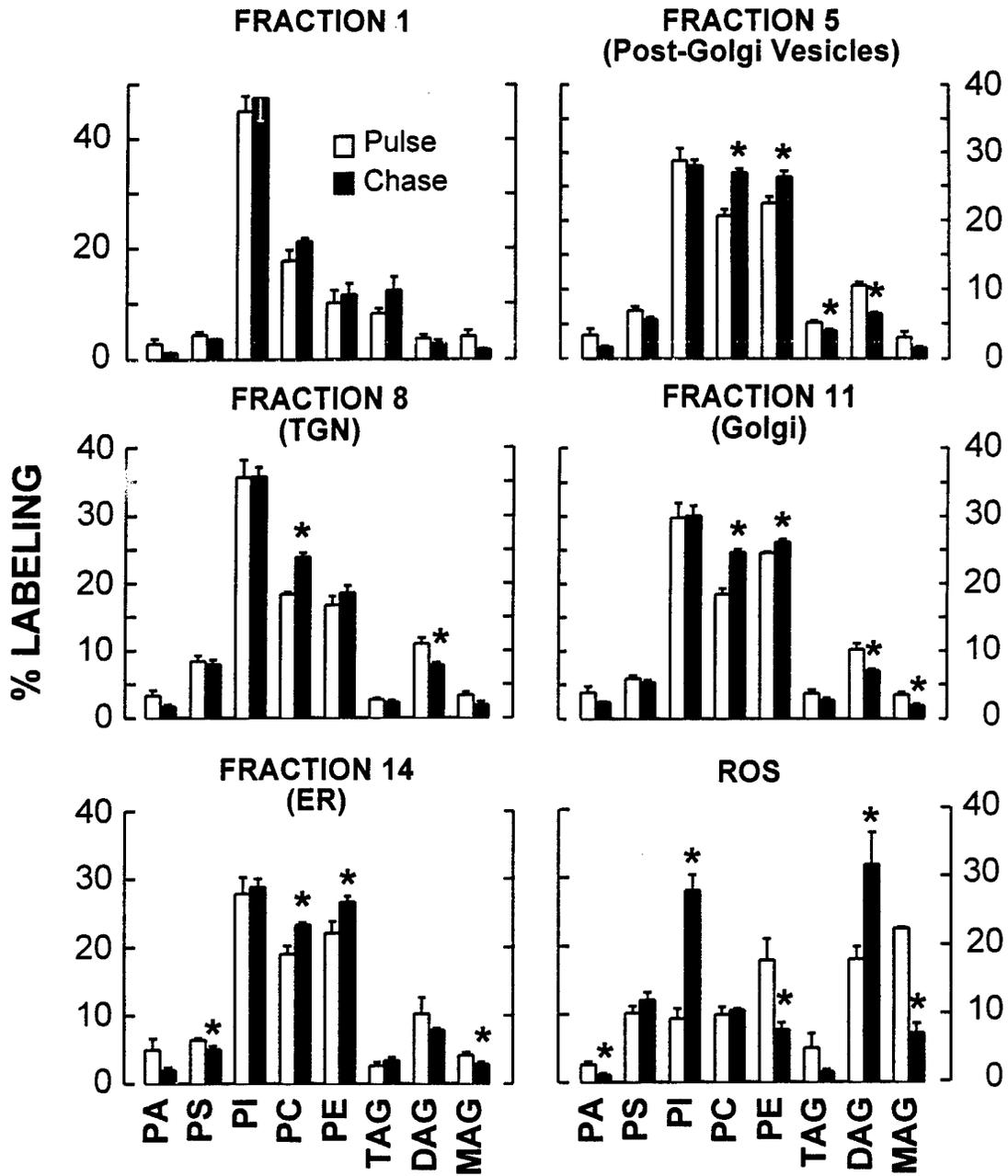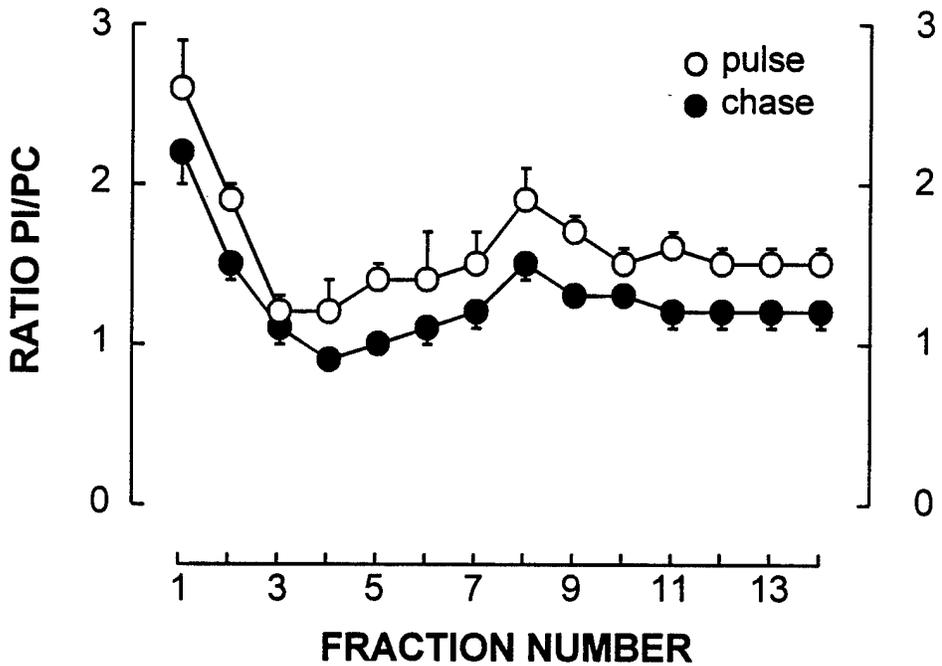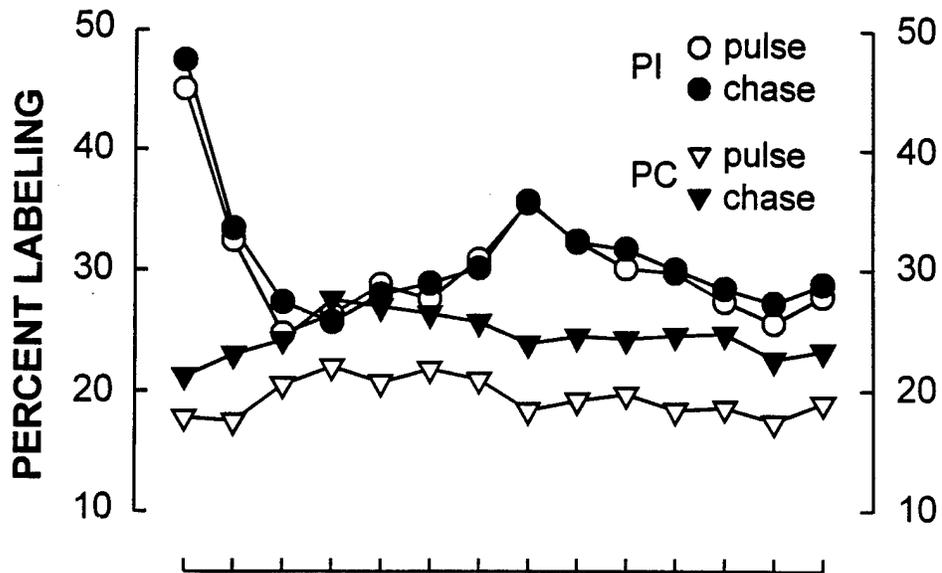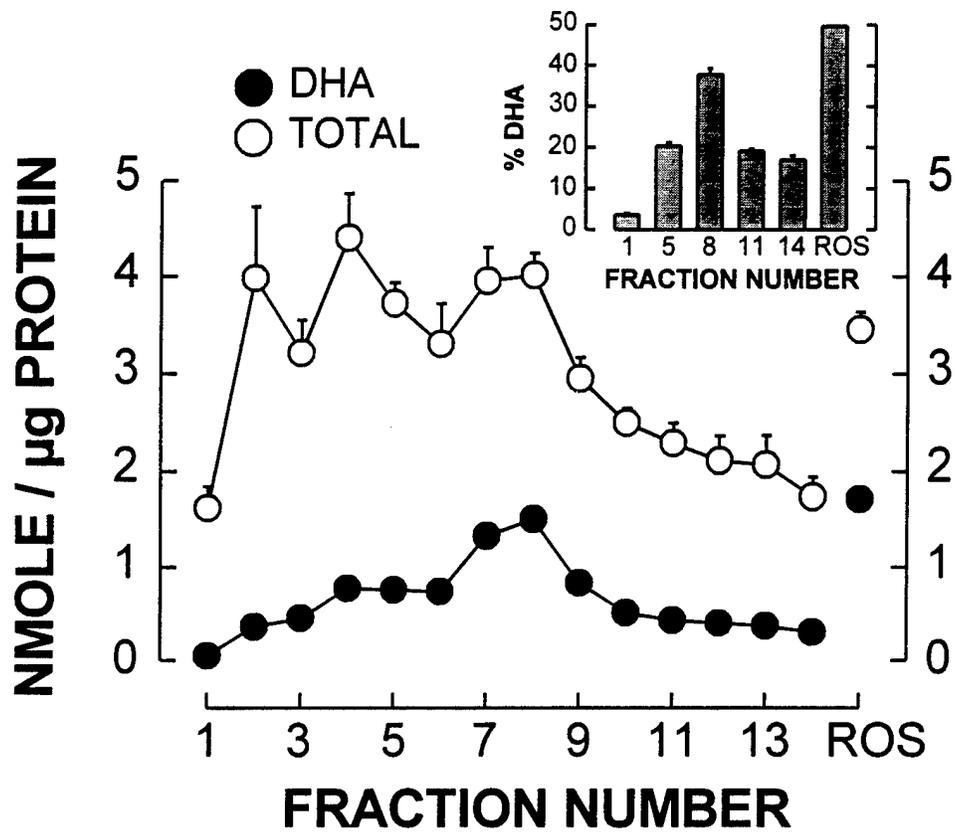
2970

THE ONSET OF LIGHT DAMAGE SELECTIVELY INDUCES THE EARLY RESPONSE GENE INDUCIBLE CYCLOOXYGENASE IN THE RAT RETINA. E.B. Rodriguez de Turco, V.L. Marcheselli, W.C. Gordon, N.G. Bazan. LSU Neuroscience Center. LSU Medical Center, New Orleans, LA 70112.

Bright light can trigger a sequence of changes in rretina that will induce apoptosis and photoreceptor cell loss, but little is known about the nature of these events. COX-2, the inducible form of prostaglandin H synthase, converts arachidonic acid to prostaglandin H2, a nodal precursor of prostaglandins, thromboxanes, and leukotrienes. We have shown that COX-2 is involved in furthering brain damage resulting from seizures or trauma. Blocking the induced expression of brain COX-2 with PAF antagonists results in protection from injury, suggesting involvement of prostaglandins. Because light damage in retina similarly culminates in apoptosis and cell loss, we examined the effects of retinal light trauma on COX-2 induction. Sprague-Dawley rats (175-200 g) were light damaged (7000 lux, 2 hr, fluorescent light) and then returned to dim light (10 lux, 4 hr). Control rats were kept in dim light. Eyecups were prepared and retinas (RPE + neural retina) cut into 4 quadrants. Inferior-temporal quadrants (areas of greatest light damage) were compared to superior-nasal quadrants (regions of least damage). Western blot analysis of COX-2 and PGDS was run and results normalized to control animal values. Tissue was also monitored histologically to quantify apoptosis and determine cell loss. By 4 hrs post-light treatment there was no evidence that apoptosis had been initiated and no cell loss had occurred. PGDS levels demonstrated no statistical difference between control and light-damaged retinas in either quadrant, and COX-2 levels in superior-nasal quadrants also showed no change. However, COX-2 was increased 100-fold in light-damaged regions. Induction of COX-2 in light-damaged areas followed the topographic pattern found for apoptosis and cell loss, but induction of this enzyme precedes these events, suggesting that prostaglandins are involved early in the apoptotic pathway. Supported by the USAMRDC contract #DAMD-17-93-V-3013.

2971

THE ROLE OF CYTOSOLIC PHOSPHOLIPASE A2 IN SIGNAL TRANSDUCTION BY INTERFERON. Bryan R.G. Williams and Vincenzo. Flati (SPON: R. Gronostajski) Cleveland Clinic Foundation Research Institute, Cleveland, OH 44195

Interferon α (IFN-α) treatment of cells results in a transient activation of phospholipase A_2 and rapid hydrolysis and release of arachidonic acid (AA). Signal transduction by IFN-α as measured by electromobility shift assays (EMSA) using the interferon stimulated response element (ISRE) as a probe or in transient transfection assays using ISRE-dpendent reporter constructs can be effectively blocked by phospholipase inhibitors. Cytosolic phospholipase A_2 (cPLA$_2$) is rapidly tyrosine phosphorylated and activated following IFN treatment in a Jak1 kinase-dependent step. Jak1 can be co-immunoprecipitated with cPLA$_2$ in cell extracts and in Jak1 kinase mutant cells there is no release of AA following exposure to IFN-α. In cells where Jak1 kinase activity has been rescued by cDNA transfection, cPLA2 activation is restored, as is formation of interferon stimulated gene factor three (ISGF3) on an ISRE. In either cell cultures or cell free systems, formation of ISGF3 which consists of a complex of transcription factors Stat1, Stat2 and p48, can be blocked by cPLA$_2$ inhibitors. However, these inhibitors do not block the IFN-α or γ induced binding of Stat1 to IR/GAS elements. Rather, the inhibitors appear to specifically block the translocation of Stat2 from membrane bound sites to the cytosol preventing the formation of ISGF3. Thus cPLA$_2$ activation occurs as an early step in the IFN response and appears to be selectively involved in the induction of ISGF3-dependent genes through mobilization of Stat2. Supported by PO1-CA62220, NIH-NCI.

2972

RECONSTITUTION OF HUMAN ARYL HYDROCARBON RECEPTOR (AhR) SIGNALING PATHWAY IN YEAST. Charles A. Miller. Tulane University School of Public Health and Center for Bioenvironmental Research, New Orleans, LA 70112.

In mammalian cells the binding of ligand (e.g., TCDD) is required for AhR to undergo translocation from the cytoplasm into the nucleus of the cell. A nuclear-localized complex of AhR and its dimerization partner ARNT regulates transcription of genes involved in metabolic regulation and signal transduction. Genes encoding human AhR and ARNT were expressed in the yeast *Saccharomyces cerevisiae*, which lacks equivalent homologs. Coexpression of AhR and ARNT specifically stimulated expression of a lacZ reporter plasmid that contained AhR-ARNT response elements upstream of a minimal yeast promoter. Surprisingly, in the yeast system transactivation was constitutive and insensitive to the AhR ligand β-napthoflavone. This result suggests that yeast either produce a natural AhR ligand or that human AhR is processed to a transcriptionally competent form that does not require ligand binding for activity. The basis of the constitutive AhR activation is being studied.

2973

PARATHYROID HORMONE STIMULATES THE *C-FOS* PROMOTER THROUGH CREB PHOSPHORYLATION AND BINDING TO THE MAJOR CRE. A.T. Pearman, M.R. Pulumati, D.R. Tyson, N.C. Partridge, St. Louis University School of Medicine, St. Louis, MO 63104.

The major CRE in the c-*fos* gene is necessary for its activation in response to parathyroid hormone (PTH) treatment in UMR 106-01 rat osteosarcoma cells as determined through transient transfection of mouse c-*fos* 5'-deletion constructs. This CRE binds protein(s) from these cells which include CREB. We now provide further evidence indicative of a role for phosphoCREB and the major CRE in PTH activation of c-*fos*. To directly assess the importance of the c-*fos* major CRE, we have mutated this element in the largest of our c-*fos* promoter constructs (-356 *fos*-CAT). This construct was transiently transfected into UMR 106-01 cells and treated with PTH (10^{-8} M). The mutation reduced basal expression to 10% of wild type. Most significantly, PTH inducibility was substantially decreased from 2.7 to 1.5 fold stimulation. Gel mobility shift confirmed that this mutation prevents CREB binding to this CRE. CREB involvement in c-*fos* promoter activity is directly addressed by cotransfection of the dominant inhibitor KCREB with the c-*fos* deletion constructs. KCREB expression substantially (average 46%) inhibits induction of all PTH-activatable promoter constructs. Of primary importance, PTH treatment causes phosphorylation of CREB protein in our cells with a time course and PTH dose dependency that parallels previously measured protein kinase A induction. These data support our hypothesis that PTH-induced phosphoCREB binds the major CRE in the c-*fos* 5' regulatory region then activates transcription of this gene in UMR 106-01 cells.

2974

CHARACTERIZATION OF A NOVEL NUCLEAR MOVEMENT PROTEIN GENE, CLONE 15 (RNUDC). S. M. Morris, G. May, P. Anaya, and L.-y. Yu-Lee. Baylor College of Med., Houston, TX 77030.

Prolactin (PRL) regulates lymphocyte proliferation through the activation of a number of genes, one of which was identified as clone 15 (c15) from a PRL-dependent T cell line, Nb2. The c15 ORF (332 aa) shows a high degree of similarity (68% of the carboxy terminus 94 aa are identical) to the nuclear movement protein encoded by the *Aspergillus nidulans mudC* (nuclear distribution) gene. The 45 kDa c15 protein has been identified in many different tissues and cell types, ranging from epithelial to neuronal. Immunocytochemistry studies have localized c15 protein expression to the cytoplasm.

To address function, complementation studies of *A. nidulans mudC* mutants with c15 have been initiated. Preliminary complementation results suggest that transformed *A. nidulans mudC* mutants, which express a full-length rat c15 protein, are rescued and exhibit a normal nuclear movement phenotype. These results suggest that rat c15 and fungal NUDC not only share similar structures, but also serve similar functions. Because of such a high degree of structural and functional similarity, c15 is likely to be the mammalian (rat) homologue of *mudC* and may be the first mammalian nuclear movement protein to be described and has therefore been renamed *RnudC*. (Supported by The Linda and Ronald Finger Lupus Research Center, Association for Women in Science, and ACS BE49J).

2975

ZETA PKC- MEDIATED PHOSPHORYLATION OF A 100 kDa NUCLEAR PROTEIN IN RESPONSE TO NGF. G. Zhou and M. W. Wooten. Dept. of Zoology, Auburn University, Auburn, AL 36849.

We have previously reported that atypical protein kinase C (PKC)-ζ is both activated and required for nerve growth factor (NGF) responses in pheochromocytoma (PC12) cells. A nuclear protein with an approximate molecular mass of 100 kDa has been characterized as a substrate of PKC-ζ. NGF treatment resulted in nuclear translocation of PKC-ζ and a ~ 2-fold increase in the phosphorylation of this nuclear protein at pH 6.5, while EGF had no effect. Phosphorylation occurred on serine-residues, independent of Ca^{2+}/CaM. Addition of PKC-ζ pseudosubstrate peptide diminished phosphorylation in a dose-dependent fashion in the range of 5 - 100 μM, whereas addition of purified PKC-ζ to nuclear extracts resulted in an incremental increase in the phosphorylation of the protein *in vitro*. Chronic PMA-treatment enhanced NGF responsiveness and neurite length in addition to elevating the phosphorylation state of this protein. Overexpression of gp140^{trk} in PC12 cells resulted in enhanced NGF-induced phosphorylation of the 100 kDa protein, whereas expression of *ras* mutant, Asn-17, which confers the dominant negative phenotype, diminished NGF-induced 100 kDa protein phosphorylation. Studies are underway to establish the identity of this protein. Our findings suggest that this protein may serve to relay signals from NGF receptor *trk/ras*- PKC-ζ pathways into the nucleus. Supported by NS-33661 (MWW).

Enhanced Expression of the Inducible Prostaglandin Synthase Gene Precedes Light-Induced Photoreceptor Apoptosis

The upstream intracellular pathways of signal transduction involved in photoreceptor cell apoptosis are not well understood. We have studied COX-2 (prostaglandin H-synthase, an early response gene that converts arachidonic acid to prostaglandin H_2, the precursor of prostaglandins, thromboxanes, and prostacyclin) in retinas undergoing light-triggered photoreceptor apoptosis. COX-2 transcriptional activation is an early event in the hippocampus in conditions leading to neuronal cell death (Marcheselli, V. L. and Bazan, N.G., J. Biol. Chem. 217:24794-24799, 1996). Sprague-Dawley rats (175-200 g) were light-damaged (7000 lux, 2 hrs, fluorescent light) and then returned to dim light (10 lux). Control rats were kept in dim light. Eyecups were prepared and retinas were cut into 4 quadrants. Inferior-temporal quadrants (the region of greatest light-induced apoptosis) were compared to superior-nasal quadrants (the region of least light damage). Western and Northern blot analyses of COX-2, COX-1 and PGDS (lipocalin-type prostaglandin D synthase, another prostaglandin synthesizing enzyme) were run and the results were normalized to control values. Tissue was also monitored histologically to quantify apoptosis and determine cell loss. By 4 hrs post-light treatment, neither apoptosis nor levels of PGDS demonstrate any statistical difference between control and light-damaged retinas in either quadrant. There was also no change in COX-2 levels in superior-nasal quadrants. However, COX-2 was increased several-fold in light-damaged retinal regions. The early induction of COX-2 preceded apoptosis while displaying the same cellular topographic pattern, which suggests that COX-2 is involved in apoptotic photoreceptor loss. Moreover, COX-2 protein was immunocytochemically localized in inner segments of photoreceptor cells. Light-induced COX-2 induction may be involved in the chain of events leading to apoptosis, functioning as part of an intracellular pathway engaged in repair/rescue responses of a photoreceptor cell when confronted with adverse, survival-threatening environmental conditions. (NIH/EY05121 and DAMD 17-93-V-3013)

PAF is a transcriptional activator of PGS-2 (COX-2): Significance for neuronal survival after injury.

Nicolas G. Bazan
LSUMC Neuroscience Center of Excellence
2020 Gravier St., Suite B
New Orleans, LA 70112

PAF activates luciferase reporter constructs driven by regulatory regions of the COX-2 gene transfected in glioblastoma-neuroblastoma NG108-15 hybrid, human SH-SY5Y neuroblastoma or in NIH 3T3 cells. Deletion of the sequences between -371 and -300 of the murine COX-2 promoter greatly reduces PAF induction. Moreover, deletion mutants containing sequences for -430 and -830 of the human COX-2 promoter are necessary for PAF induction. BN 50730, a potent intracellular PAF antagonist, blocks COX-2 induction by PAF, using either murine or human COX-2 promoter constructs.

COX-2 transcription and protein expression are upregulated in the hippocampus in kainic acid induced epileptogenesis. Although the expression of other early-response genes is also increased under these conditions (e.g. *zif*-268, AP1), there is a selectively elevated induction of COX-2 (several fold) by kainic acid preceding neuronal cell death. BN 50730 administered by icv injection blocks seizure-induced COX-2 induction. DNA-binding activities for NFKB, AP2, STAT3, and NFIL6 increases both in cells in culture (human IM-9) exposed to PAF as well as in hippocampus during seizures. In both instances, BN 50730 inhibits these DNA-binding activities. Since consensus sequences for these DNA-binding activities are present in the COX-2 promoter, transcription factors recognizing these sequences may be involved in PAF-induction of COX-2. PAF stimulated signal transduction pathways are major components of seizure-induced expression of COX-2 in neurons. We are exploring the significance of the PAF-COX-2 route in cell death, both in light-induced rod photoreceptor cell apoptosis, as well as in kainic acid-induced neuronal apoptosis. (NIH NS23002 and DAMD 17-93-V-3013)